

THE UNIVERSITY OF CALGARY

Load-Deflection Characteristics of Spherical Inflatables

by

Mark Robert Sawa

A THESIS

SUBMITTED TO THE FACULTY OF GRADUATE STUDIES
IN PARTIAL FULFILLMENT OF THE REQUIREMENTS FOR THE
DEGREE OF MASTER OF SCIENCE

DEPARTMENT OF MECHANICAL ENGINEERING

CALGARY, ALBERTA

FEBRUARY, 1996

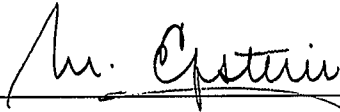
©Mark Robert Sawa 1996

THE UNIVERSITY OF CALGARY
FACULTY OF GRADUATE STUDIES

The undersigned certify that they have read, and recommend to the Faculty of Graduate Studies for acceptance, a thesis entitled "Load-Deflection Characteristics of Spherical Inflatables" submitted by Mark Robert Sawa in partial fulfillment of the requirements for the degree of Master of Science.



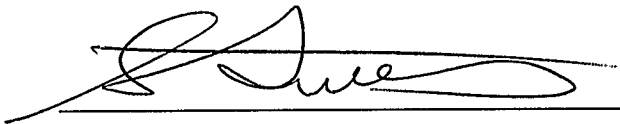
Supervisor, Dr. P.G. Glockner, Department of Mechanical Engineering



Dr. M. Epstein, Department of Mechanical Engineering



Dr. R. Loov, Department of Civil Engineering



Dr. S. Lukasiewicz, Department of Mechanical Engineering

96.05.06

Date

Abstract

A contributing factor to the unexplained collapse of a number of large-scale inflatable structures is ponding instability. In this thesis, the load-deflection characteristics will be examined for a spherical membrane of radius R_o , central half angle β_o , and internal pressure p_o subjected to concentrated axisymmetric apex loads, hydrostatic loads, or a combination of hydrostatic and concentrated axisymmetric apex loading. A full range of geometries, from shallow to very lofty, will be treated and the entire range of the ponding medium's nondimensional density will be allowed. The analysis will also take support wrinkling into account. The deflected configuration is considered in an Eulerian description with open boundary conditions. Equations of equilibrium, the Gauss-Codazzi relation and compatibility are used to solve the governing differential equations numerically using an iterative scheme based on a fourth order Runge-Kutta method.

The results indicate limit-point behavior for all loading conditions examined if the geometry of the structure is sufficiently lofty. The engineer is presented with the critical concentrated axisymmetric apex load which can be applied safely to the structure or the minimum allowable central half angle for a given nondimensional density such that snap-through behavior can be avoided. The engineer should then be able to use spherical inflatable structures without fear of snap-through behavior.

Table of Contents

Table of Contents	iv
List of Figures	vii
List of Variables	xi
1 INTRODUCTION	1
1.1 Introduction	1
1.2 Historical Development	2
1.3 Summary	4
2 CONCENTRATED AXISYMMETRIC APEX LOADING	6
2.1 Introduction	6
2.2 Assumptions and Definitions	6
2.3 Physical Arrangement	8
2.4 Theory	8
2.4.1 General Formulation	8
2.4.2 Support Wrinkling	16
2.5 Numerical Procedure	18
2.6 Load-Deflection Characteristics	18
2.7 Results	22
3 HYDROSTATIC LOADING	25
3.1 Introduction	25

3.2	Physical Arrangement	25
3.3	Theory	27
3.4	Load-Deflection Characteristics	33
3.5	Results	36
3.5.1	Critical Nondimensional Density	36
3.5.2	The "Takeoff" Curve	40
3.5.3	Central Half Angle	42
3.5.4	Nondimensional Density	47
3.5.5	Load-Deflection Curves	50
4	HYDROSTATIC AND CONCENTRATED AXISYMMETRIC APEX	
	LOADING	66
4.1	Introduction	66
4.2	Physical Arrangement	66
4.3	Theory	68
4.4	Load-Deflection Characteristics	75
4.5	Results	80
4.5.1	Nondimensional Density	80
4.5.2	Central Half Angle	88
4.5.3	Design	96
4.6	Summary	101
5	DISCUSSION AND CONCLUSIONS	102
5.1	Limitations	102
5.2	Conclusions	104

5.3 Future Research	107
Bibliography	109

List of Figures

2.1	Spherical Membrane Subjected to Internal Overpressure	7
2.2	Spherical Membrane Subjected to Concentrated Axisymmetric Apex Load	9
2.3	Membrane of Revolution with Support Wrinkling	17
2.4	Typical Load-Deflection Curve for a Spherical Membrane Subjected to a Concentrated Axisymmetric Apex Load ($\beta_o = 45^\circ$)	19
2.5	Load-Deflection Curves for a Spherical Membrane Subjected to a Concentrated Axisymmetric Apex Loading with Support Wrinkling	23
3.1	Spherical Membrane Subjected to Axisymmetric Hydrostatic Apex Loading	26
3.2	Load-Deflection Curve for a Spherical Membrane Subjected to Hydrostatic Axisymmetric Loading with no Support Wrinkling	34
3.3	Effect of Nondimensional Density on the Existence of a Maximum Load	37
3.4	“Takeoff” and Maximum Points for Hydrostatic Loading of a Spherical Membrane	38
3.5	The Complete “Takeoff” Curve for Hydrostatic Loading of a Spherical Membrane	41
3.6	Effect of Nondimensional Density on the Load-Deflection Behavior of a Spherical Membrane Under Axisymmetric Hydrostatic Loading with no Support Wrinkling ($\beta_o = 120^\circ$)	43

3.7	Effect of Nondimensional Density on the Load-Deflection Behavior of a Spherical Membrane Under Axisymmetric Hydrostatic Loading with no Support Wrinkling ($\beta_o = 60^\circ$)	44
3.8	Effect of Nondimensional Density on the Load-Deflection Behavior of a Spherical Membrane Under Axisymmetric Hydrostatic Loading with no Support Wrinkling ($\beta_o = 30^\circ$)	45
3.9	Effect of Nondimensional Density on the Minimum Neutral Stability Point ($\beta_o = 60^\circ$)	48
3.10	Effect of Nondimensional Density on the Minimum Neutral Stability Point ($\beta_o = 30^\circ$)	49
3.11	Load-Deflection Curves for a Spherical Membrane Subjected to Axisymmetric Hydrostatic Loading with Support Wrinkling ($\bar{\gamma} = 1.8$) . .	51
3.12	Load-Deflection Curves for a Spherical Membrane Subjected to Axisymmetric Hydrostatic Loading with Support Wrinkling ($\bar{\gamma} = 2.8$) . .	52
3.13	Load-Deflection Curves for a Spherical Membrane Subjected to Axisymmetric Hydrostatic Loading with Support Wrinkling ($\bar{\gamma} = 3.4$) . .	53
3.14	Load-Deflection Curves for a Spherical Membrane Subjected to Axisymmetric Hydrostatic Loading with Support Wrinkling ($\bar{\gamma} = 4.55$) .	54
3.15	Load-Deflection Curves for a Spherical Membrane Subjected to Axisymmetric Hydrostatic Loading with Support Wrinkling ($\bar{\gamma} = 9$) . . .	55
3.16	Load-Deflection Curves for a Spherical Membrane Subjected to Axisymmetric Hydrostatic Loading with Support Wrinkling ($\bar{\gamma} = 15$) . .	56
3.17	Load-Deflection Curves for a Spherical Membrane Subjected to Axisymmetric Hydrostatic Loading with Support Wrinkling ($\bar{\gamma} = 30$) . .	57

3.18	Load-Deflection Curves for a Spherical Membrane Subjected to Axisymmetric Hydrostatic Loading with Support Wrinkling ($\bar{\gamma} = 50$) . .	59
3.19	Load-Deflection Curves for a Spherical Membrane Subjected to Axisymmetric Hydrostatic Loading with Support Wrinkling ($\bar{\gamma} = 100$) .	60
3.20	Load-Deflection Curves for a Spherical Membrane Subjected to Axisymmetric Hydrostatic Loading with Support Wrinkling ($\bar{\gamma} = 200$) .	61
3.21	Load-Deflection Curves for a Spherical Membrane Subjected to Axisymmetric Hydrostatic Loading with Support Wrinkling ($\bar{\gamma} = 500$) .	62
3.22	Load-Deflection Curves for a Spherical Membrane Subjected to Axisymmetric Hydrostatic Loading with Support Wrinkling ($\bar{\gamma} = 1000$) .	63
3.23	Load-Deflection Curves for a Spherical Membrane Subjected to Axisymmetric Hydrostatic Loading with Support Wrinkling ($\bar{\gamma} = 2000$) .	64
3.24	Load-Deflection Curves for a Spherical Membrane Subjected to Axisymmetric Hydrostatic Loading with Support Wrinkling ($\bar{\gamma} = 4000$) .	65
4.1	Spherical Membrane Subjected to Hydrostatic and Concentrated Axisymmetric Apex Loading	67
4.2	Typical Load-Deflection Surface for a Spherical Membrane Subjected to Combined Hydrostatic and Concentrated Axisymmetric Apex Loading with no Support Wrinkling ($\beta_o = 60^\circ$ and $\bar{\gamma} = 4.55$)	77
4.3	Load-Deflection Surface for a Spherical Membrane Subjected to Combined Hydrostatic and Concentrated Axisymmetric Apex Loading ($\bar{\gamma} = 2.8$ and $\beta_o = 60^\circ$)	81

4.4	Load-Deflection Surface for a Spherical Membrane Subjected to Combined Hydrostatic and Concentrated Axisymmetric Apex Loading ($\bar{\gamma} = 4.55$ and $\beta_o = 60^\circ$)	82
4.5	Load-Deflection Surface for a Spherical Membrane Subjected to Combined Hydrostatic and Concentrated Axisymmetric Apex Loading ($\bar{\gamma} = 4000$ and $\beta_o = 60^\circ$)	83
4.6	Load-Deflection Surface for a Spherical Membrane Subjected to Combined Hydrostatic and Concentrated Axisymmetric Apex Loading ($\bar{\gamma} = 4.55$ and $\beta_o = 120^\circ$)	89
4.7	Load-Deflection Surface for a Spherical Membrane Subjected to Combined Hydrostatic and Concentrated Axisymmetric Apex Loading ($\bar{\gamma} = 4.55$ and $\beta_o = 60^\circ$)	90
4.8	Load-Deflection Surface for a Spherical Membrane Subjected to Combined Hydrostatic and Concentrated Axisymmetric Apex Loading Neglecting Support Wrinkling ($\bar{\gamma} = 4.55$ and $\beta_o = 30^\circ$)	91
4.9	Load-Deflection Surface for a Spherical Membrane Subjected to Combined Hydrostatic and Concentrated Axisymmetric Apex Loading with Support Wrinkling ($\bar{\gamma} = 4.55$ and $\beta_o = 30^\circ$)	94
4.10	Minimum Allowable Central Half Angle for a Given Nondimensional Density	97
4.11	The Critical Concentrated Axisymmetric Apex Load for a Given Nondimensional Density	100

List of Variables

A - A point on the membrane of revolution defined as the start of the load wrinkling domain.

B - A point on the membrane defined by the change in curvature due to hydrostatic loading.

C - A point on the load-deflection curve or surface defining an equilibrium configuration with a completely filled depression.

C_H - A point on the C curve which corresponds to hydrostatic loading (page 75).

C_M - A point on the C curve defined by the maximum concentrated axisymmetric apex load which produces a completely filled depression.

D - A point on a load-deflection curve or surface at which the load wrinkling domain first reaches the supports.

E - A point on the membrane defining the end of the load wrinkling domain.

F - The total load applied to the membrane.

\bar{F} - The nondimensional total load applied to the membrane.

G - A point on a load-deflection curve or surface for which the load is a local maximum.

h - The orthonormal coordinate in the vertical direction.

\bar{h} - The nondimensional orthonormal coordinate in the vertical direction.

h_A - The height to point A.

\bar{h}_A - The nondimensional height to point A.

\bar{h}_E - The nondimensional height to point E.

H_o - The depth of the hydrostatic load to the apex.

\bar{H}_o - The nondimensional depth of the hydrostatic load to the apex.
 J - An arbitrary constant.
 k - A variable equal to 1 or -1.
 L - A point on the membrane defining the boundary between hydrostatic and non-hydrostatic loading.
 M - An arbitrary constant.
 N_θ - The circumferential stress resultant.
 N_ϕ - The meridional stress resultant.
 O - The origin.
 p - The net pressure.
 \bar{p} - The nondimensional net pressure.
 p_o - The internal overpressure.
 P - The concentrated axisymmetric apex force.
 \bar{P} - The nondimensional concentrated axisymmetric apex force.
 \bar{P}_G - The nondimensional concentrated axisymmetric apex force for which the membrane's equilibrium configuration has an angle ϕ_E equal to the central half angle.
 P_L - The concentrated axisymmetric apex force which initiates support wrinkling.
 \bar{P}_L - The nondimensional concentrated axisymmetric apex force which initiates support wrinkling.
 \bar{P}_M - The maximum nondimensional concentrated axisymmetric apex force which produces a completely filled depression when hydrostatic loading is applied.
 Q - The total vertical force.
 \bar{Q} - The nondimensional total vertical force.
 Q_L - The point on the load-deflection curve to which the membrane snaps-through

when loading.

Q_{UL} - The point on the load-deflection curve to which the membrane snaps-through when unloading.

r - The orthonormal coordinate in the radial direction.

\bar{r} - The nondimensional orthonormal coordinate in the radial direction.

R - A point on the load-deflection curve or surface where the effects of support wrinkling terminate.

r_L - The radius of point L on the membrane.

\bar{r}_o - The nondimensional radius to the point on the membrane at which the slope is horizontal.

R_o - The radius of the sphere.

r_s - The radial distance to the supports.

R_ϕ - The meridional radius of curvature.

s - The arc length.

\bar{s} - The nondimensional arc length.

S - A point on the load-deflection curve or surface at which the effects of support wrinkling initiate.

T - A point on the load-deflection curve or surface at which the load is a local minimum.

U - A point on the load-deflection curve or surface which represents the end of the load-deflection curve or surface.

V - The volume of the hydrostatic load at any loading stage.

\bar{V} - The nondimensional volume of the hydrostatic load.

\bar{V}_A - The nondimensional volume of the hydrostatic load at point A.

V_L - The volume of the hydrostatic load at point L.
 \bar{V}_L - The nondimensional volume of the hydrostatic load at point L.
 W - The total liquid load.
 \bar{W} - The total nondimensional liquid load.
 β_o - The central half angle.
 $\hat{\beta}_o$ - The central half angle due to support wrinkling.
 γ - The density.
 $\bar{\gamma}$ - The nondimensional density.
 δ - The apex deflection.
 $\bar{\delta}$ - The nondimensional apex deflection.
 $\hat{\delta}_o$ - The nondimensional apex deflection due to support wrinkling.
 $\bar{\delta}_{ULT}$ - The nondimensional apex deflection of the ultimate point.
 ϕ - The meridional angle measured from the vertical to the normal passing through a point on the membrane.
 ϕ_A - The meridional angle to point A.
 ϕ_B - The meridional angle to point B.
 ϕ_E - The meridional angle to point E.
 $\phi_{E_{HC}}$ - The meridional angle to the end of the load wrinkling domain for a hydrostatic loading's C point.
 $\phi_{E_{HG}}$ - The meridional angle to the end of the load wrinkling domain for a hydrostatic loading's G point.
 $\phi_{E_{PG}}$ - The meridional angle to the end of the load wrinkling domain for a concentrated axisymmetric apex loading's G point.
 ϕ_L - The meridional angle to point L.

Chapter 1

INTRODUCTION

1.1 Introduction

In recent years, the use of polyvinyl pneumatic structures has gained popularity. The acceptance of these types of structures can be attributed to reasons such as: improved look and quality of the polyvinyl fabric; ease of construction, ease of assembly of the structures at a site; the portability of the structure; and its low cost compared to conventional structures. In most cities they can be spotted as sports facilities, green houses, storage facilities, and as temporary structures for equipment or people at special events.

Although inflatable structures are in use today, the problems associated with the loading characteristics have not been completely addressed. The applications stated above result in the need for various loads to be attached to the structure such as lighting, speaker systems, or watering systems. In most cases these loads are attached symmetrically around the apex of the structure. These concentrated loads will cause a depression to form at the apex which in turn allows rain, snow, or ice to accumulate. This type of loading scenario can lead to the failure of the structure.

The most popular configurations for pneumatic membrane structures are the spherical and cylindrical shapes. This thesis will address the load-deflection characteristics of spherical inflatable structures.

1.2 Historical Development

The identification of the need for research in this area was first done by Dr. Peter Glockner in the seventies. Although research was conducted on both spherical and cylindrical pneumatic structures, only the historical work done on the spherical inflatables will be discussed here. The profiles of the spherical inflatables investigated varied from shallow to very lofty profiles. In the literature the profile of the structure is defined by the central half angle which, for a very lofty structure, nears 0° . Over the years, the research developed into three distinct areas: combined hydrostatic and concentrated axisymmetric apex loads, concentrated axisymmetric apex loads, and hydrostatic loads. Each will be discussed in turn.

The problem of determining the load-deflection and stability characteristics of low profiled spherical membranes subjected to a combined hydrostatic and concentrated axisymmetric apex load was first examined by Malcolm and Glockner [20] in 1981. In their research, they derived the differential equations for a membrane of revolution with a critical concentrated axisymmetric apex load such that the resulting depression was completely filled with liquid. The results determined the critical central weight for various densities, internal pressures, and radii of the structure. Their efforts also included experimental work for comparison with theoretical predictions.

Preliminary work was also done by Lukasiewicz and Glockner [17, 18, 19] in 1983 and Szyszkowski and Glockner [14] in 1984. Lukasiewicz and Glockner established critical loads for a membrane with a completely filled depression utilizing an energy method. Szyszkowski and Glockner, on the other hand, established load-deflection curves for membranes under combined hydrostatic and concentrated axisymmetric

apex loading by numerically solving the governing differential equations. The curves obtained determined the axisymmetric concentrated apex load which resulted in the depression being completely filled with liquid.

The research on concentrated axisymmetric apex loads began with Szyszkowski and Glockner [25] in 1983. The model included an inextensible spherical membrane which had a vertical concentrated load hung at the apex. The loading caused a wrinkled domain to form around the apex. They developed a set of differential equations which satisfied the equations of equilibrium and the Gauss-Codazzi relation for the wrinkled region of the membrane. The equations were solved numerically to determine points on the structure's load-deflection curve. Load-deflection curves were established for a range of profiles, not including very lofty structures. The results included snap-through and ultimate behavior of the structures.

In 1988, Dacko and Glockner [6] took another look at the problem. Their research extended the earlier work and included the full range of geometries, from very flat to very high profile structures. Their solution technique resulted in convergence for low values of the central half angle, down to 20° . They also investigated the effect of membrane extensibility and found that the load-deflection curves were within a few percent of those for the inextensible case. In addition, they admitted in their analysis the phenomenon of support wrinkling which occurs in very lofty structures. In an attempt to determine the load-deflection curves for central half angles below 20° , Dacko and Glockner [7], in 1989, reformulated the differential equations in terms of the arc length. This resulted in load-deflection curves for central half angles down to 5° .

The final development in the research on concentrated axisymmetric apex loads

for spherical membranes was also conducted by Dacko and Glockner [8, 9] in 1989. This work concentrated on the effects of support conditions on the load-deflection behavior of spherical membranes. Supports examined included stove-pipe-like supports and a horizontal support surface.

In 1983 Szyszkowski and Glockner [26] also began research on spherical membranes subjected to hydrostatic loading. They developed the governing differential equations for an inextensible membrane of revolution with an axisymmetric depression at the apex which was completely or partially filled with liquid. Their results included a curve representing membranes with a completely filled depression for various nondimensional densities. It also included the stable domains of the load-deflection curve for a nondimensional density of 4.55. The unstable portion of the load-deflection curve, however, was not obtained in its entirety due to convergence difficulties.

In the nineties, Stanuszek and Glockner [23, 24] refined the numerical method used to solve the differential equations for the hydrostatic loading case. This allowed them to determine the unstable portion of the load-deflection curve. Their research also incorporated support wrinkling of the structure. The results included load-deflection curves for nondimensional densities ranging from 2.78 to 30.0 and for central half angles down to 5° . Presently research continues on this topic.

1.3 Summary

The following material will be covered in the remainder of this thesis. In Chapter 2 the notation, theory, and results for a spherical membrane with concentrated ax-

isymmetric apex loading will be briefly discussed. Chapter 3 will discuss the theory and results for a spherical membrane under hydrostatic loads while Chapter 4 provides a detailed analysis of the theory for the combined hydrostatic and concentrated axisymmetric apex loading of a spherical membrane. The chapter will also present load-deflection surfaces for three nondimensional densities and three central half angles. Finally, this thesis concludes with a summary of the results and suggestions for further research in Chapter 5.

Chapter 2

CONCENTRATED AXISYMMETRIC APEX LOADING

2.1 Introduction

Chapter 2 provides a brief summary of the background, theory and results pertaining to this thesis on spherical membranes under concentrated axisymmetric apex loading. This chapter's importance lies in the fact that it provides most of the definitions, assumptions, and procedures applicable to all loading conditions discussed in the thesis. For detailed information on this loading condition see Szyszkowski and Glockner [25] and Dacko and Glockner [6, 7, 8, 9].

2.2 Assumptions and Definitions

Figure 2.1 shows a spherical membrane of radius R_o subjected to an internal overpressure, p_o . There is no other load applied to the structure. The membrane is attached to the ground through hinged supports. In the event of support wrinkling, it will be assumed that the wrinkled membrane around the supports lays itself flat on the adjacent ground. This type of support is termed a horizontal support and is discussed in detail in Dacko and Glockner [6]. The internal overpressure is assumed to be constant even though the internal volume of the spherical membrane may change during loading. This can only be justified if it is further assumed that

an infinite reservoir exists below the supports, or that a pump system is in place which maintains a constant internal pressure.

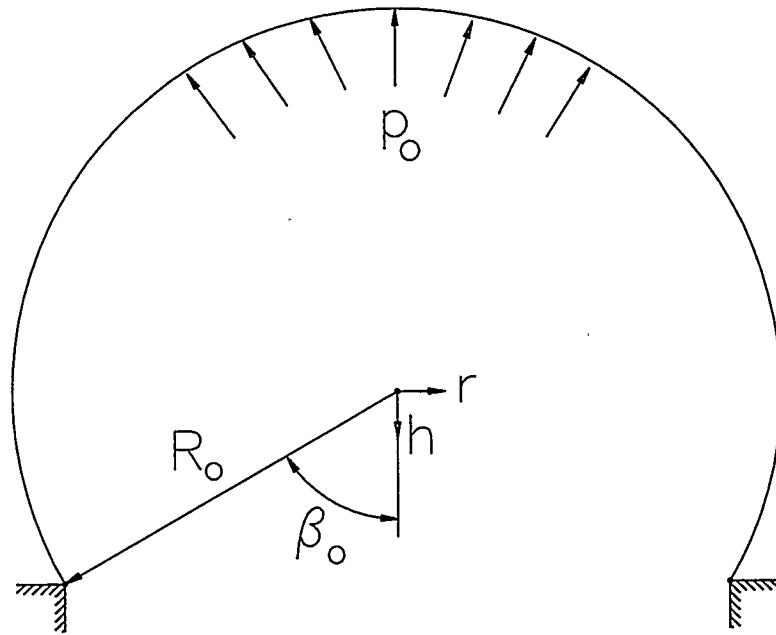


Figure 2.1: Spherical Membrane Subjected to Internal Overpressure

The loftiness of the spherical structure is defined by the central half angle, β_0 . A shallow spherical membrane, which typifies most realistic structures, has a central half angle between 120° and 180° , while a very lofty structure has a central half angle between 0° and 60° .

The properties of the membrane itself were assumed to be as follows: self weight is negligible; zero flexural rigidity; suitably small thickness allowing stresses to be defined on the “mean” surface; and inextensible. The last assumption was relaxed by Dacko and Glockner [6] and the membrane’s extensibility was found to have little effect on the overall large deflection and stability behavior of such structures. This

assumption eliminates the need to define strains and constitutive relations for the membrane, thus greatly simplifying the model.

Finally, when the membrane structure is loaded, it is assumed that the region around the apex undergoes wrinkling. The definition of the load wrinkling region assumed in the papers and this thesis is that the circumferential stress resultant, N_θ , vanishes. Furthermore, it is assumed that the wrinkling is uniform and that the wrinkled domain is approximated by a surface with a “mean” radius.

2.3 Physical Arrangement

Figure 2.2 shows a spherical membrane subjected to a concentrated axisymmetric load, P , applied at the apex which is labeled as point A. The angle between the tangent to the deformed membrane and the vertical is defined by ϕ_A . Point E defines the end of the wrinkled domain which started at point A. The angle between the vertical and the tangent to the deformed membrane at point E, is defined by ϕ_E . The deflection undergone by the concentrated axisymmetric load, P , is defined as δ , representing the vertical movement of the apex.

2.4 Theory

2.4.1 General Formulation

In this thesis, all equations and results are stated in nondimensional terms. This allows greater freedom for the designer in that the engineer is not limited to a few specific values for the internal pressure or the sphere’s radius. The dimensionless variables for this chapter are:

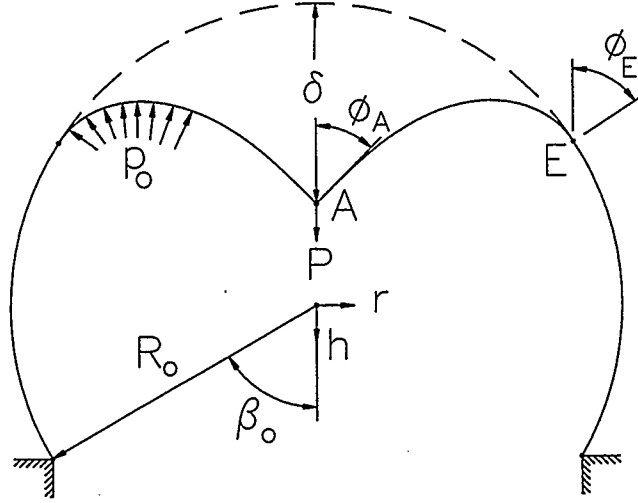


Figure 2.2: Spherical Membrane Subjected to Concentrated Axisymmetric Apex Load

$$\bar{r} = \frac{r}{R_0} \quad (2.1)$$

$$\bar{h} = \frac{h}{R_0} \quad (2.2)$$

$$\bar{p} = \frac{p}{p_0} \quad (2.3)$$

$$\bar{Q} = \frac{Q}{\pi R_0^2 p_0} \quad (2.4)$$

$$\bar{P} = \frac{P}{\pi R_0^2 p_0} \quad (2.5)$$

$$\bar{\delta} = \frac{\delta}{R_o} \quad (2.6)$$

$$\bar{s} = \frac{s}{R_o} \quad (2.7)$$

where \bar{r} , \bar{h} , \bar{p} , \bar{Q} , \bar{P} , $\bar{\delta}$, and \bar{s} are the nondimensional radial coordinate referenced to the center of the sphere, nondimensional height coordinate referenced to the center of the sphere, nondimensional net pressure, nondimensional total vertical force, nondimensional concentrated axisymmetric apex load, nondimensional vertical deflection, and nondimensional arc length, respectively.

Based on the equations of equilibrium and the Gauss-Codazzi relation for a membrane of revolution, Szyszkowski and Glockner [25] developed three first order differential equations which govern the behavior of the spherical membrane with a concentrated axisymmetric apex load. The differential equations were rewritten in terms of the arc length by Dacko and Glockner [7] as the earlier formulation resulted in convergence difficulties for very lofty structures.

In the load wrinkling region, the circumferential stress resultant, N_θ , vanishes and the two nonzero equations of equilibrium for a membrane of revolution become:

$$\frac{d}{d\phi}(rN_\phi) = 0 \quad (2.8)$$

$$\frac{N_\phi}{R_\phi} = p \quad (2.9)$$

where N_ϕ is the meridional stress resultant, ϕ is the meridional angle, and R_ϕ is the meridional radius of curvature. When Q , the total vertical force exerted on the

membrane, is introduced into equations 2.8 and 2.9 the meridional stress resultant N_ϕ can be eliminated to give:

$$\frac{Q}{2\pi r \sin \phi} = R_\phi p \quad (2.10)$$

$$Q = 2\pi \int_0^\phi p R_\phi r \cos \phi d\phi \quad (2.11)$$

Using the single nontrivial Gauss-Codazzi equation for a membrane of revolution

$$R_\phi = \frac{1}{\cos \phi} \frac{dr}{d\phi} \quad (2.12)$$

to eliminate R_ϕ from Equations 2.10 and 2.11, the resulting two differential equations are written as:

$$\frac{dr}{d\phi} = \frac{Q}{2\pi r p \tan \phi} \quad (2.13)$$

$$\frac{dQ}{dr} = 2\pi r p \quad (2.14)$$

Finally, the shape of the wrinkled membrane, when defined in terms of the orthogonal coordinates r and h , is given by:

$$\frac{dh}{dr} = \tan \phi \quad (2.15)$$

Equations 2.13, 2.14, and 2.15 are the three first order differential equations derived by Szyszkowski and Glockner [25]. The equations were derived without considering the loading state. As such, the differential equations are valid for all loading cases discussed in this thesis.

The nondimensional form of differential equations 2.13, 2.14, and 2.15 in terms of the radius are:

$$\frac{d\phi}{d\bar{r}} = \frac{2\bar{r} \tan \phi}{\bar{Q}} \quad (2.16)$$

$$\frac{d\bar{Q}}{d\bar{r}} = 2\bar{r} \quad (2.17)$$

$$\frac{d\bar{h}}{d\bar{r}} = \tan \phi \quad (2.18)$$

In the case of a concentrated axisymmetric apex load, the net pressure p is equal to the internal pressure, p_o , which is constant. By integrating Equation 2.17 and using the boundary condition $\bar{Q}(\bar{r} = 0) = -\bar{P}$, the following explicit equation can be determined for \bar{Q} :

$$\bar{Q} = \bar{r}^2 - \bar{P} \quad (2.19)$$

When Equation 2.19 is substituted into differential equation 2.16, the system is reduced to the following two differential equations:

$$\frac{d\phi}{d\bar{r}} = \frac{2\bar{r} \tan \phi}{\bar{r}^2 - \bar{P}} \quad (2.20)$$

$$\frac{d\bar{h}}{d\bar{r}} = \tan \phi \quad (2.21)$$

For computational accuracy, it is advantageous to rewrite differential equations 2.20 and 2.21 in terms of the nondimensional arc length \bar{s} . The resulting differential equations are:

$$\frac{d\phi}{ds} = \frac{2\bar{r} \sin \phi}{\bar{r}^2 - P} \quad (2.22)$$

$$\frac{d\bar{h}}{ds} = \sin \phi \quad (2.23)$$

In transforming the differential equations, the relation

$$\frac{d\bar{r}}{ds} = \cos \phi \quad (2.24)$$

has been used.

As well as determining the behavior of the spherical membrane, Equations 2.22, 2.23, and 2.24 must also satisfy the boundary conditions at points A and E. If the wrinkled domain has not reached the supports yet, the boundary conditions at point A are:

$$\left. \begin{aligned} \phi &= -\phi_A \\ \bar{h} &= 0 \\ \bar{r} &= 0 \end{aligned} \right\} \quad (2.25)$$

while the boundary conditions at point E are:

$$\left. \begin{aligned} \phi &= \phi_E \\ \bar{h} &= \bar{h}_E \\ \bar{r} &= \sin \phi_E \end{aligned} \right\} \quad (2.26)$$

It can be seen that, with the height of point E, \bar{h}_E , and angles ϕ_A and ϕ_E , there are three unknown quantities. The problem can be reduced to two unknowns because

differential equation 2.20 was solved analytically by Szyszkowski and Glockner [25].

The analytical solution is:

$$\bar{r}(\phi) = \sqrt{\bar{P} - J \sin \phi} \quad (2.27)$$

where J is a constant of integration. To eliminate J , the boundary condition $\phi = -\phi_A$ at $\bar{r} = 0$ was used. The resulting equation is:

$$\bar{r}(\phi) = \sqrt{\bar{P} \left(1 + \frac{\sin \phi}{\sin \phi_A} \right)} \quad (2.28)$$

Now a relationship can be established between ϕ_A and ϕ_E by substituting the boundary condition $\phi = \phi_E$ at $\bar{r} = \sin \phi_E$ into Equation 2.28. The result is:

$$\sin \phi_A = \frac{\bar{P} \sin \phi_E}{\sin^2 \phi_E - \bar{P}} \quad (2.29)$$

The boundary value problem now has two unknowns, \bar{h}_E and ϕ_E . However, only one differential equation remains. The second independent equation required to solve the boundary value problem comes from the inextensibility condition, namely:

$$\bar{s} = \phi_E \quad (2.30)$$

Equations 2.19 through 2.30 define the theory for the membrane of revolution under a concentrated axisymmetric apex load when the wrinkled domain has not yet reached the supports. Once the wrinkled domain reaches the supports, the boundary conditions at point E in Equation 2.26 no longer apply. They become:

$$\left. \begin{aligned} \phi &= \phi_E \\ \bar{h} &= \bar{h}_E \\ \bar{r} &= \sin \beta_o \end{aligned} \right\} \quad (2.31)$$

The new boundary conditions at point E require equations 2.29 and 2.30 to be rederived. When the boundary condition $\phi = \phi_E$ at $\bar{r} = \sin \beta_o$ is introduced into Equation 2.28, the relationship between ϕ_A and ϕ_E for a fully wrinkled membrane becomes:

$$\sin \phi_A = \frac{\bar{P} \sin \phi_E}{\sin^2 \beta_o - \bar{P}} \quad (2.32)$$

while the inextensibility condition for a fully wrinkled membrane requires:

$$\bar{s} = \pi - \beta_o \quad (2.33)$$

Once again, the boundary value problem has two unknowns and can be solved.

Finally, when the load-deflection curves are generated, the vertical deflection at the apex, $\bar{\delta}$, is given by:

$$\bar{\delta} = \bar{h}_E + 1 - \cos \phi_E \quad (2.34)$$

when the wrinkled domain has not yet reached the supports, and by:

$$\bar{\delta} = \bar{h}_E + 1 - \cos \beta_o \quad (2.35)$$

when the wrinkled domain has reached the supports. Refer to Szyszkowski and Glockner [25] or Dacko and Glockner [6, 7, 8, 9] for further information concerning the theory related to concentrated axisymmetric apex loading of spherical membranes.

2.4.2 Support Wrinkling

For very lofty structures, the phenomenon of support wrinkling becomes a concern. When the forces at the supports are examined, it can be seen that:

$$\pi r_s^2 p_o - P = 2\pi r_s (N_\phi \sin \beta_o) \quad (2.36)$$

where r_s is the radius of the support which is given by $R_o \sin \beta_o$. When loading of the structure begins $P < \pi r_s^2 p_o$ and the meridional stress resultant at the supports is in tension. However, it is possible for N_ϕ at the support to vanish if:

$$P_L = \pi r_s^2 p_o \quad (2.37)$$

or:

$$\bar{P}_L = \sin^2 \beta_o \quad (2.38)$$

where \bar{P}_L is the nondimensional concentrated axisymmetric apex load which initiates support wrinkling and results in lateral instability of the structure as a whole. Any additional loading will cause the wrinkled membrane at the support to collapse onto the horizontal support as shown in Figure 2.3. With the membrane laying on top of the horizontal support, a new central half angle, $\hat{\beta}_o$, exists. The value of $\hat{\beta}_o$ is given by:

$$\hat{\beta}_o = \sin^{-1} \sqrt{\bar{P}} \quad (2.39)$$

whenever $\bar{P} > \bar{P}_L$.

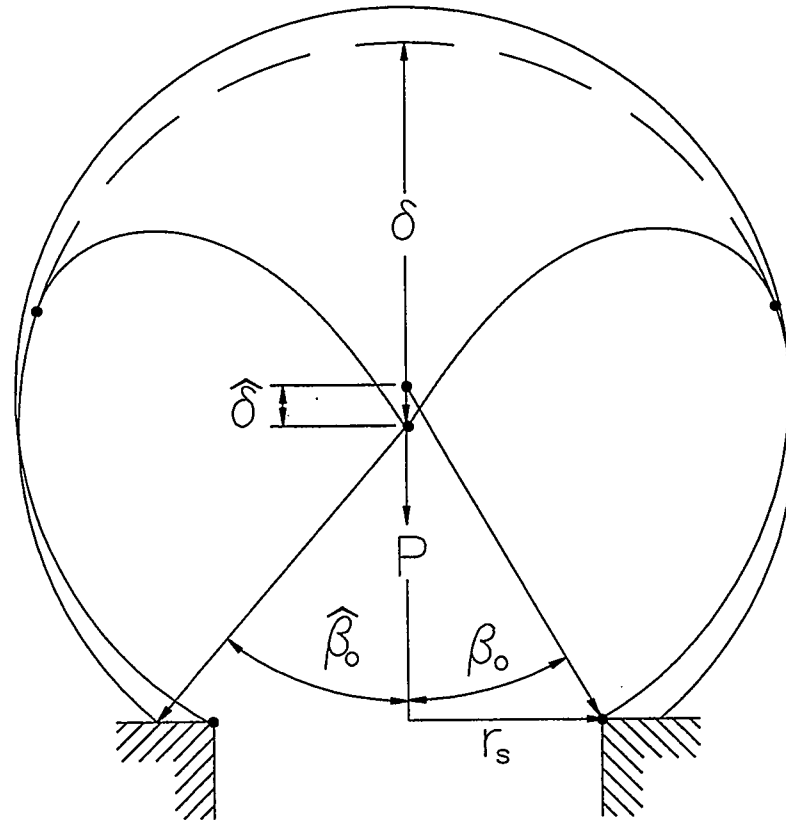


Figure 2.3: Membrane of Revolution with Support Wrinkling

As the support wrinkling produces an additional deflection, $\hat{\delta}$, of the apex, it must be added to the displacement produced by the loading to give the total deflection of the apex. The value of $\hat{\delta}$ is given by:

$$\hat{\delta} = (\cos\beta_0 - \cos\hat{\beta}_0) \quad (2.40)$$

2.5 Numerical Procedure

In this section the basics for the numerical procedure will be discussed. The approach used to solve the boundary value problem is termed a “shooting method”. The “shooting method” starts at one boundary and, using the differential equations, “shoots” to the second boundary. At that point, a test is carried out to see if the correct solution was found.

In the case of a spherical membrane under a concentrated axisymmetric apex load, the starting point for the “shooting method” is point A. Next, a Runge-Kutta fourth order method was used to solve the differential equations 2.22, 2.23, and 2.24 in successive steps until point E was reached. At this point, to ensure that the correct solution was obtained, the inextensibility condition, equation 2.30 or 2.33, was checked. If the difference between the actual nondimensional arc length and calculated nondimensional arc length was less than $1.0 * 10^{-8}$ then the solution was deemed to be correct. Otherwise new values were selected at point A and the entire procedure repeated.

2.6 Load-Deflection Characteristics

Once the numerical procedure is completed, a load-deflection curve can be generated. Figure 2.4 will be used to explain in detail the behavioral characteristics exhibited by a spherical membrane under axisymmetric apex loading. The load-deflection curve was generated for a central half angle of 45° .

The load-deflection curve begins at the origin, designated O on Figure 2.4. As the concentrated axisymmetric apex loading increases so too does the apex deflec-

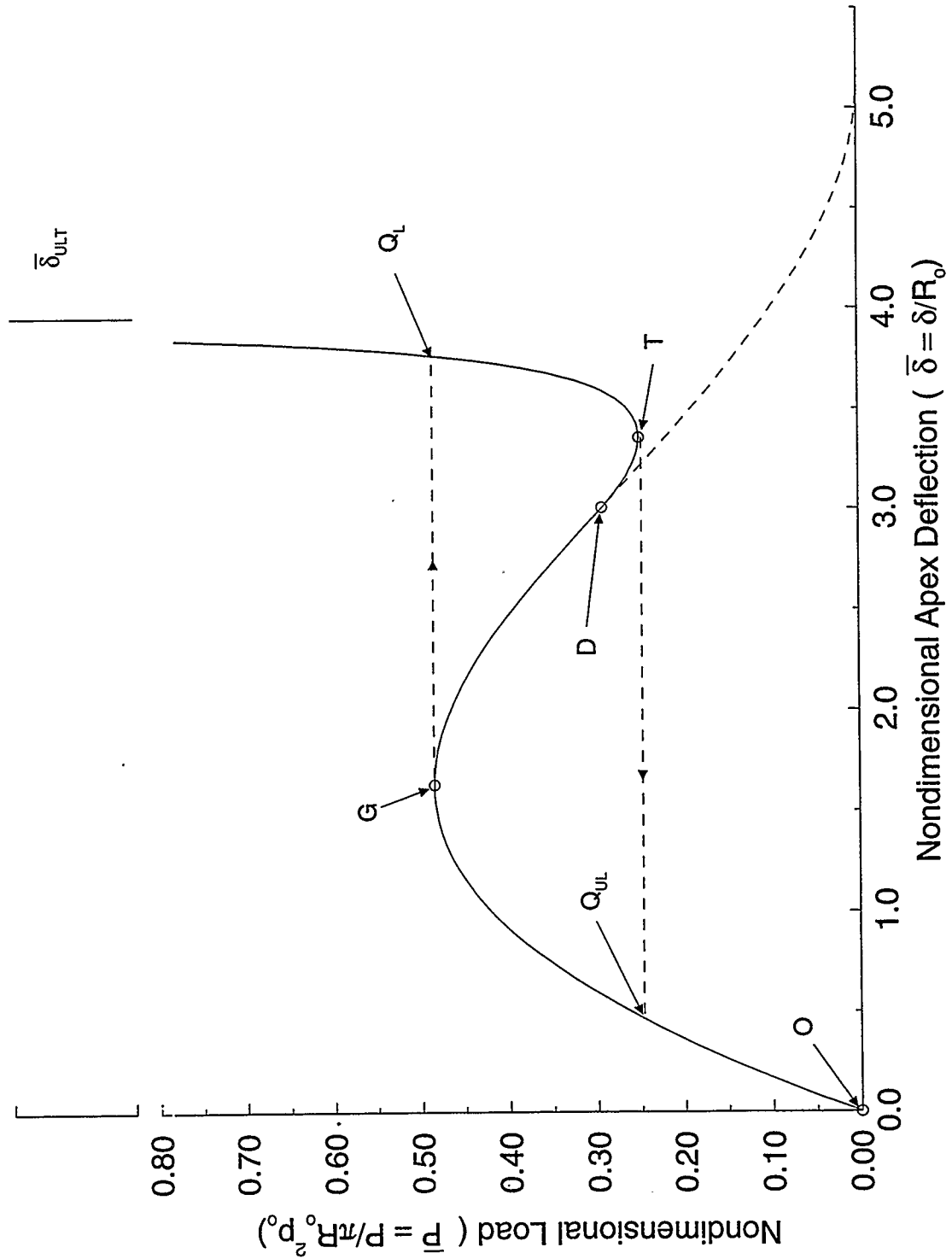


Figure 2.4: Typical Load-Deflection Curve for a Spherical Membrane Subjected to a Concentrated Axisymmetric Apex Load ($\beta_0 = 45^\circ$)

tion. This is the monotonically stiffening domain of the load-deflection curve. If the concentrated axisymmetric apex loading continues to increase, a state of neutral equilibrium will be attained at the point designated as G in Figure 2.4. This is the maximum concentrated axisymmetric apex load which can be applied to the spherical membrane before snap-through occurs. If the loading on the structure is increased slightly, snap-through occurs, with the structure moving to a new state of stable equilibrium designated by point Q_L in Figure 2.4.

However, if after reaching point G the concentrated axisymmetric apex load is decreased, the unstable portion of the load-deflection curve can be found. The unstable portion of the load-deflection curve is between points G and T on Figure 2.4. As it is unstable, a real structure would never achieve any of these equilibrium states.

The unstable portion of the load-deflection curve continues as the concentrated axisymmetric apex load is decreased until the wrinkled domain reaches the supports. Up to this point the load-deflection curve corresponded to the main load-deflection curve which is defined as the load-deflection curve for the full range of geometries for a spherical membrane subjected to concentrated axisymmetric apex loading. Once the wrinkling has reached the supports, the load-deflection curve begins to deviate from the main curve. This is designated point D in Figure 2.4 and the deviated portion of the load-deflection curve will be referred to as the deviated curve. Even though a departure from the main curve has occurred, the equilibrium is still unstable and the concentrated axisymmetric apex load continues to decrease. Eventually, the concentrated axisymmetric apex load decreases to the point at which a state of neutral equilibrium exists. This is designated by point T on Figure 2.4 and represents

the local minimum attained in the unloading process after reaching the G point.

From point T on, the concentrated axisymmetric apex loading increases and the equilibrium is once again stable. When snap-through occurs, stable equilibrium is reestablished on the stable portion of the deviated load-deflection curve. As the loading increases it would eventually lead to an ultimate point. This is defined as the ultimate load and ultimate deflection for the spherical structure. Due to the fact that the membrane is supported by the internal overpressure, the structure's walls will always have some curvature. Only in the limit, when the concentrated axisymmetric apex load reaches infinity, will the membrane walls become straight lines and attain the ultimate deflection. For this reason the load axis of Figure 2.4 has been broken. When the concentrated axisymmetric apex load reaches infinity, the ultimate deflection or $\bar{\delta}_{ULT}$, which is governed solely by the central half angle, is given by:

$$\bar{\delta}_{ULT} = \sqrt{(\pi - \beta_o)^2 - \sin^2(\pi - \beta_o)} + 1 - \cos(\pi - \beta_o) \quad (2.41)$$

where β_o is given in radians.

It should also be noted that the T point is also important when unloading from the ultimate point as snap-through can occur. As the concentrated axisymmetric apex load decreases below the concentrated axisymmetric apex load of the T point, snap-through occurs from point T to point Q_{UL} on the main curve as shown in Figure 2.4.

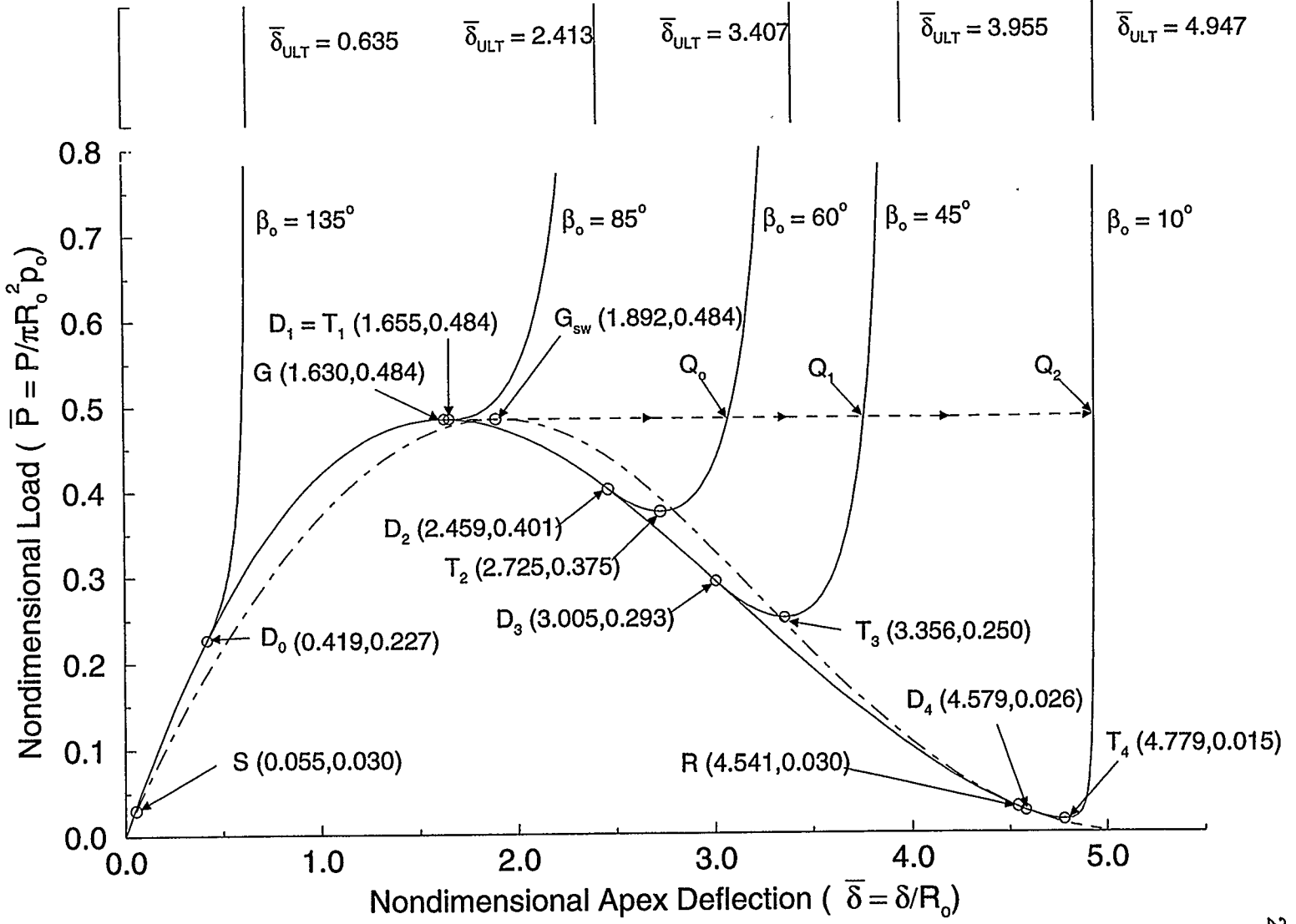
2.7 Results

Load-deflection curves for central half angles of 135° , 85° , 60° , 45° , and 10° are shown in Figure 2.5. The numerical procedure used was capable of determining equilibrium points on the main curve down to a central half angle of 5° . Below this point the main curve was extrapolated to $\beta_o = 0^\circ$ and is shown as a dashed line in Figure 2.5. The deflection at this point was $\bar{\delta} = 2 + \pi = 5.142$.

The effect of support wrinkling is also included in Figure 2.5. When a concentrated axisymmetric apex load is being applied to a spherical membrane with central half angles below 44.1° , support wrinkling will occur. This angle was obtained by substituting $\bar{P} = 0.484$ into Equation 2.39. As can be seen from the figure, only the load-deflection curve for $\beta_o = 10^\circ$ is affected. Its load-deflection curve, when support wrinkling is taken into account, is indicated as the dashed-dot curve. The effect of the additional deflection is readily apparent. The points from which the support wrinkling load-deflection curve deviates from the main load deflection curve and returns to it are indicated by points S and R, respectively. It can be seen that the curve rejoins the main load-deflection curve prior to reaching point D. One final point is that the regions of support wrinkling and load wrinkling around the apex never intersect one another.

Of special note in Figure 2.5 is the effect of the central half angle β_o on the load-deflection curves. For central half angles of 85.85° or greater, only monotonically stiffening behavior is observed. The value of point G is also of special note. The maximum concentrated axisymmetric apex load which can be applied to a spherical membrane with no snap-through behavior is $\bar{P} = 0.484$. If the designer is concerned

Figure 2.5: Load-Deflection Curves for a Spherical Membrane Subjected to a Concentrated Axisymmetric Apex Loading with Support Wrinkling



with preventing snap-through of the structure, two possibilities exist. If the central half angle of the structure is greater than 85.85° there is no concern as only monotonically stiffening behavior exists. However, if the central half angle is less than 85.85° , the designer must ensure that the nondimensional concentrated axisymmetric apex load used does not exceed 0.484. Finally, the calculated values of all G,D, and T points on Figure 2.5 are in agreement with those published by Dacko and Glockner [6] in 1987.

Chapter 3

HYDROSTATIC LOADING

3.1 Introduction

This chapter will present the set up, theory, and results pertaining to a spherical membrane subjected to axisymmetric hydrostatic loading. The theory was taken from [26] where it was first derived.

3.2 Physical Arrangement

In this thesis, hydrostatic loads will be restricted to natural substances such as rain water and dry snow pellets which will pond in the membrane's depression rather than deposit as piles. The depression in which the ponding medium accumulates is assumed to be caused by an imperfection in the membrane or by a tie down which may become slack once the hydrostatic load begins to accumulate.

Figure reffig5 shows the basic layout of a spherical membrane subjected to an axisymmetric hydrostatic load. The ponding medium has a density, γ , and fills the depression to a height H_o . If the ponding medium's height, H_o , reaches the total depth of the depression, then any additional liquid will overflow without affecting the load or deflection of the membrane.

The apex of the membrane of revolution is defined as point O rather than point A in the figure. This is because point A specifically refers to the point on the mem-

brane where wrinkling begins. Between points O and A, the membrane takes the shape of an inverted sphere. The reason for this is that at point O a singularity exists at which the membrane is in a state of tension. As the circumferential stress resultant N_θ equals the meridional stress resultant N_ϕ , the region around point O cannot be wrinkled. It takes the distance between points O and A before the circumferential stress resultant N_θ vanishes. The shape of an inverted sphere results from the assumption of inextensibility of the membrane.

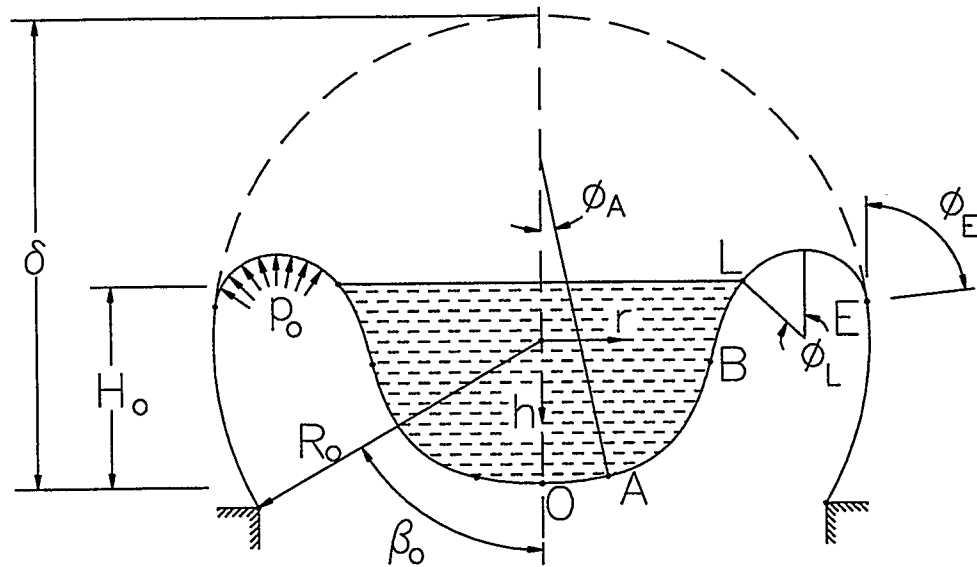


Figure 3.1: Spherical Membrane Subjected to Axisymmetric Hydrostatic Apex Loading

Point A is defined by angle ϕ_A which is measured from the vertical passing through point O. Once wrinkling initiates at point A, it continues to point B. At point B the net pressure, p , is equal to zero and a change in the membrane's curvature results. From point B, wrinkling continues to the pond-air interface which is designated as point L. Finally, wrinkling continues from point L until point E is reached which

indicates the boundary between wrinkled and unwrinkled membrane.

3.3 Theory

In addition to the nondimensional terms defined in Chapter 2, the following additional nondimensional terms are required when hydrostatic loading occurs:

$$\bar{\gamma} = \frac{\gamma R_o}{p_o} \quad (3.1)$$

$$\bar{V} = \frac{V}{\pi R_o^3} \quad (3.2)$$

where $\bar{\gamma}$ and \bar{V} represent the nondimensional density and the nondimensional liquid volume, respectively.

As differential equations 2.13, 2.14, and 2.15 were derived without reference to a loading condition, they are valid for hydrostatic loading and will be the starting point for this theory section. Unlike the concentrated axisymmetric apex loading, the net pressure p is no longer a constant. Instead, it is defined piece-wise. Between points A and L on the membrane the net pressure is given by:

$$p = p_o - \gamma(H_o + h) \quad (3.3)$$

and by:

$$p = p_o \quad (3.4)$$

between points L and E. By integrating Equations 3.3 and 3.4, a piece-wise definition of the total vertical force Q can also be obtained. Between points A and L, Q is:

$$Q = \pi r^2 [p_o - \gamma(H_o + h)] - \gamma V \quad (3.5)$$

while between point L and E it is:

$$Q = \pi r^2 p_o - \gamma V_L \quad (3.6)$$

where V_L is the total volume of the ponding medium and V , the volume at any particular loading stage, is given by:

$$V = V_A - k \int_{r_A}^r \pi r^2 \tan \phi dr \quad (3.7)$$

or

$$\frac{dV}{dr} = -k\pi r^2 \tan \phi \quad (3.8)$$

where

$$k = \begin{cases} -1 & \text{between points A and B} \\ 1 & \text{between points B and L} \end{cases} \quad (3.9)$$

When Equations 3.3, 3.5, and 3.8 are substituted into Equations 2.13, 2.14, and 2.15 and converted into nondimensional terms, the differential equations defining the behavior of the membrane between points A and L, in terms of arc length, are:

$$\frac{d\phi}{ds} = \frac{2\bar{r}\bar{p} \sin \phi}{\bar{r}^2\bar{p} - \bar{V}\gamma} \quad (3.10)$$

$$\frac{d\bar{V}}{ds} = -k\bar{r}^2 \sin \phi \quad (3.11)$$

$$\frac{d\bar{h}}{d\bar{s}} = k \sin \phi \quad (3.12)$$

$$\frac{d\bar{r}}{d\bar{s}} = \cos \phi \quad (3.13)$$

When equation 3.6 is substituted into Equations 2.16, 2.17, and 2.18, the nondimensional differential equations defining the membrane's behavior between points L and E become:

$$\frac{d\phi}{d\bar{s}} = \frac{2\bar{r} \sin \phi}{r^2 - \gamma \bar{V}_L} \quad (3.14)$$

$$\frac{d\bar{h}}{d\bar{s}} = \sin \phi \quad (3.15)$$

$$\frac{d\bar{r}}{d\bar{s}} = \cos \phi \quad (3.16)$$

As well as defining the behavior of the membrane of revolution, the differential equations must also satisfy the various boundary and continuity conditions. For a membrane of revolution under hydrostatic loading, it is particularly difficult as the boundary and continuity conditions exist at points A, B, L, and E and the differential equations are defined piece-wise. In an attempt to simplify the explanation, these conditions will be explained in the order required to solve the numerical method. In this case point A was the start and point E was the finish.

At point A, the membrane's behavior is defined by differential equations 3.10, 3.11, 3.12, and 3.13 and the boundary conditions are:

$$\left. \begin{aligned} \phi &= \phi_A \\ \bar{V} &= \bar{V}_A = (1 - \cos \phi_A)(2 - \cos \phi_A - \cos^2 \phi_A) \\ \bar{r} &= \sin \phi_A \\ \bar{h} &= \bar{H}_o - (1 - \cos \phi_A) \end{aligned} \right\} \quad (3.17)$$

As \bar{H}_o is an input variable, the only unknown at boundary A is ϕ_A for which an initial guess is made in the numerical method. Differential equations 3.10, 3.11, 3.12, and 3.13 are then used to increment from point A to point B. The numerical method realizes it has reached point B when the net pressure is zero. The test used was:

$$\bar{p} = 1 - \bar{\gamma}(\bar{H}_o + \bar{h}) = 0 \quad (3.18)$$

At point B the value of k in Equations 3.11 and 3.12 is changed to 1 and the angle ϕ_B is changed to $-\phi_B$. The numerical procedure is then continued from point B until point L is reached. As point L is where the liquid loading ceases, the test used by the numerical procedure was:

$$\bar{H}_o + \bar{h} = 0 \quad (3.19)$$

The conditions at point L are:

$$\left. \begin{aligned} \phi &= \phi_L \\ \bar{V} &= \bar{V}_L \\ \bar{r} &= \sin \phi_L \\ \bar{h} &= -\bar{H}_o \end{aligned} \right\} \quad (3.20)$$

all of which are numerically determined. At this point, differential equations 3.10, 3.11, 3.12, and 3.13 are no longer valid and differential equations 3.14, 3.15, and 3.16 are used. The numerical procedure would then continue until point E is reached which is defined by the following boundary conditions:

$$\left. \begin{aligned} \phi &= \phi_E \\ \bar{r} &= \sin \phi_E \\ \bar{h} &= \bar{h}_E \end{aligned} \right\} \quad (3.21)$$

Unfortunately, the value for ϕ_E is unknown. To obtain a value for ϕ_E , differential equation 3.14 was solved explicitly, as was done in Chapter 2, in the form:

$$\bar{r} = \sqrt{\gamma \bar{V}_L + J \sin \phi} \quad (3.22)$$

where J is an arbitrary constant of integration. When the boundary condition $\bar{r} = \sin \phi_E$ at $\phi = \phi_E$ is used, the value of J can be determined and Equation 3.22 becomes:

$$\bar{r} = \bar{r}_o \sqrt{1 + \left[\frac{\sin^2 \phi_E}{\bar{r}_o^2} - 1 \right] \frac{\sin \phi}{\sin \phi_E}} \quad (3.23)$$

where

$$\bar{r}_o = \sqrt{\bar{V}_L \gamma} \quad (3.24)$$

is the value of \bar{r} at $\phi = 0$. A relationship can be established between ϕ_L and ϕ_E if the boundary condition $\bar{r} = \sin \phi_L$ at $\phi = \phi_L$ is used in Equation 3.23. The relationship is:

$$\sin \phi_E = \frac{(\sin^2 \phi_L - \bar{r}_o^2) + \sqrt{(\sin^2 \phi_L - \bar{r}_o^2)^2 + 4\bar{r}_o^2}}{2} \quad (3.25)$$

Since \bar{V}_L and ϕ_L are known, the values for \bar{r}_o and ϕ_E can be obtained for Equations 3.24 and 3.25. The numerical procedure now continues to point E. To determine if the assumed value of ϕ_A was correct, the inextensibility condition:

$$\bar{s} = \phi_E \quad (3.26)$$

was used. If incorrect, a new guess is made for ϕ_A and the process is repeated.

However, once the wrinkling has reached the supports, Equations 3.23, 3.25, and 3.26 are no longer valid due to a change in the boundary conditions at point E. The new boundary conditions are:

$$\left. \begin{aligned} \phi &= \phi_E \\ \bar{r} &= \sin \beta_o \\ \bar{h} &= \bar{h}_E \end{aligned} \right\} \quad (3.27)$$

When Equation 3.23 is rederived with the boundary condition $\bar{r} = \sin \beta_o$ at $\phi = \phi_E$ the result is:

$$\bar{r} = \bar{r}_o \sqrt{1 + \left[\frac{\sin^2 \beta_o}{\bar{r}_o^2} - 1 \right] \frac{\sin \phi}{\sin \phi_E}} \quad (3.28)$$

Now when the boundary condition $\bar{r} = \sin \phi_L$ at $\phi = \phi_L$ is used, the relationship between ϕ_L and ϕ_E for a fully wrinkled membrane becomes:

$$\sin \phi_E = \frac{(\sin^2 \beta_o - \bar{r}_o^2)}{(\sin^2 \phi_L - \bar{r}_o^2)} \sin \phi_L \quad (3.29)$$

Once the numerical procedure reaches point E at the supports, the test to determine if ϕ_A was correct is given by the inextensibility condition:

$$\bar{s} = \pi - \beta_o \quad (3.30)$$

Support wrinkling also occurs when hydrostatic loads are applied to very lofty spherical membranes. The treatment of support wrinkling is identical to the theory discussed in Chapter 2 with the only difference being the substitution of the hydrostatic load, \bar{W} , for the concentrated axisymmetric apex load, \bar{P} . This concludes the theory relating to a spherical membrane subjected to hydrostatic loading in which the depression can be completely or partially filled with a ponding medium of nondimensional density $\bar{\gamma}$.

3.4 Load-Deflection Characteristics

Figure 3.2 shows a typical load-deflection curve for a spherical membrane subjected to hydrostatic loading. The nondimensional density and central half angle for this particular curve are 4.55 and 30° , respectively.

Unlike the concentrated axisymmetric apex load's load-deflection curve which starts at the origin, the load-deflection curve for hydrostatic loading begins at a point which will be designated as C. On Figure 3.2 it can be seen that point C lies on a dotted curve which will be termed the "takeoff" curve in this thesis. The "takeoff" curve is a compilation of all the C points for the entire range of nondimensional densities. The C point represents the load and apex deflection of a membrane the depression of which is completely filled with the ponding medium. It was not possible

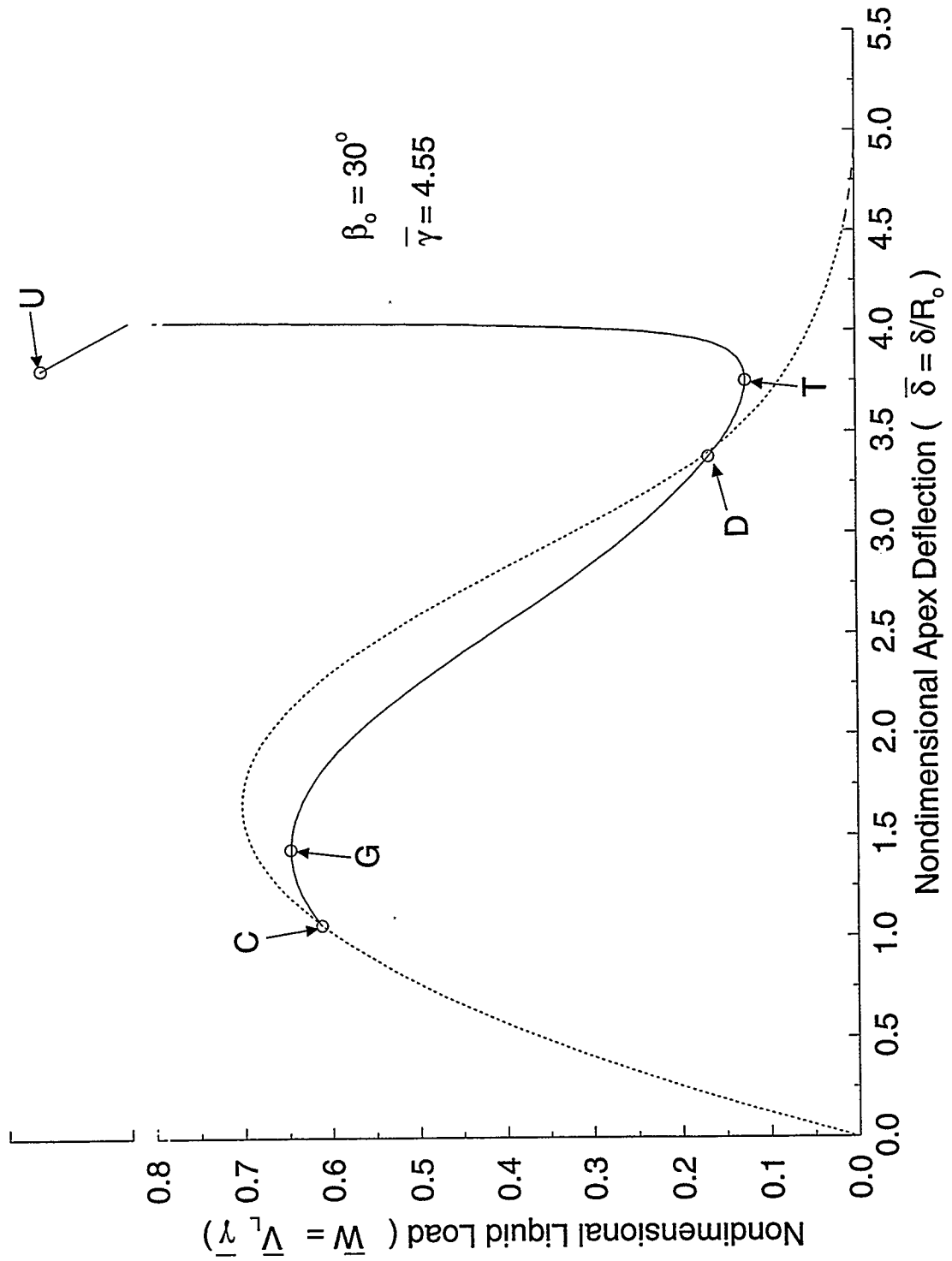


Figure 3.2: Load-Deflection Curve for a Spherical Membrane Subjected to Hydrostatic Axisymmetric Loading with no Support Wrinkling

to determine equilibrium configurations to the left of point C.

To the right of point C, the load-deflection curve exists with the depression partially filled by the ponding medium. This is accomplished by adding liquid without completely filling the depression. The load-deflection curve then progresses in a manner similar to the concentrated axisymmetric apex load's load-deflection curve. A G point is reached which is defined as the maximum load at which neutral equilibrium exists. An unstable portion of the load-deflection curve then exists until the entire membrane is in a wrinkled state. This is the definition of point D. The load-deflection curve continues to point T which is defined as the local minimum load at which neutral equilibrium exists.

After point T, the load-deflection curve comprises, once again, stable equilibrium configurations. This is the portion of the load-deflection curve which is reached when the structure incurs snap-through. At this point the similarities with the concentrated axisymmetric apex load's load-deflection curves cease. The first difference which can be seen on Figure 3.2 is that the maximum deflection of the structure does not occur at the ultimate point which is designated by U. The maximum deflection of the structure occurs where the slope of the load-deflection curve is vertical. The second difference is that the ultimate point has a finite deflection and load. This is because, at the ultimate point, the membrane's depression is once again completely filled with the ponding medium. Any additional liquid added to the depression flows off. As the structure does not attain the shape of an inverted sphere due to the internal pressure, the test used to determine whether the structure reached the ultimate point was to check if $\phi_L = \phi_E$. For if $\phi_L = \phi_E$ then the height of the ponding medium was at the same height as the supports.

3.5 Results

Before presenting the load-deflection curves, some new results which arose during the research will be discussed in detail.

3.5.1 Critical Nondimensional Density

During the research conducted on spherical membranes subjected to hydrostatic loads it was established that, for a particular nondimensional density, the structure's depression was completely filled with liquid while it is in a state of neutral equilibrium. In other words the G and C points coincide. This particular nondimensional density is termed the critical nondimensional density. The reason it is termed critical is that for a nondimensional density lower than the critical nondimensional density the load-deflection curve departs from the "takeoff" curve in a state of unstable equilibrium.

In previous research by Szyszkowski and Glockner [26] and Stanuszek and Glockner [23, 24] it was established that the "takeoff" curve had a point at which the slope of the curve was horizontal. Furthermore, the nondimensional density corresponding to this point was established as $\bar{\gamma} = 2.86$ by Szyszkowski and Glockner [26] and was further refined by Stanuszek and Glockner [23] to be $\bar{\gamma} = 2.78$. It was assumed by these researchers that the slope of the actual load-deflection curve for this density was also zero and that a G point existed. Consequently, it was concluded that $\bar{\gamma} = 2.86$ (or 2.78) was the critical nondimensional density.

The previous researchers, however, had calculated load-deflection curves for nondimensional densities of $\bar{\gamma} = 4.55$ and for the nondimensional density corresponding

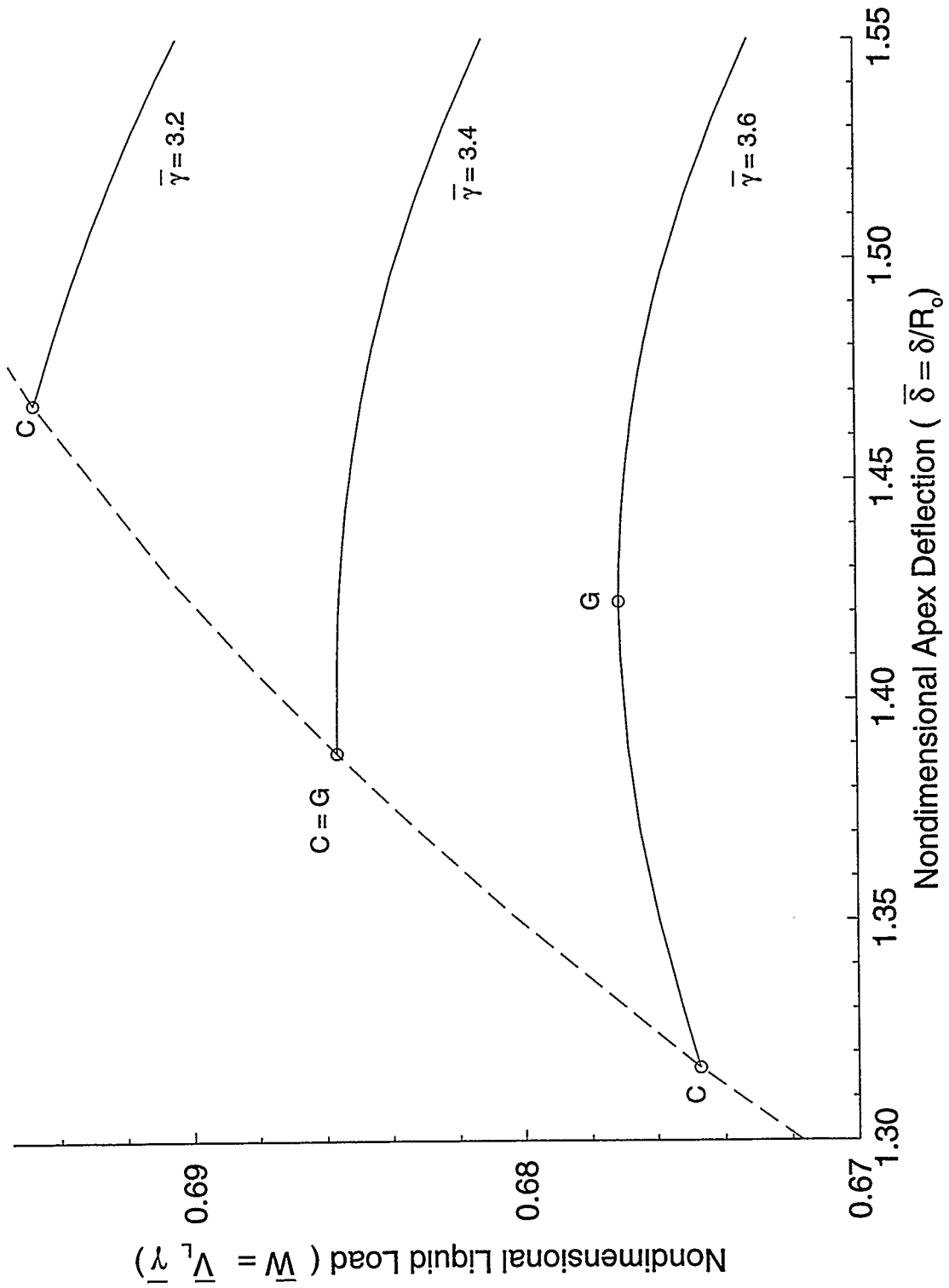
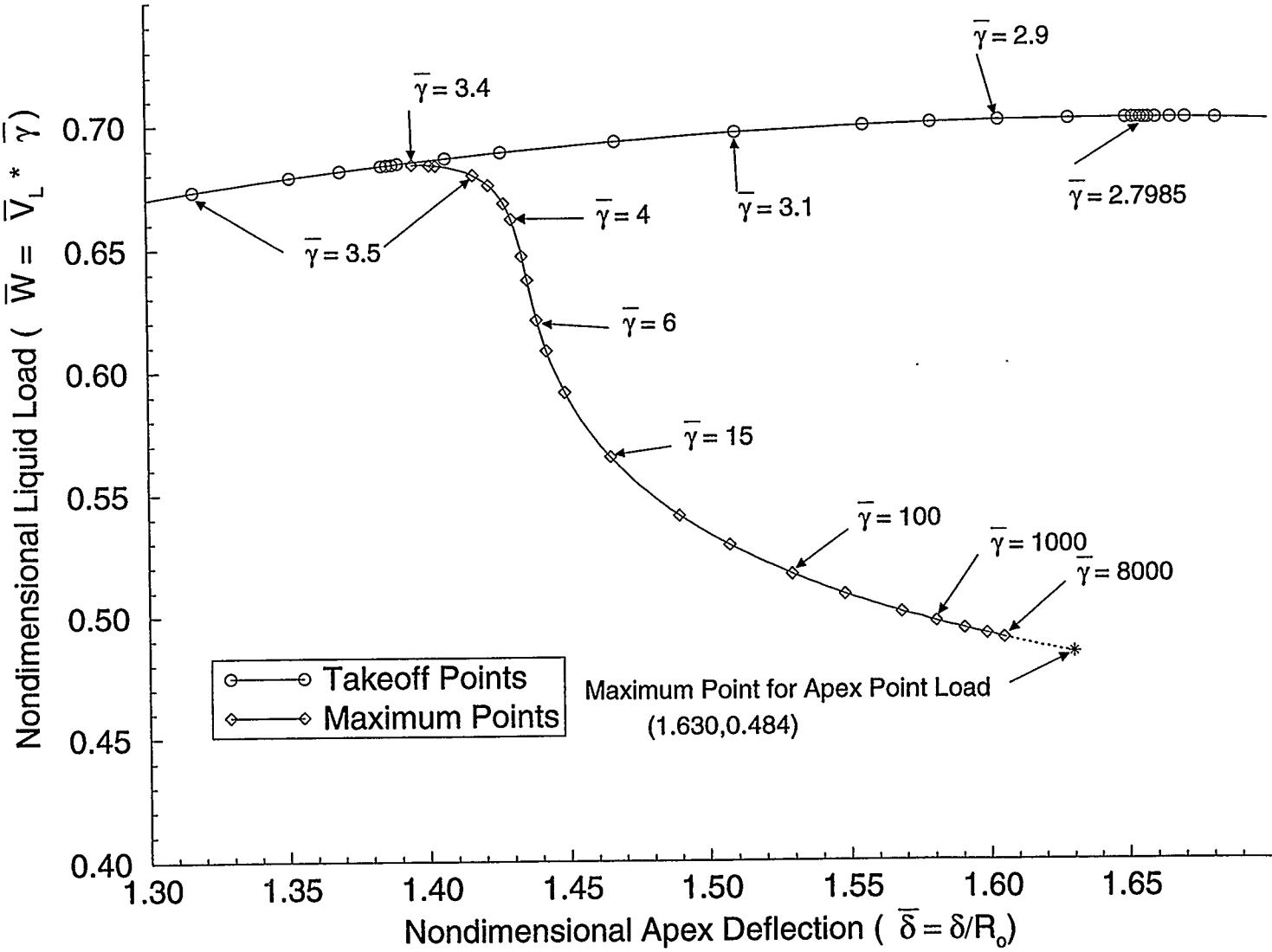


Figure 3.3: Effect of Nondimensional Density on the Existence of a Maximum Load

Figure 3.4: "Takeoff" and Maximum Points for Hydrostatic Loading of a Spherical Membrane



to the “takeoff” curve’s apex. In the course of the present research, load-deflection curves for nondimensional densities between $\bar{\gamma} = 2.78$ and $\bar{\gamma} = 4.55$ were calculated and Figure 3.3 was produced. It can be seen clearly that the load-deflection curve for $\bar{\gamma} = 3.6$ departs from the “takeoff” curve with a positive slope while the load-deflection curve for $\bar{\gamma} = 3.2$ leaves the “takeoff” curve with a negative slope. It was determined, in the course of the research, that the load-deflection curve for $\bar{\gamma} = 3.4$ was in neutral equilibrium when it departed from the “takeoff” curve and is the critical nondimensional density.

As this is a new development in the research and it conflicted with previous published values for the critical density it was deemed necessary to confirm the results. As load-deflection curves are continuous entities, it was felt that a curve composed of points representing states of neutral equilibrium would smoothly tend towards the lowest nondimensional density for which neutral equilibrium corresponded to a filled depression. Figure 3.4 which is comprised of two curves was produced as a result. The first curve is a portion of the “takeoff” curve which is a hypothetical curve composed of points representing equilibrium configurations for which the membrane’s depression is completely filled with liquid for various nondimensional densities. The second curve is a hypothetical curve composed of points representing neutral equilibrium configurations at G points for various nondimensional densities. As can be seen from the figure, the two curves are smooth and continuous and intersect at a nondimensional density of $\bar{\gamma} = 3.4$.

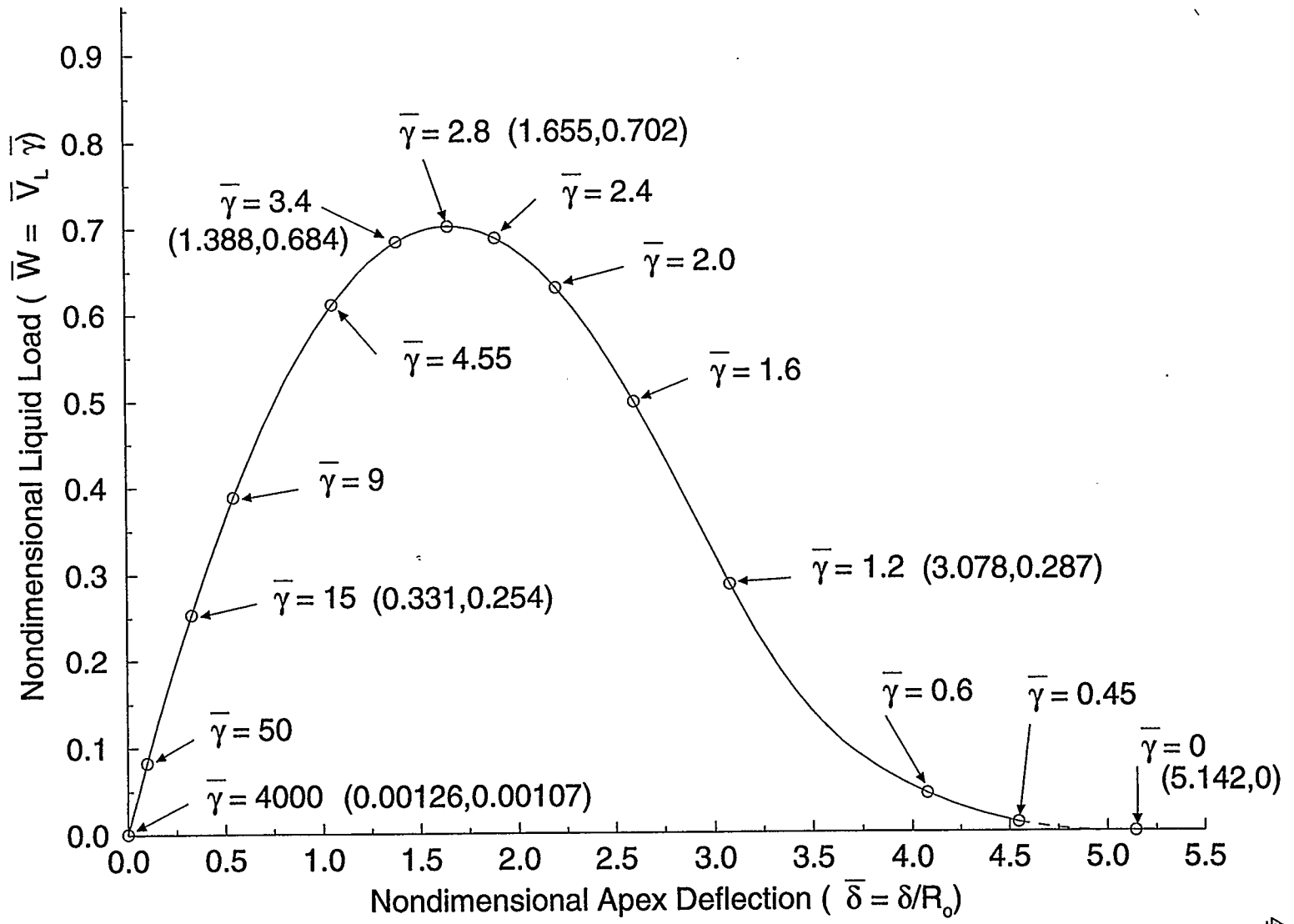
As a final proof to the value of the critical density, the slopes of the load-deflection curves as they left the “takeoff” curve were calculated. The calculations revealed that the slope for $\bar{\gamma} = 3.405$ was positive while the slope for $\bar{\gamma} = 3.395$ was negative. By

extrapolation of the slopes, the nondimensional density for which the slope was zero was confirmed to be $\bar{\gamma} = 3.400$. The “takeoff” curve is now broken into two distinct regions. The first region is for $\bar{\gamma} < 3.4$ in which the load-deflection curves departing from the “takeoff” curve start with configurations corresponding to a completely filled depression in unstable equilibrium. The other region is for $\bar{\gamma} > 3.4$ in which all load-deflection curves depart the “takeoff” curve with a configuration in stable equilibrium. The load-deflection curve for $\bar{\gamma} = 3.4$ leaves the “takeoff” curve with a membrane configuration in neutral equilibrium and represents the boundary between the two regions.

3.5.2 The “Takeoff” Curve

As was stated earlier, the “takeoff” curve is a collection of points for which the membrane is in a state of equilibrium with the depression completely filled with liquid. As such, it represents the collection of C points for the entire range of nondimensional densities. It was assumed in past research that all points on the “takeoff” curve were stable equilibrium configurations since the “takeoff” curve was never considered for values smaller than $\bar{\gamma} = 2.86$. Based on this assumption, past researchers logically concluded that the “takeoff” curve terminated at its apex. Their reasoning was that, if the “takeoff” curve existed past the apex, its slope would be negative and the C points would be in unstable equilibrium. At the time they felt this was impossible. However, as was stated in the prior section, points on the “takeoff” curve are in a state of unstable equilibrium for nondimensional densities below $\bar{\gamma} = 3.4$. This being the case, the current research for this thesis investigated the possibility of the existence of the “takeoff” curve past its apex.

Figure 3.5: The Complete "Takeoff" Curve for Hydrostatic Loading of a Spherical Membrane



It can be seen on Figure 3.4 that the nondimensional density which defines the apex of the “takeoff” curve is $\bar{\gamma} = 2.7985$. However, in determining the nondimensional density which corresponded to the apex, unstable equilibrium configurations with completely filled depressions were found for nondimensional densities below $\bar{\gamma} = 2.7985$. In fact, as can be seen on Figure 3.5, the “takeoff” curve for nondimensional densities was calculated down to $\bar{\gamma} = 0.45$. The remainder of the “takeoff” curve was then extrapolated down to $\bar{\gamma} = 0.0$ which is shown as a dashed line in the figure. As the “takeoff” curve exists down to $\bar{\gamma} = 0.0$, load-deflection curves also exist for nondimensional densities down to $\bar{\gamma} = 0.0$. In fact load-deflection curves for $\bar{\gamma} = 1.8$ will be presented later in this thesis.

3.5.3 Central Half Angle

Next, the effect of the central half angle on the load-deflection behavior of a spherical membrane will be discussed. Figure 3.6 shows a variety of load-deflection curves for various nondimensional densities when the central half angle of the structure is held constant at $\beta_o = 120^\circ$. As all the curves exhibit monotonically stiffening behavior, the only effect the nondimensional density appears to have on the load-deflection curves is their starting points on the “takeoff” curve. Special attention should be paid to the load-deflection curve for $\bar{\gamma} = 5.7961$ as its configuration when the depression is completely filled coincides with the membrane being completely wrinkled. In other words its C and D points are identical for this value of β_o . This does not mean, however, that load-deflection curves do not exist for nondimensional densities below $\bar{\gamma} = 5.7961$. Load deflection curves were generated down to a nondimensional density of $\bar{\gamma} = 4.8942$ but as they fall very close to the load-deflection curve for $\bar{\gamma} = 5.7961$

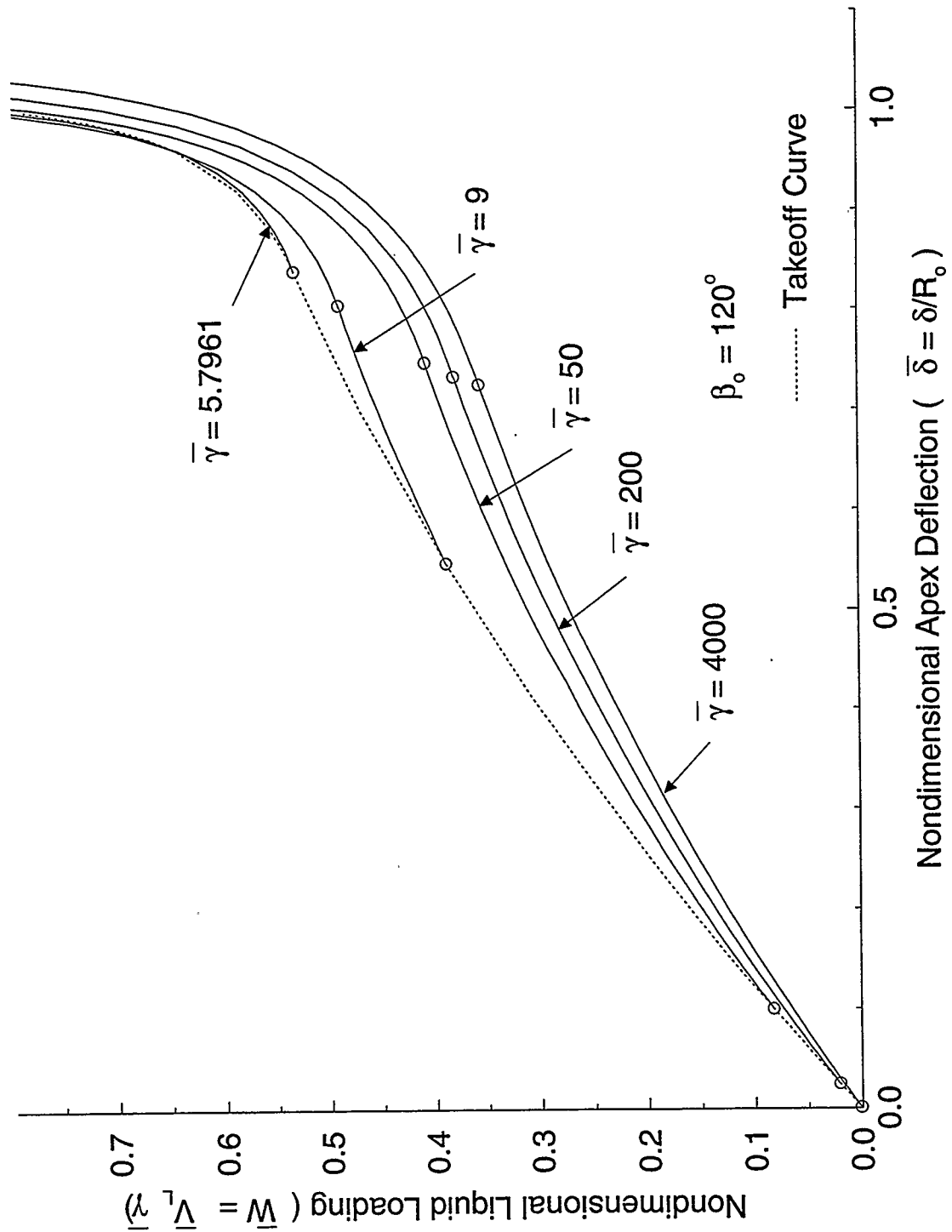


Figure 3.6: Effect of Nondimensional Density on the Load-Deflection Behavior of a Spherical Membrane Under Axisymmetric Hydrostatic Loading with no Support Wrinkling ($\beta_0 = 120^\circ$)

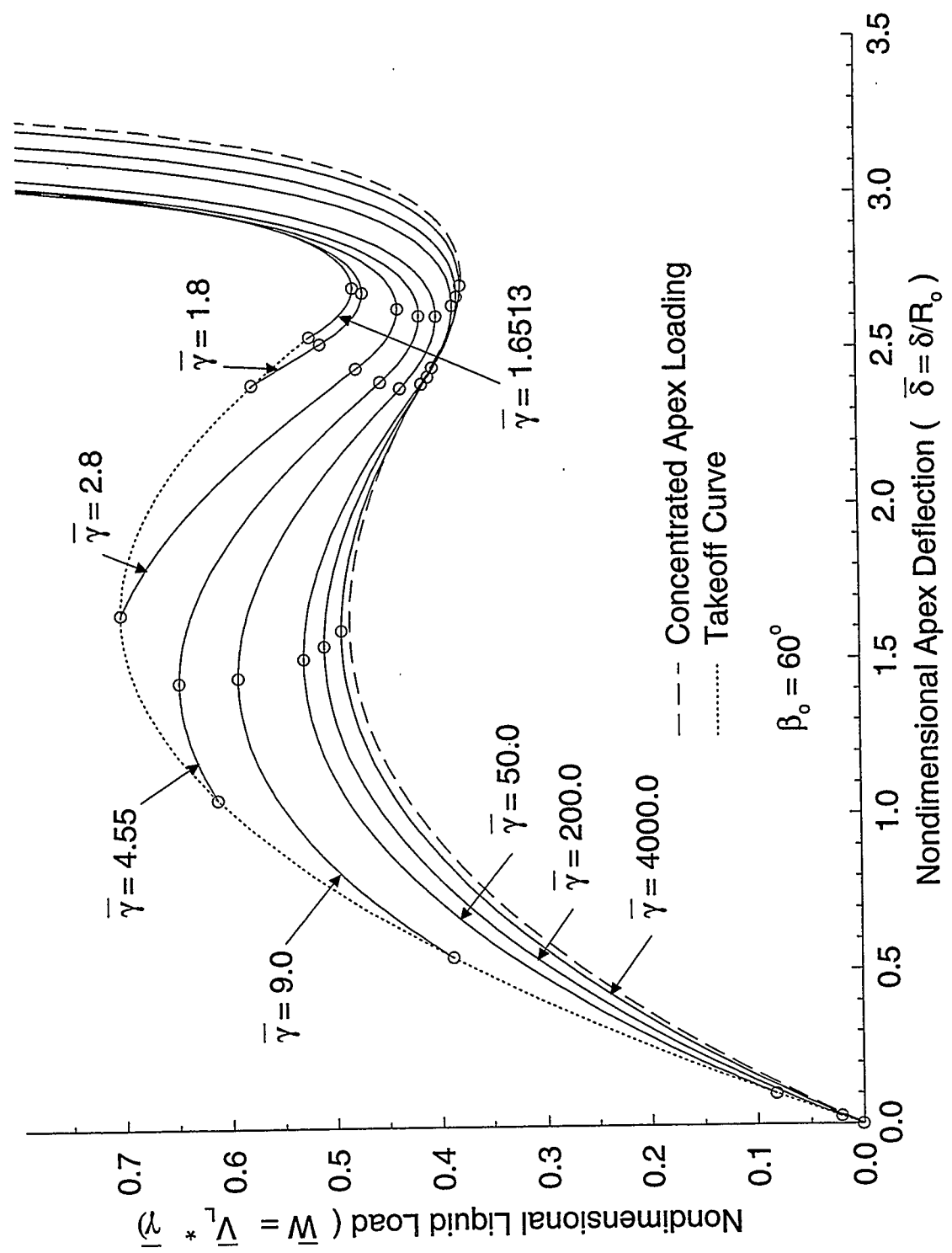


Figure 3.7: Effect of Nondimensional Density on the Load-Deflection Behavior of a Spherical Membrane Under Axisymmetric Hydrostatic Loading with no Support Wrinkling ($\beta_0 = 60^\circ$)

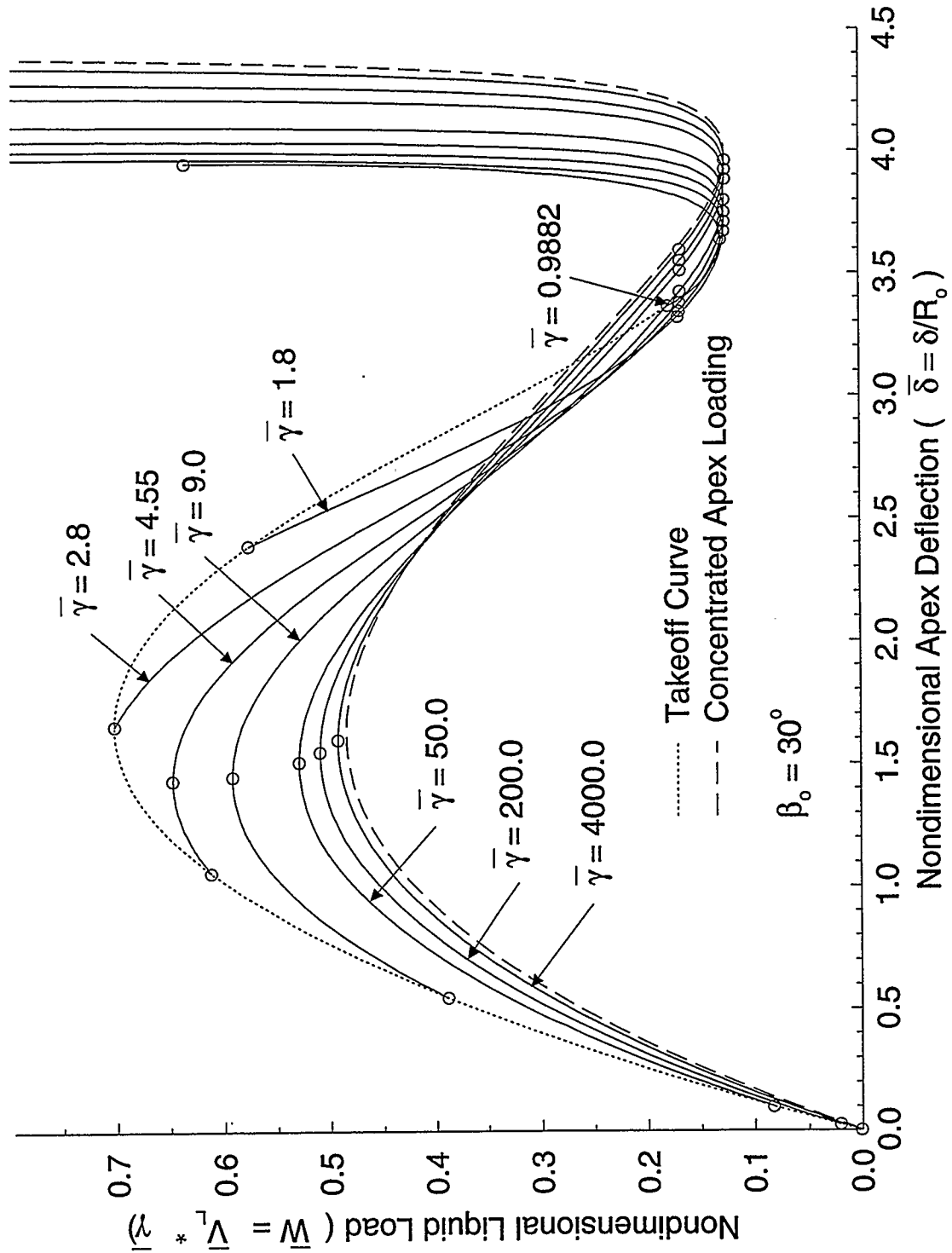


Figure 3.8: Effect of Nondimensional Density on the Load-Deflection Behavior of a Spherical Membrane Under Axisymmetric Hydrostatic Loading with no Support Wrinkling ($\beta_0 = 30^\circ$)

they were not included in Figure 3.6. As nondimensional densities below $\bar{\gamma} = 5.7961$ have load-deflection curves consisting of fully wrinkled membrane configurations for $\beta_o = 120^\circ$, their C points comprise a deviated “takeoff” curve as shown in Figure 3.6. For example, the load-deflection curve for $\bar{\gamma} = 5.2$ would start on the deviated portion of the “takeoff” curve and exhibit monotonically stiffening behavior until its ultimate point is reached. As the nondimensional density decreases, the loading difference between the C and ultimate point decreases until the two coincide. For $\beta_o = 120^\circ$ this occurs for a nondimensional density of $\bar{\gamma} = 4.8942$ and no load-deflection curves exist with lower nondimensional densities for this particular central half angle.

Figure 3.7 shows the load-deflection curves for various nondimensional densities when the structure’s central half angle is $\beta_o = 60^\circ$. By changing the central half angle from $\beta_o = 120^\circ$ to $\beta_o = 60^\circ$, the load-deflection curves are affected in two ways. First by the fact that load-deflection curves now exist with partially wrinkled membranes for nondimensional densities between $\bar{\gamma} = 5.7961$ and $\bar{\gamma} = 1.6513$. The “takeoff” curve, although not indicated on Figure 3.7, deviates at $\bar{\gamma} = 1.6513$ which is the nondimensional density for which the C and D point coincide. The second effect of increasing the central half angle is that it allows unstable equilibrium to exist for nondimensional densities between $\bar{\gamma} = 4000$ and $\bar{\gamma} = 3.4$. For nondimensional densities below 3.4 stable equilibrium exists only after the membrane has become fully wrinkled.

Finally Figure 3.8 shows load-deflection curves for a central half angle of $\beta_o = 30^\circ$. The nondimensional density for which the C and D points coincide is $\bar{\gamma} = 0.9882$. Otherwise the load-deflection curves are similar in appearance to those for $\beta_o = 60^\circ$,

the only difference being the unstable portion of the load-deflection curve which is extended because it takes longer for the structure to become fully wrinkled due to the extra arc length a higher profile central half angle provides.

3.5.4 Nondimensional Density

In Subsection 3.5.2 it was shown that load-deflection curves existed for nondimensional densities down to $\bar{\gamma} = 0.0$. The question then arose during the course of this research as to what the effect of increasing the value of the nondimensional density had on the load-deflection curves. In past research, when the membrane was subjected solely to hydrostatic loads, the highest nondimensional density for which a load-deflection curve was generated was $\bar{\gamma} = 30.0$. To determine an answer, load-deflection curves were calculated for nondimensional densities up to $\bar{\gamma} = 4000.0$ and individual points on the load-deflection curve were calculated for $\bar{\gamma} = 8000.0$.

On examination of Figures 3.7 and 3.8 it can be seen that a dashed line was included to show the load-deflection curve for concentrated axisymmetric apex loading. Both figures clearly show that as the nondimensional density increases, the load-deflection curves approach the concentrated axisymmetric apex loading's load-deflection curve. To further illustrate the point, Figures 3.9 and 3.10 show, for $\beta_o = 60^\circ$ and $\beta_o = 30^\circ$, how the minimum points of neutral stability (T points) for hydrostatic loading approach the T point for concentrated axisymmetric apex loading as the nondimensional density approaches infinity. As further proof, it can be seen in Figure 3.4 that the curve composed of maximum points of neutral equilibrium (G points) also approaches the G point for concentrated axisymmetric apex loads as the nondimensional density increases.

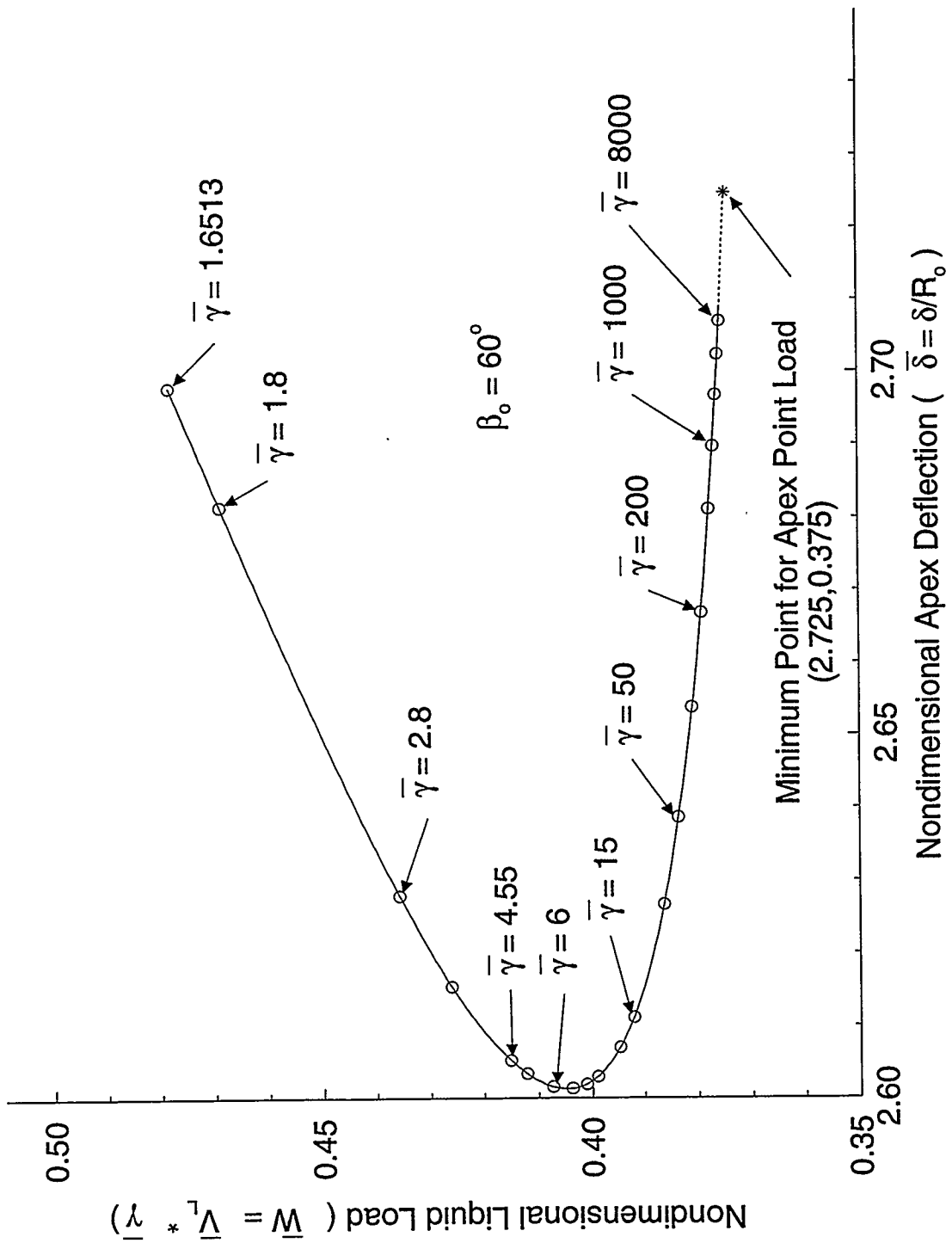
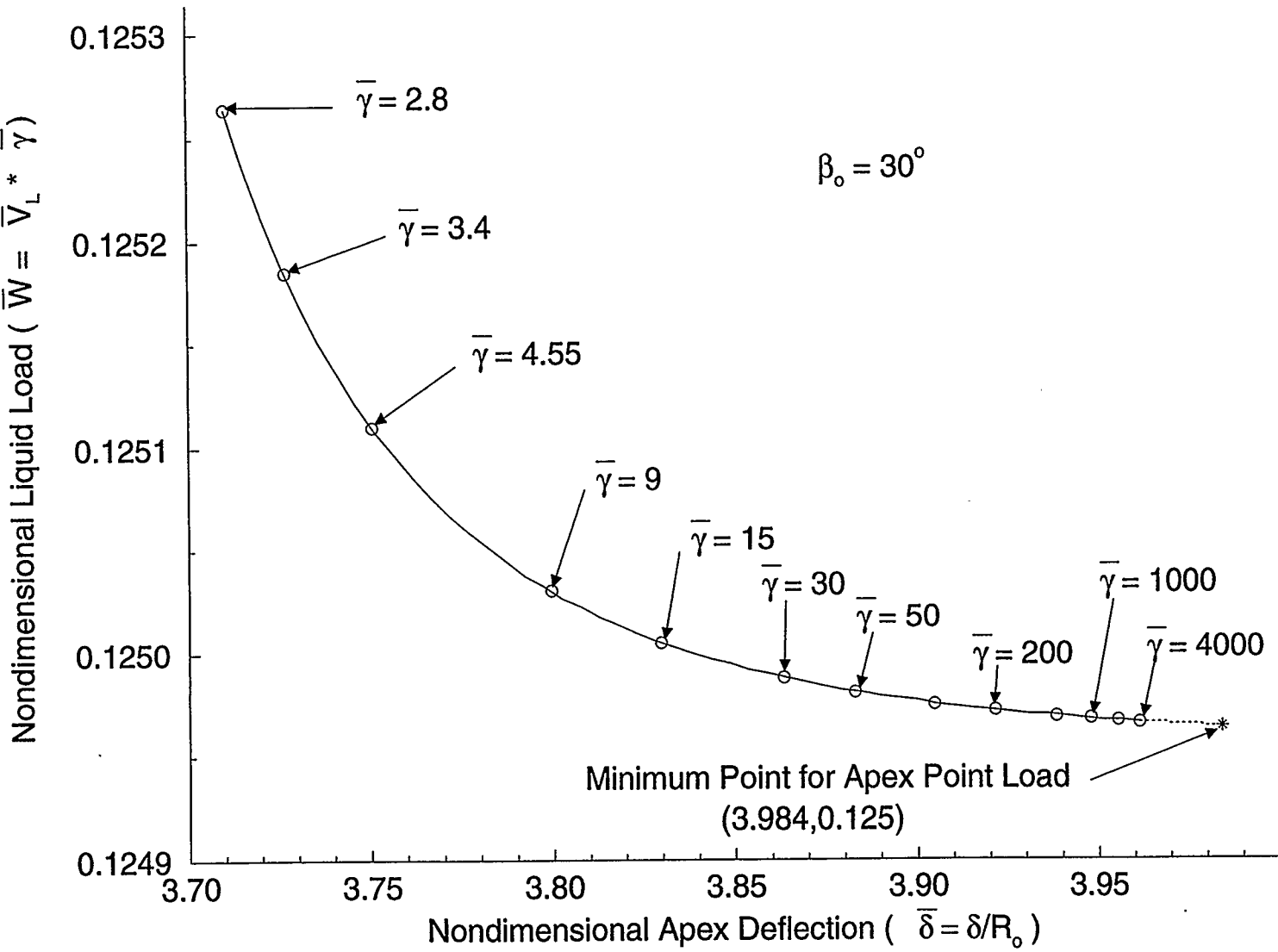


Figure 3.9: Effect of Nondimensional Density on the Minimum Neutral Stability Point ($\beta_0 = 60^\circ$)

Figure 3.10: Effect of Nondimensional Density on the Minimum Neutral Stability Point ($\beta_o = 30^\circ$)



To explain the fact that, as the nondimensional density approaches infinity, the membrane's behavior tends toward that of a membrane under concentrated axisymmetric apex loading, the following reasoning was used. As the nondimensional density applied increases, the volume of liquid required for equilibrium decreases. As this trend continues, the loading becomes a very small volume of liquid with a very high nondimensional density situated at the apex of the membrane. This is very close to the model of a concentrated axisymmetric apex load and if the nondimensional density could reach infinity, it is proposed that the load-deflection curve for hydrostatic loading would be identical to that of concentrated axisymmetric apex loading.

3.5.5 Load-Deflection Curves

Figures 3.11 to 3.24 conclude Chapter 3 with the presentation of load-deflection curves for nondimensional densities ranging from $\bar{\gamma} = 1.8$ to $\bar{\gamma} = 4000$. For each nondimensional density, load-deflection curves were included for central half angles of $\beta_o = 120^\circ$, $\beta_o = 60^\circ$, and $\beta_o = 30^\circ$ where applicable. Each Figure also includes load and deflection values for all C, G, D, T and U points where applicable.

The effect of support wrinkling is included in the results as the long dashed curves in the figures. In general the only curves affected in this thesis are those for $\beta_o = 30^\circ$. It should be noted that in this thesis all load-deflection curves that include the effect of support wrinkling with a nondimensional density satisfying $\bar{\gamma} < 15.2$ are broken into two segments. The first segment is a dotted line showing the effect of support wrinkling on the "takeoff" curve. The second portion of the curve is long dashed and represents the effect of support wrinkling on the load-deflection curve. The reason

Figure 3.11: Load-Deflection Curves for a Spherical Membrane Subjected to Axisymmetric Hydrostatic Loading with Support Wrinkling ($\bar{\gamma} = 1.8$)

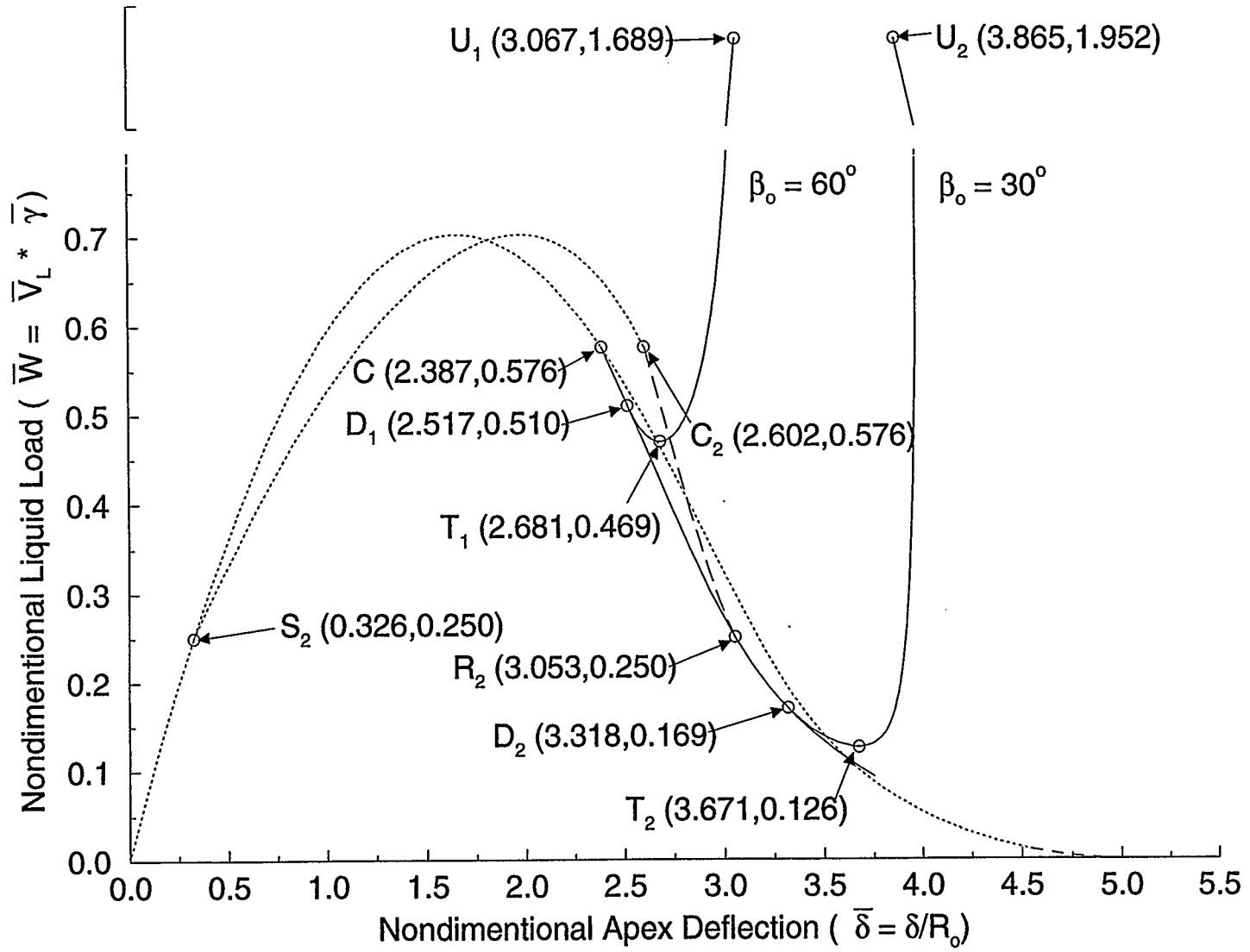


Figure 3.12: Load-Deflection Curves for a Spherical Membrane Subjected to Axisymmetric Hydrostatic Loading with Support Wrinkling ($\bar{\gamma} = 2.8$)

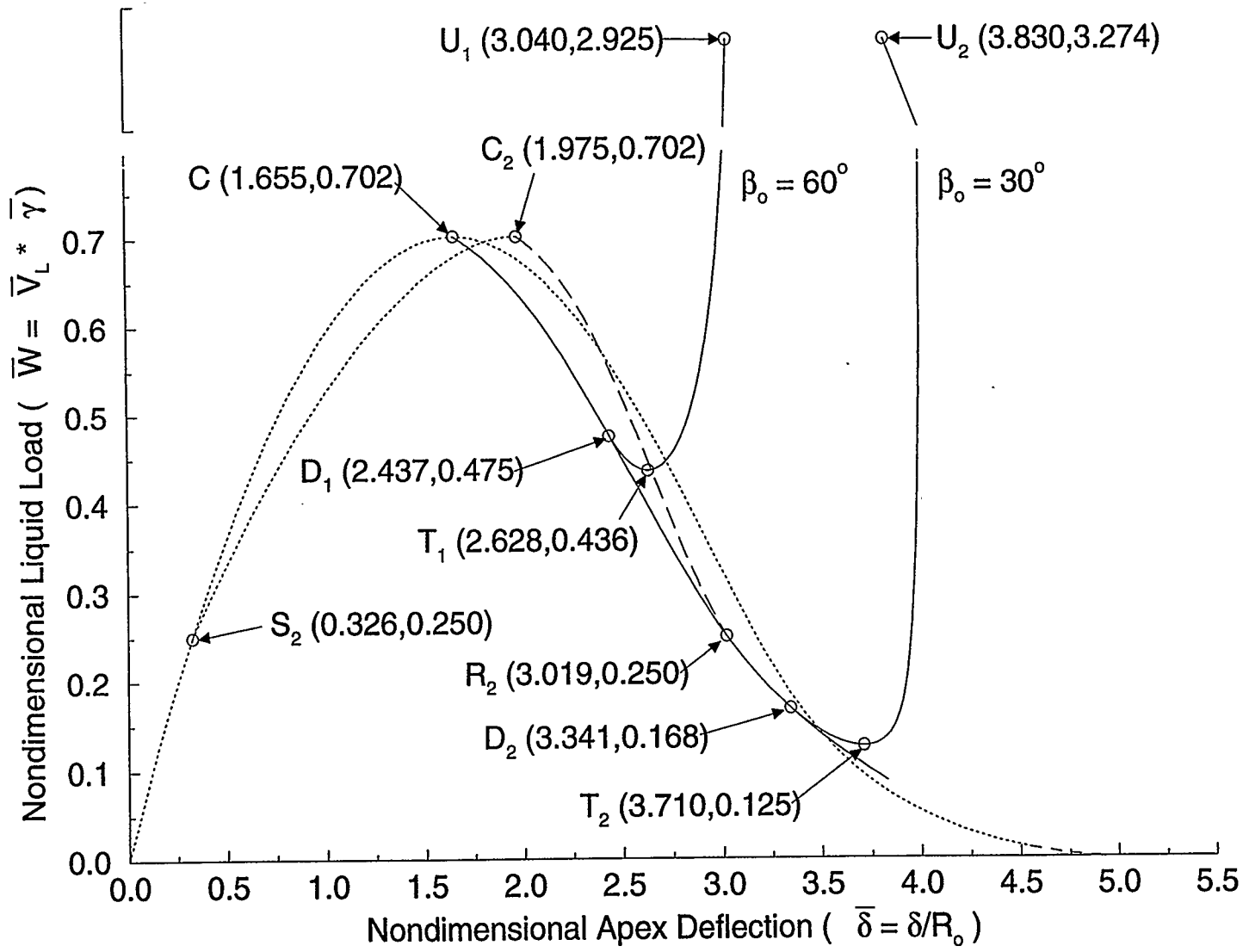


Figure 3.13: Load-Deflection Curves for a Spherical Membrane Subjected to Axisymmetric Hydrostatic Loading with Support Wrinkling ($\bar{\gamma} = 3.4$)

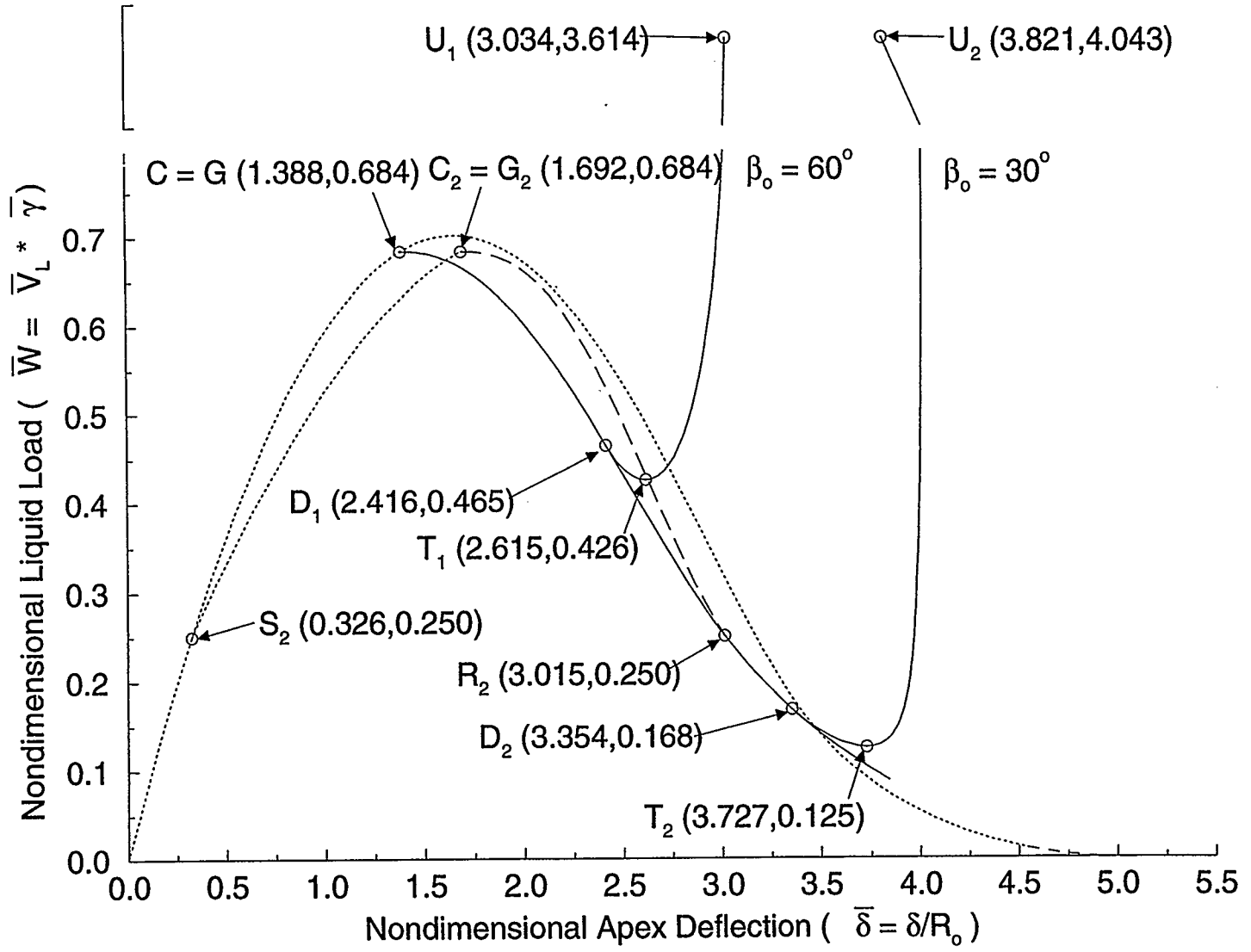


Figure 3.14: Load-Deflection Curves for a Spherical Membrane Subjected to Axisymmetric Hydrostatic Loading with Support Wrinkling ($\bar{\gamma} = 4.55$)

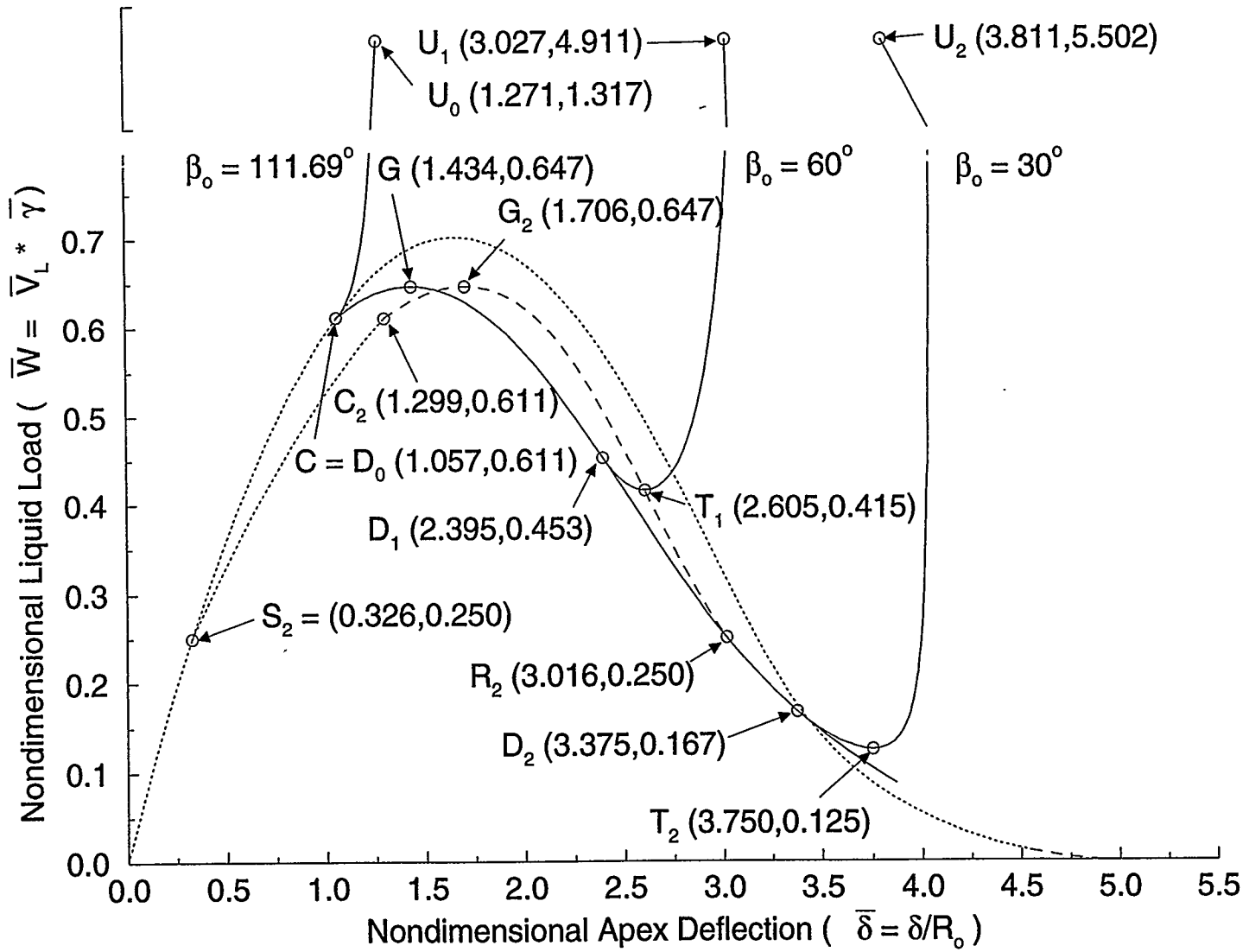


Figure 3.15: Load-Deflection Curves for a Spherical Membrane Subjected to Axisymmetric Hydrostatic Loading with Support Wrinkling ($\bar{\gamma} = 9$)

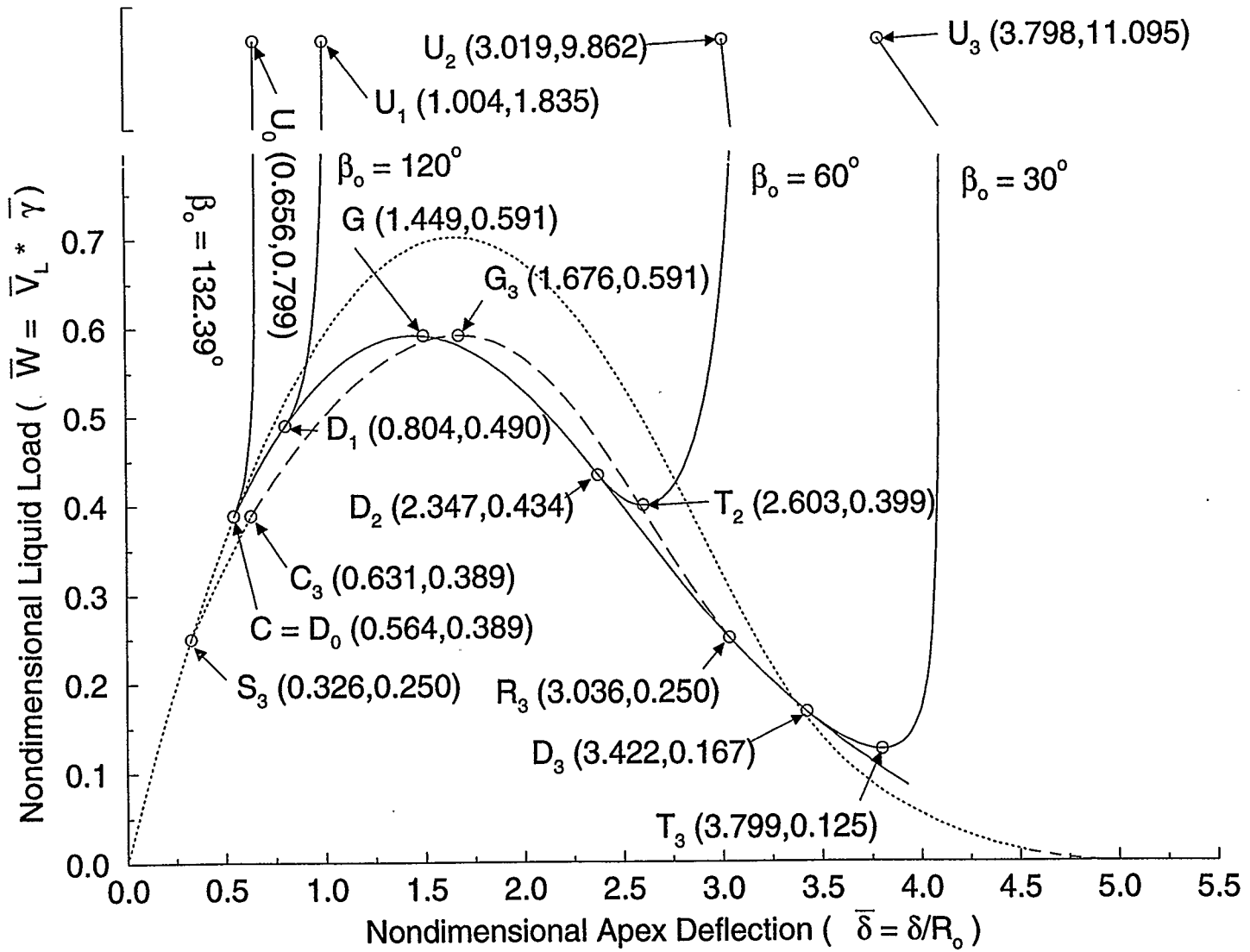


Figure 3.16: Load-Deflection Curves for a Spherical Membrane Subjected to Axisymmetric Hydrostatic Loading with Support Wrinkling ($\bar{\gamma} = 15$)

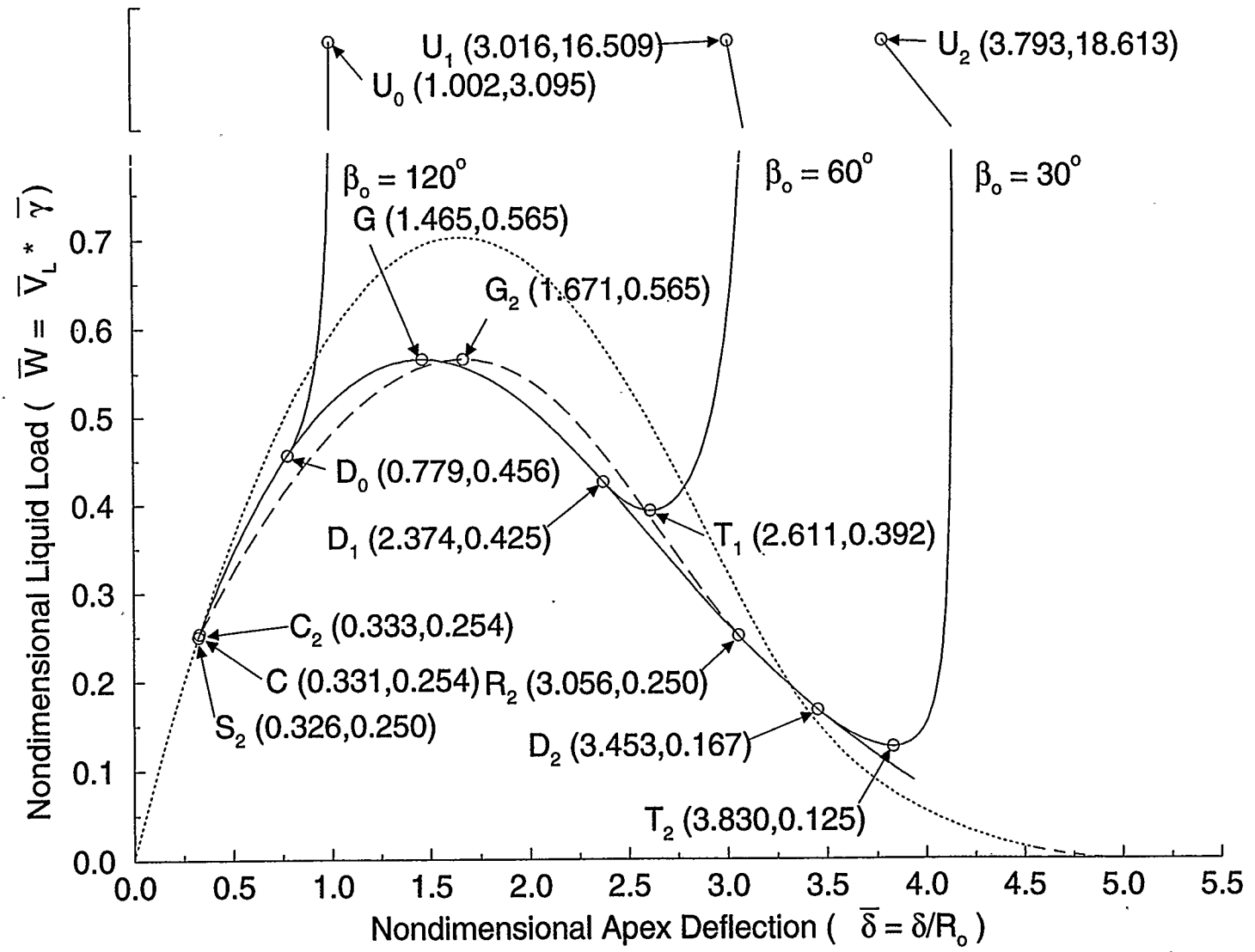
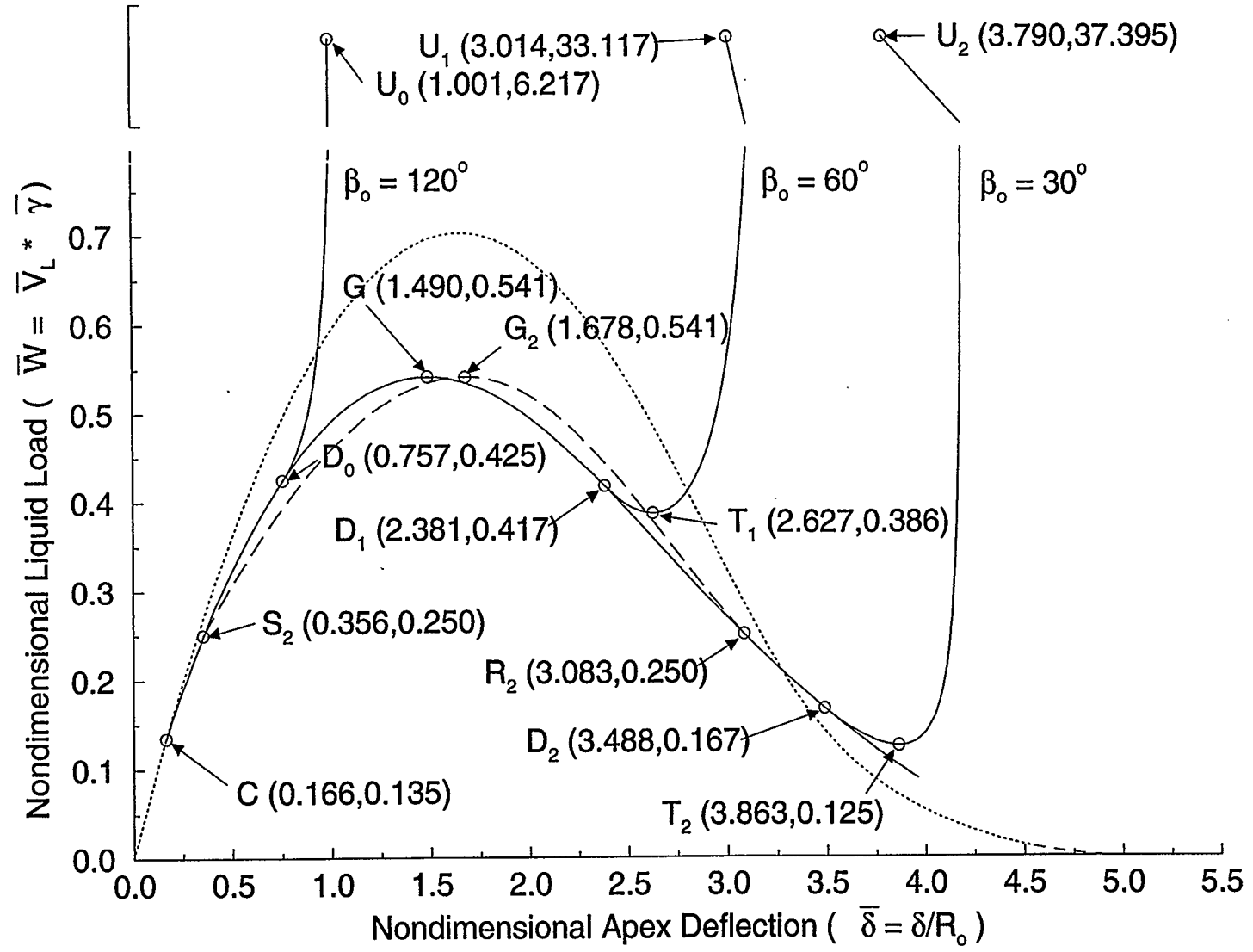


Figure 3.17: Load-Deflection Curves for a Spherical Membrane Subjected to Axisymmetric Hydrostatic Loading with Support Winkling ($\bar{\gamma} = 30$)



for the two segments is that the C points for $\bar{\gamma} < 15.2$ occur at a nondimensional force which is greater than the nondimensional force required for the onset of support wrinkling.

One important characteristic of support wrinkling is the maximum value of β_o for which support wrinkling first occurs for a particular nondimensional density. The maximum value of the central half angle is determined by substituting the maximum nondimensional liquid load that occurs on the load-deflection curve for the particular nondimensional density into Equation 2.39. In general the load used will correspond to the nondimensional liquid load of the G point. However, when hydrostatic loads were being examined it was determined that G points only existed for $\bar{\gamma}$ between infinity and 3.4. In this region the value of β_o for which support wrinkling first occurs varies from $\beta_o = 44.1^\circ$ for an infinite nondimensional density (concentrated loading) to $\beta_o = 55.8^\circ$ for $\bar{\gamma} = 3.4$. For nondimensional densities below 3.4, for which the load-deflection curves do not possess a G point, the maximum force on the load-deflection curve corresponds to the nondimensional force at the C point and is used to determine the angle β_o for which support wrinkling first occurs. As the nondimensional density $\bar{\gamma} = 2.8$ has the largest nondimensional liquid load for a C point, it defines the maximum value of β_o for which support wrinkling first appears at $\beta_o = 56.93^\circ$.

It should be noted that the load-deflection curve for $\bar{\gamma} = 4.55$ was first published by Szyszkowski and Glockner [26] while load-deflection curves for $\bar{\gamma} = 2.78$, $\bar{\gamma} = 4.55$, $\bar{\gamma} = 9$, $\bar{\gamma} = 15$, and $\bar{\gamma} = 30$ were published by Stanuszek and Glockner [23] and [24]. This concludes the chapter on hydrostatic loading.

Figure 3.18: Load-Deflection Curves for a Spherical Membrane Subjected to Axisymmetric Hydrostatic Loading with Support Wrinkling ($\bar{\gamma} = 50$)

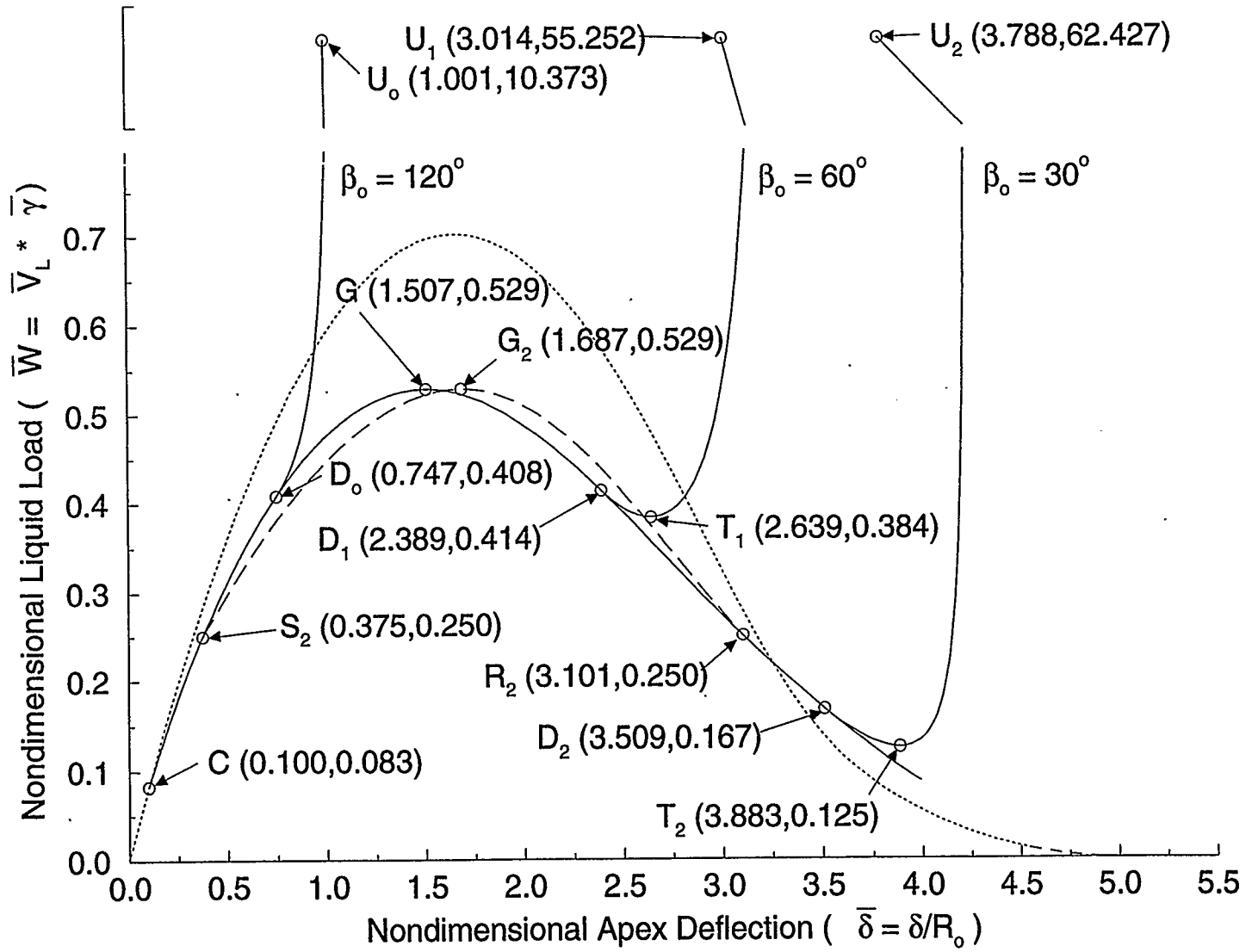


Figure 3.19: Load-Deflection Curves for a Spherical Membrane Subjected to Axisymmetric Hydrostatic Loading with Support Wrinkling ($\bar{\gamma} = 100$)

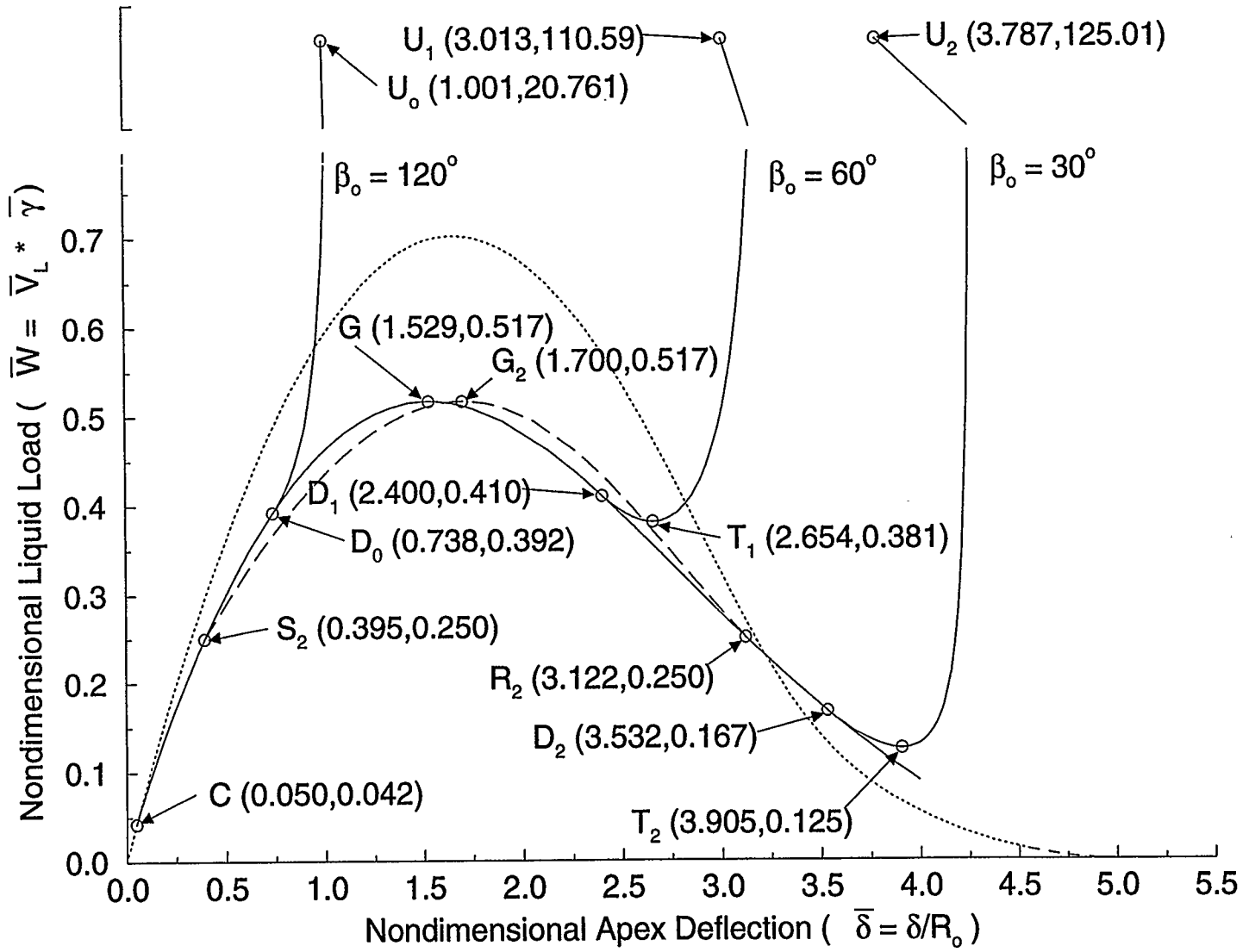


Figure 3.20: Load-Deflection Curves for a Spherical Membrane Subjected to Axisymmetric Hydrostatic Loading with Support Wrinkling ($\bar{\gamma} = 200$)

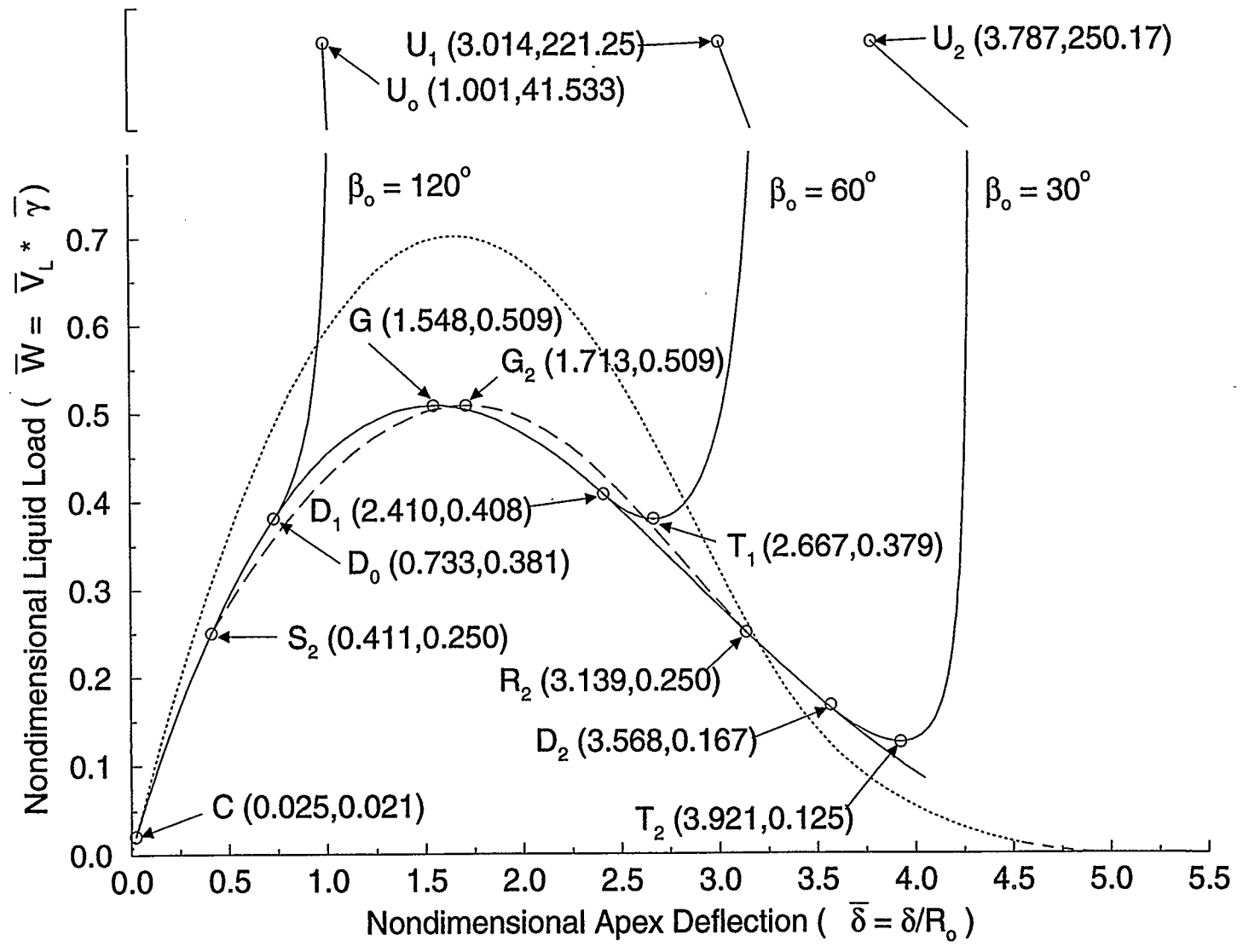


Figure 3.21: Load-Deflection Curves for a Spherical Membrane Subjected to Axisymmetric Hydrostatic Loading with Support Wrinkling ($\bar{\gamma} = 500$)

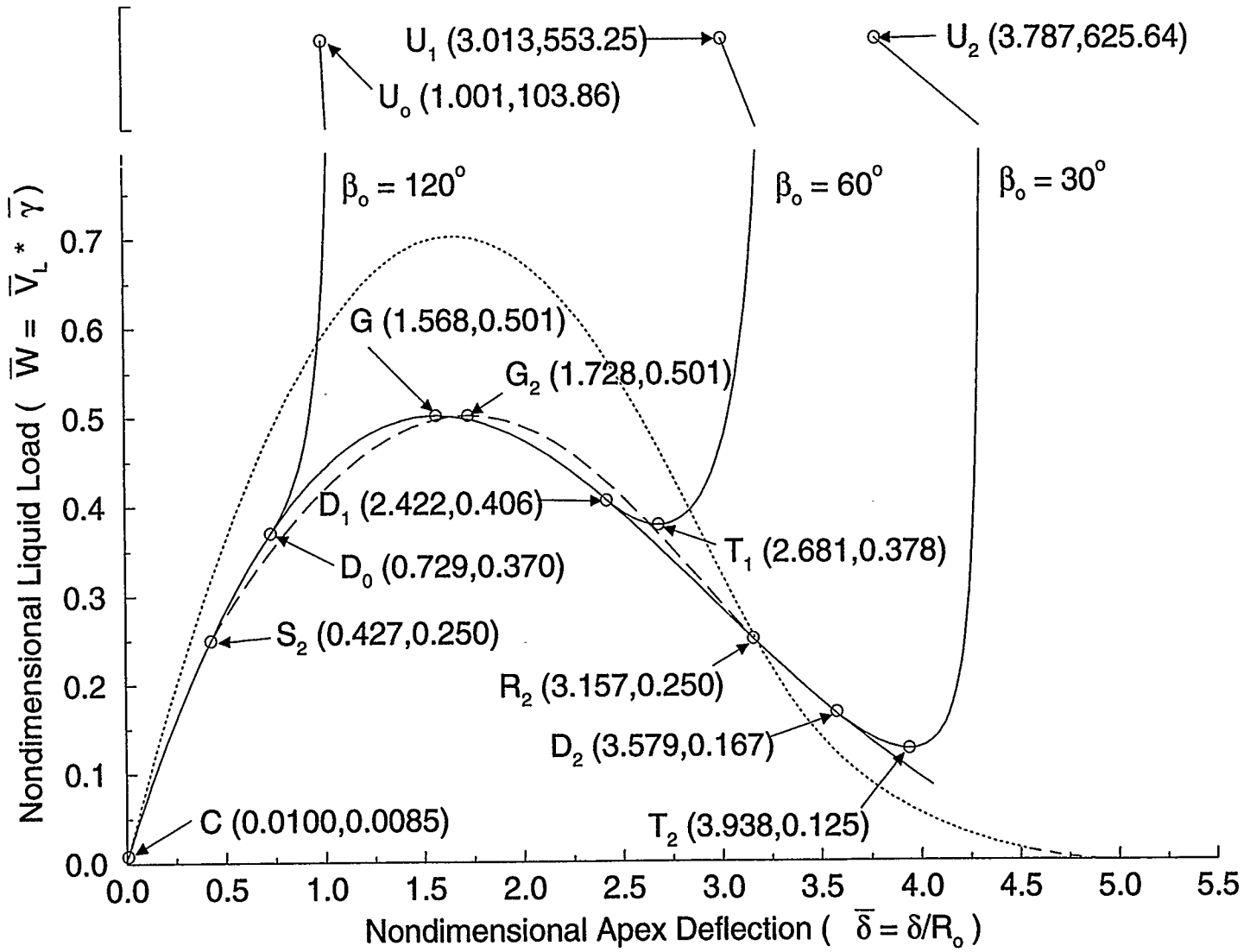


Figure 3.22: Load-Deflection Curves for a Spherical Membrane Subjected to Axisymmetric Hydrostatic Loading with Support Wrinkling ($\bar{\gamma} = 1000$)

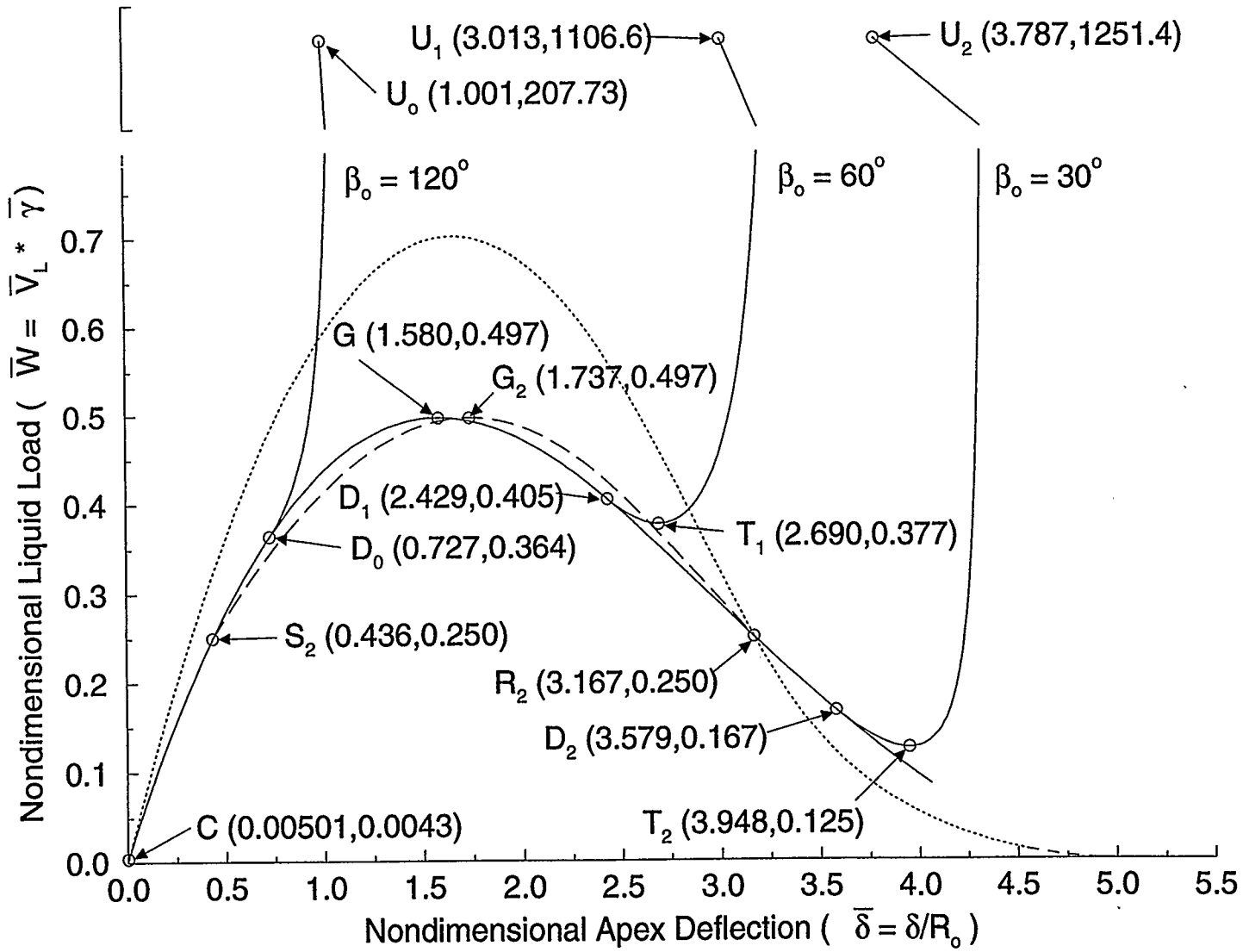


Figure 3.23: Load-Deflection Curves for a Spherical Membrane Subjected to Axisymmetric Hydrostatic Loading with Support Wrinkling ($\bar{\gamma} = 2000$)

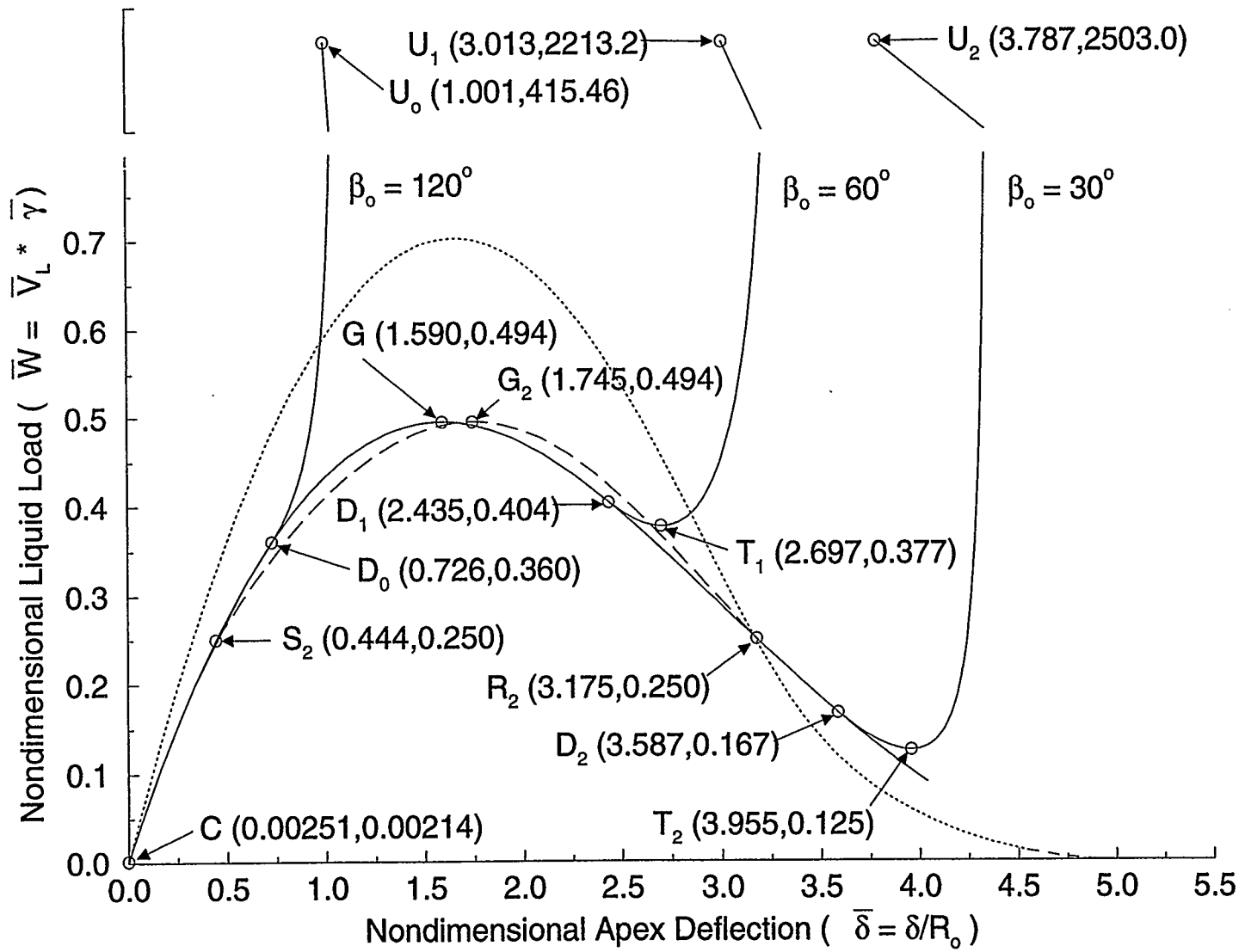
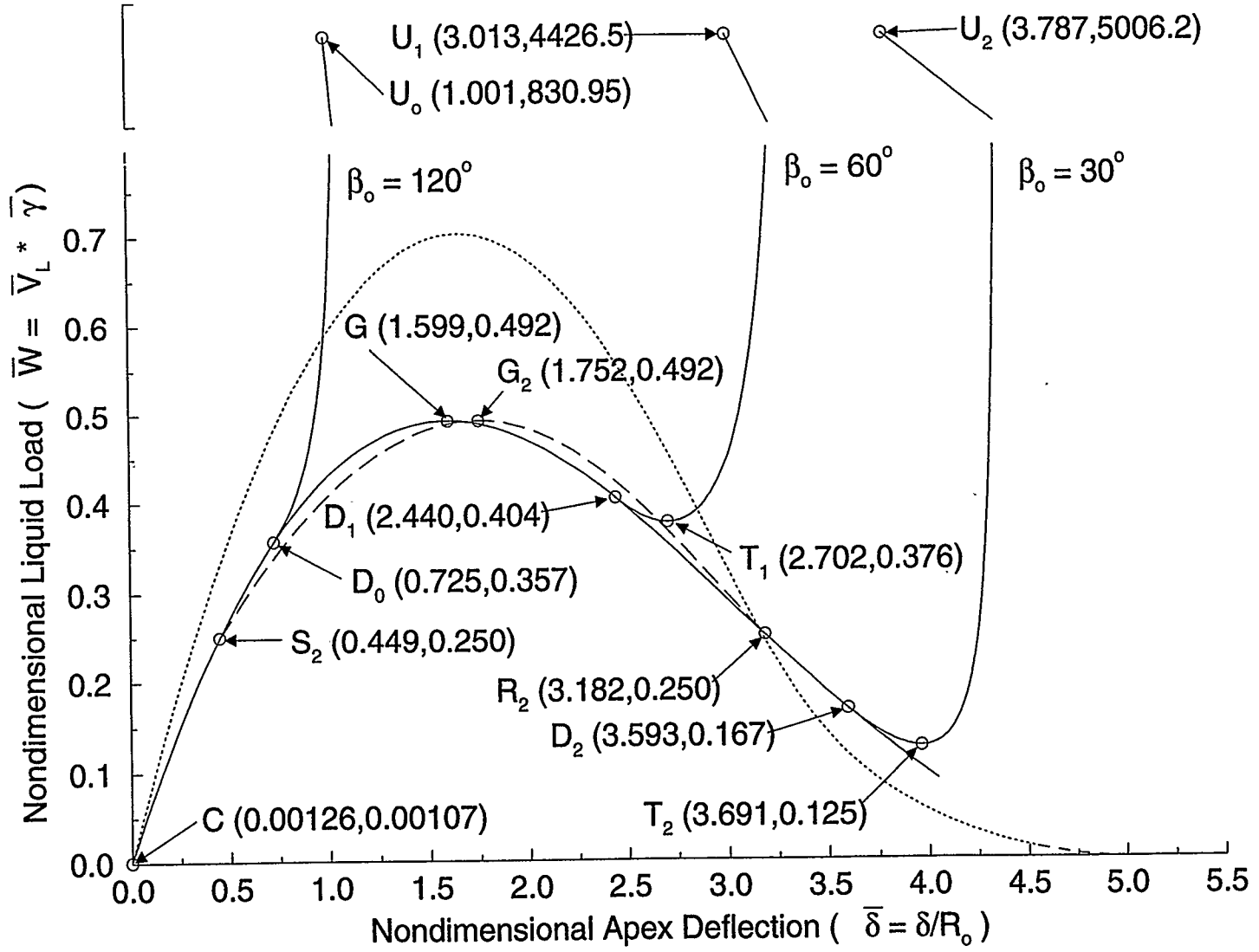


Figure 3.24: Load-Deflection Curves for a Spherical Membrane Subjected to Axisymmetric Hydrostatic Loading with Support Wrinkling ($\bar{\tau} = 4000$)



Chapter 4

HYDROSTATIC AND CONCENTRATED AXISYMMETRIC APEX LOADING

4.1 Introduction

In Chapter 4 the original problem proposed and investigated by Malcolm and Glockner [20] will be investigated. However, unlike the original study which focused on low profile structures, this chapter will present load-deflection surfaces for a wide range of geometries and nondimensional densities. The theory follows closely to that in [14] where it was first derived.

4.2 Physical Arrangement

In Chapter 3, the hydrostatic load accumulated due to an initial imperfection in the membrane or due to a depression caused by a tie down. A third method to produce a depression and allow the ponding medium to accumulate, which is also the most probable from an engineering standpoint, is to apply a concentrated axisymmetric apex load. The resulting depression is then readily available for a ponding medium to accumulate. The question then arises as to what the value is of the maximum concentrated axisymmetric apex load, or critical concentrated axisymmetric apex load, which can be applied to the membrane's apex such that the membrane's depression completely fills with the ponding medium without causing collapse.

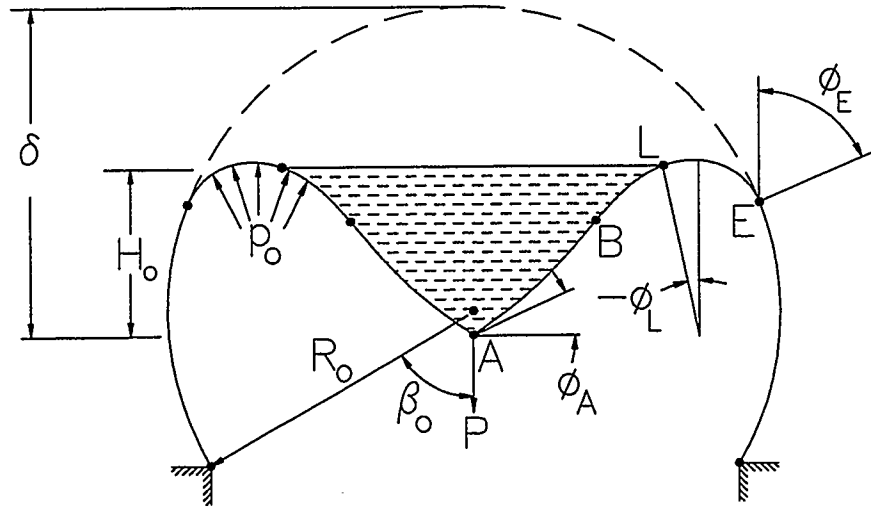


Figure 4.1: Spherical Membrane Subjected to Hydrostatic and Concentrated Axisymmetric Apex Loading

Figure 4.1 shows a spherical inflatable of radius R_0 with an internal pressure p_0 subjected to a concentrated axisymmetric apex load, P , and a hydrostatic load of density γ to a depth of H_0 measured from the apex. As can be seen from the figure, point A defines the beginning of the wrinkled region at the apex where the concentrated axisymmetric apex load is applied. Angle ϕ_A defines the slope of the tangent at point A and is measured from the tangent to the membrane at point A to the horizontal. The curvature of the wrinkled membrane changes at point B and the end of the hydrostatic loading occurs at point L. When angle ϕ_L is equal to zero the depression is completely filled and any additional liquid will flow off the membrane. Finally the wrinkled domain terminates at point E where the slope is defined by angle ϕ_E .

The supports are identical to those described in the preceding two chapters and support wrinkling is taken into account for the high profile structures.

4.3 Theory

Unlike the theory presented in Chapters 2 and 3, which was previously developed and published, the following theory on combined hydrostatic and concentrated axisymmetric apex loading is being presented for the first time in terms of the volume instead of the total vertical force, Q , and the differential equations are in terms of the arc length. However, as the methodology mirrors that of the theory for Chapter 3, the equations presented will appear familiar.

The development of the theory begins, once again, with the following differential equations which were derived in Chapter 2:

$$\frac{d\phi}{dr} = \frac{2\pi r p \tan \phi}{Q} \quad (4.1)$$

$$\frac{dQ}{dr} = 2\pi r p \quad (4.2)$$

$$\frac{dh}{dr} = k \tan \phi \quad (4.3)$$

As was the case with hydrostatic loading, the net pressure, p is not constant and furthermore must be defined piece-wise due to the change in loading domains at point L. Its definition is:

$$p = \begin{cases} p_o - \gamma(H_o + h) & \text{between points A and L} \\ p_o & \text{between points L and E} \end{cases} \quad (4.4)$$

When Equation 4.4 is substituted into differential equation 4.2 and the resulting differential equation is integrated, the following piece-wise definition for the total vertical force, Q , is obtained:

$$Q = \begin{cases} \pi r^2 [p_o - \gamma(H_o + h)] + k\gamma \int_{h_A}^h \pi r^2 dh + J & \text{between points A and L} \\ \pi r^2 p_o + M & \text{between points L and E} \end{cases} \quad (4.5)$$

where J and M are arbitrary constants of integration. To eliminate the arbitrary constant J from equation 4.5, the boundary condition $Q(r = 0) = -P$ was used which resulted in $J = -P$. Next, Equation 4.5 being continuous across point L, was used to eliminate constant M . Thus, substituting $r = r_L$ and $h = -H_o$ into both equations for Q and equating them resulted in $M = -\gamma V_L - P$. Now the equation for the total vertical load, Q , is:

$$Q = \begin{cases} \pi r^2 [p_o - \gamma(H_o + h)] + k\gamma \int_{h_A}^h \pi r^2 dh - P & \text{between points A and L} \\ \pi r^2 p_o - \gamma V_L - P & \text{between points L and E} \end{cases} \quad (4.6)$$

As the integral in Equation 4.6 represents the total volume of liquid accumulated in the depression at height, h , the volume is defined as:

$$V = -k \int_{h_A}^h \pi r^2 dh \quad (4.7)$$

or

$$\frac{dV}{dh} = -k\pi r^2 \quad (4.8)$$

When the definition for V is substituted into Equation 4.6, the result is:

$$Q = \begin{cases} \pi r^2[p_o - \gamma(H_o + h)] - \gamma V - P & \text{between points A and L} \\ \pi r^2 p_o - \gamma V_L - P & \text{between points L and E} \end{cases} \quad (4.9)$$

By transforming Equation 4.8 into a differential equation in terms of r and substituting Equation 4.9 into differential equations 4.1, 4.2, and 4.3 they become:

$$\frac{d\phi}{dr} = \frac{2\pi r p \tan \phi}{\pi r^2 p - \gamma V - P} \quad (4.10)$$

$$\frac{dV}{dr} = -k\pi r^2 \tan \phi \quad (4.11)$$

$$\frac{dh}{dr} = k \tan \phi \quad (4.12)$$

between points A and L and:

$$\frac{d\phi}{dr} = \frac{2\pi r p_o \tan \phi}{\pi r^2 p_o - \gamma V_L - P} \quad (4.13)$$

$$\frac{dh}{dr} = \tan \phi \quad (4.14)$$

between points L and E. It is a simple procedure to convert these differential equations into nondimensional form as well as in terms of arc length. Differential equations 4.10, 4.11, and 4.12 are thus written as:

$$\frac{d\phi}{d\bar{s}} = \frac{2\bar{r}\bar{p} \sin \phi}{\bar{r}^2\bar{p} - \bar{\gamma}\bar{V} - \bar{P}} \quad (4.15)$$

$$\frac{d\bar{V}}{d\bar{s}} = -k\bar{r}^2 \sin \phi \quad (4.16)$$

$$\frac{d\bar{h}}{d\bar{s}} = k \sin \phi \quad (4.17)$$

$$\frac{d\bar{r}}{d\bar{s}} = \cos \phi \quad (4.18)$$

It must be noted that, even though there are now four differential equations, only three are independent as differential equations 4.17 and 4.18 can be combined to represent one differential equation, namely the nondimensional form of differential equation 4.12. Similarly, differential equations 4.13 and 4.14 written in terms of arc length and nondimensional terms results in:

$$\frac{d\phi}{d\bar{s}} = \frac{2\bar{r} \sin \phi}{\bar{r}^2 - \bar{\gamma}\bar{V}_L - \bar{P}} \quad (4.19)$$

$$\frac{d\bar{h}}{d\bar{s}} = \sin \phi \quad (4.20)$$

$$\frac{d\bar{r}}{d\bar{s}} = \cos \phi \quad (4.21)$$

Again it should be noted that only two of these are independent. It is encouraging to note that, if \bar{P} in differential equations 4.15 through 4.21 is zero, they reduce to differential equations 3.10 through 3.16 for hydrostatic loading. Similarly, when

$\bar{\gamma}$ and \bar{V} are zero, the differential equations reduce to differential equations 2.22 through 2.24 for concentrated axisymmetric apex loading.

Now that the differential equations are defined, all that remains is to satisfy the boundary and continuity conditions and the inextensibility criterion. Once again, the conditions will be discussed in the order they are used in the numerical procedure. Point A, as with hydrostatic loading, is the starting point and has the following boundary conditions:

$$\left. \begin{aligned} \phi &= \phi_A \\ \bar{V} &= 0 \\ \bar{r} &= 0 \\ \bar{h} &= 0 \end{aligned} \right\} \quad (4.22)$$

It is apparent that the only unknown variable is ϕ_A for which an initial guess was made. As point A is also the apex, the nondimensional arc length, \bar{s} , is set to zero. As there are two input variables, namely \bar{H}_o and \bar{P} , it was decided that \bar{P} would be held constant while individual points were established for various liquid depths, \bar{H}_o , until an entire load-deflection curve was obtained. Once this was accomplished, the value of \bar{P} was incremented and its corresponding new load-deflection curve developed.

The numerical method then solves for ϕ , \bar{V} , \bar{r} , and \bar{h} along the membrane using the Runge-Kutta fourth order method until point B is reached. The test used was whether the net pressure was zero which is determined by:

$$\bar{p} = 1 - \bar{\gamma}(\bar{H}_o + \bar{h}) = 0 \quad (4.23)$$

Once point B is reached, the values of k and ϕ_B must be changed to $-k$ and

$-\phi_B$, respectively. The numerical procedure continues with differential equations 4.15, 4.16, 4.17, and 4.18 until point L is reached. As point L marks the end of the liquid loading domain, the test to determine if point L was reached is:

$$\bar{H}_o + \bar{h} = 0 \quad (4.24)$$

The boundary conditions at point L, which are all determined numerically, are:

$$\left. \begin{aligned} \phi &= \phi_L \\ \bar{V} &= \bar{V}_L \\ \bar{r} &= \sin \phi_L \\ \bar{h} &= -\bar{H}_o \end{aligned} \right\} \quad (4.25)$$

As the liquid loading domain is finished, the numerical method switches to differential equations 4.19, 4.20, and 4.21 until point E is reached. Point E is defined by the following boundary conditions:

$$\left. \begin{aligned} \phi &= \phi_E \\ \bar{r} &= \sin \phi_E \\ \bar{h} &= \bar{h}_E \end{aligned} \right\} \quad (4.26)$$

of which ϕ_E and \bar{h}_E are unknown. At this point it became necessary to predict the correct value of ϕ_E . As was the case in Chapter 3, the first step is to solve differential equation 4.19 explicitly. The solution was originally derived by Szyszkowski and Glockner [14], and their result was:

$$\bar{r} = \sqrt{\gamma \bar{V}_L + \bar{P} + J \sin \phi} \quad (4.27)$$

where J is an arbitrary constant of integration. Before solving for J , an important value is obtained when $\phi = 0$ is substituted into Equation 4.27. The value of \bar{r} is renamed \bar{r}_o and is equal to:

$$\bar{r}_o = \sqrt{\gamma \bar{V}_L + \bar{P}} \quad (4.28)$$

The radius, \bar{r}_o , occurs at the highest point on the deformed membrane or, in other words, where the membrane's slope is horizontal. When the membrane's depression is completely filled with liquid, the values for \bar{r}_o and \bar{r}_L coincide. Now, to determine the value of the arbitrary constant J , the boundary condition $\bar{r} = \sin \phi_E$ at $\phi = \phi_E$ is used. Once equation 4.28 is substituted, the resulting equation for \bar{r} is:

$$\bar{r} = \bar{r}_o \sqrt{1 + \left[\frac{\sin^2 \phi_E}{\bar{r}_o^2} - 1 \right] \frac{\sin \phi}{\sin \phi_E}} \quad (4.29)$$

At this point it is possible to establish a relationship between ϕ_E and ϕ_L by substituting the boundary condition $\bar{r} = \sin \phi_L$ at $\phi = \phi_L$ into equation 4.29. Utilizing the quadratic equation, the value of ϕ_E can now be predicted at point L by:

$$\sin \phi_E = \frac{(\sin^2 \phi_L - \bar{r}_o^2) + \sqrt{(\sin^2 \phi_L - \bar{r}_o^2)^2 + 4\bar{r}_o^2}}{2} \quad (4.30)$$

The numerical procedure can then proceed to point E where the inextensibility condition is used to determine if the initial guess made for ϕ_A was correct. The inextensibility criterion demands:

$$\bar{s} = \phi_E \quad (4.31)$$

If this condition is satisfied the solution is correct and the liquid level, \bar{H}_o is incremented and a new initial guess for ϕ_A is made. Otherwise, the current value of ϕ_A is incorrect and a new guess for ϕ_A must be made.

The procedure outlined above is only valid in predicting ϕ_E if the wrinkled domain has not reached the supports. Once the wrinkling reaches the supports, the boundary conditions for point E alter. The procedure for handling this case is identical to the theory presented in Chapter 3 as outlined by equations 3.27 through 3.30.

Finally, the production of load-deflection curves requires a value for the total vertical deflection, $\bar{\delta}$. Equations 2.34 and 2.35 in Chapter 2 are still valid.

Once again, support wrinkling is handled as outlined in Section 2.4.2. It should be noted that the combined load, \bar{F} , must be used, which is defined as:

$$\bar{F} = \bar{W} + \bar{P} \quad (4.32)$$

where $\bar{W} = \bar{\gamma}\bar{V}_L$ is the total hydrostatic load.

4.4 Load-Deflection Characteristics

The presentation of load-deflection results for a spherical membrane structure subjected to combined hydrostatic and concentrated axisymmetric apex loading differs from Chapters 2 and 3 as there are now two independent loading variables. As such, it was deemed appropriate to create a load-deflection surface with the three axes being the nondimensional apex deflection, the nondimensional liquid load, and the nondimensional concentrated axisymmetric apex load. Figure 4.2 shows a sample surface in order to highlight its features prior to presenting the results. The load-

deflection surface was generated for a nondimensional density of $\bar{\gamma} = 4.55$ and a central half angle of $\beta_o = 60^\circ$.

Examining Figure 4.2, it is evident that, when the value of the concentrated axisymmetric apex load remains constant at a value of zero, the resulting curve produced on the surface is for hydrostatic loading as seen in Chapter 3. Similarly, when the hydrostatic load applied to the membrane is constant with a value of zero, the resulting curve produced on the load-deflection surface is that for concentrated axisymmetric apex loading as seen in Chapter 2. Thus a load-deflection surface provides a complete representation of the behavior of a spherical membrane whether it is subjected to hydrostatic loading, concentrated axisymmetric apex loading, or a combination of the two.

Before examining combined hydrostatic and concentrated axisymmetric apex loading it is helpful to keep the physical arrangement of the loading in mind. The spherical membrane is initially loaded by a concentrated axisymmetric apex load and the depression resulting from applying the concentrated axisymmetric apex load is then allowed to fill with the ponding medium. This being the case, every concentrated axisymmetric apex load between $\bar{P} = 0$ and $\bar{P} = 0.484$ will undergo hydrostatic loading which is in stable equilibrium until one of the two situations discussed below occurs.

The first possibility is that the liquid added eventually fills the depression so that no additional liquid loading can occur. This is indicated on Figure 4.2 as the C curve. Specifically, it occurs when the concentrated axisymmetric apex load is between $\bar{P} = 0$ and $\bar{P} = \bar{P}_M$, where \bar{P}_M is the concentrated axisymmetric apex load which produces a load-deflection curve which is tangent to the C curve. The

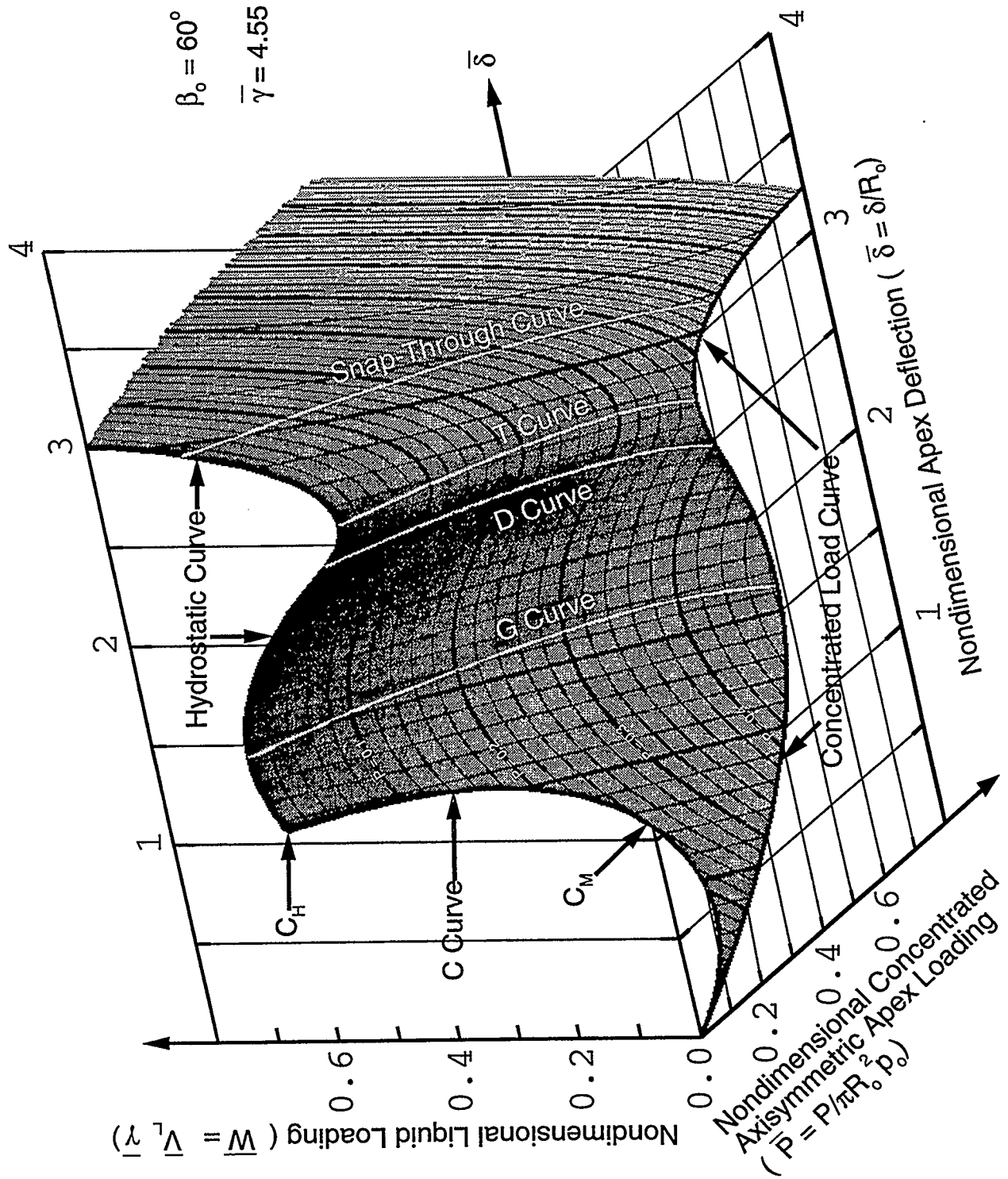


Figure 4.2: Typical Load-Deflection Surface for a Spherical Membrane Subjected to Combined Hydrostatic and Concentrated Axisymmetric Apex Loading with no Support Wrinkling ($\beta_0 = 60^\circ$ and $\bar{\gamma} = 4.55$)

tangent point is indicated on Figure 4.2 as point C_M on the C curve. Points on the C curve between C_M and C_H on Figure 4.2 also represent membranes with completely filled depressions with a concentrated axisymmetric apex load between $\bar{P} = 0$ and $\bar{P} = \bar{P}_M$. However, these configurations can only be reached by unloading from a configuration with a greater apex deflection than the configuration on the C curve. The point C_H on the C curve represents the C point when only hydrostatic loading occurs.

The second possibility occurs if the concentrated axisymmetric apex load is between $\bar{P} = \bar{P}_M$ and $\bar{P} = 0.484$ or is between $\bar{P} = 0$ and $\bar{P} = \bar{P}_M$ and is on the C curve in the direction of increasing apex deflection from point C_M . In this case, as the hydrostatic load continues to be applied, the membrane continues to be in stable equilibrium until the hydrostatic load is increased to the point that neutral equilibrium exists. In Chapters 2 and 3 this was the definition of a G point, however, in the case of combined hydrostatic and concentrated axisymmetric apex loading, where every concentrated axisymmetric apex load between $\bar{P} = 0$ and $\bar{P} = 0.484$ has a G point, a G curve is produced on the load-deflection surface as indicated in Figure 4.2. If the hydrostatic load is increased slightly once the G curve has been reached, then the membrane structure snaps through to the fourth white line from the left on Figure 4.2 which is labeled the snap-through curve. When snap-through occurs, only the apex deflection changes as the concentrated axisymmetric apex load and hydrostatic load at the G point remain the same.

If after reaching the G curve the hydrostatic load is decreased, an unstable portion of the load-deflection surface can be attained. As the load is decreased and the deflection increases, the wrinkled region eventually reaches the supports. At

this point the load-deflection surface deviates from the main load-deflection surface which would have been realized if a smaller central half angle were employed. As this occurs for every concentrated axisymmetric apex load between $\bar{P} = 0$ and $\bar{P} = 0.401$, a curve is formed which is termed the D curve. The value $\bar{P} = 0.401$ was taken from Chapter 2 and corresponds to the concentrated axisymmetric apex load which caused the load wrinkling domain on the membrane to reach the supports for $\beta_o = 60^\circ$. For the purpose of this thesis, the portion of the load-deflection surface to the left of the D curve, which consists of partially wrinkled membrane configurations, will be referred to as the main portion of the load-deflection surface. The remainder of the load-deflection surface, which consists of fully wrinkled membranes, will be referred to as the “deviated portion” of the load-deflection surface. The hydrostatic load continues to decrease on the deviated portion of the load-deflection surface until neutral equilibrium is reached once again. As this occurs for all concentrated axisymmetric apex loads between $\bar{P} = 0$ and $\bar{P} = 0.375$, a T curve is formed which is indicated on Figure 4.2. The value $\bar{P} = 0.375$ was also obtained from Chapter 2 for a central half angle of $\beta_o = 60^\circ$. From the T curve on, any additional hydrostatic loading produces stable equilibrium. For concentrated axisymmetric apex loads between $\bar{P} = 0.375$ and $\bar{P} = 0.484$, the hydrostatic unloading continues after the G curve until there is no longer any liquid remaining in the depression. This represents the unstable portion of the concentrated axisymmetric apex load’s load-deflection curve.

The portion of the load-deflection surface to the right of the T curve will be referred to as the stable deviated portion of the load-deflection surface, representing stable equilibrium configurations. In terms of concentrated axisymmetric apex loads, the stable deviated load-deflection surface is valid for loads between $\bar{P} = 0$ and

$\bar{P} = \infty$. However, as the depression is being loaded by a liquid, it will eventually fill. In terms of hydrostatic load this results in the deviated load-deflection surface terminating along a curve which will be referred to as the ultimate curve. The ultimate curve is not indicated on Figure 4.2 but it will be documented and discussed in the Results Section.

4.5 Results

4.5.1 Nondimensional Density

In order to illustrate how the load-deflection surface changes when the nondimensional density of the ponding medium changes, Figures 4.3, 4.4, and 4.5 were created. The central half angle for these figures is held constant with a value of $\beta_o = 60^\circ$ while the nondimensional density was varied. The nondimensional density has a value of $\bar{\gamma} = 2.8$, $\bar{\gamma} = 4.55$, and $\bar{\gamma} = 4000$ for Figures 4.3, 4.4, and 4.5 respectively.

One effect of varying the nondimensional density for a constant central half angle has already been touched upon in Chapter 3. Namely, that as the nondimensional density increases, the results for hydrostatic loading tend towards those for the concentrated axisymmetric apex load case. When Figures 4.3 through 4.5 are examined the load-deflection surface for $\bar{\gamma} = 4000$ appears symmetrical about a plane oriented at 45° to the concentrated axisymmetric apex load and apex deflection plane. The explanation for this phenomenon was discussed in Chapter 3 but it should be noted that it also applies for a membrane with a combined hydrostatic and concentrated axisymmetric apex load.

By examining the G, T, D and Snap-Through curves in Figures 4.3 through

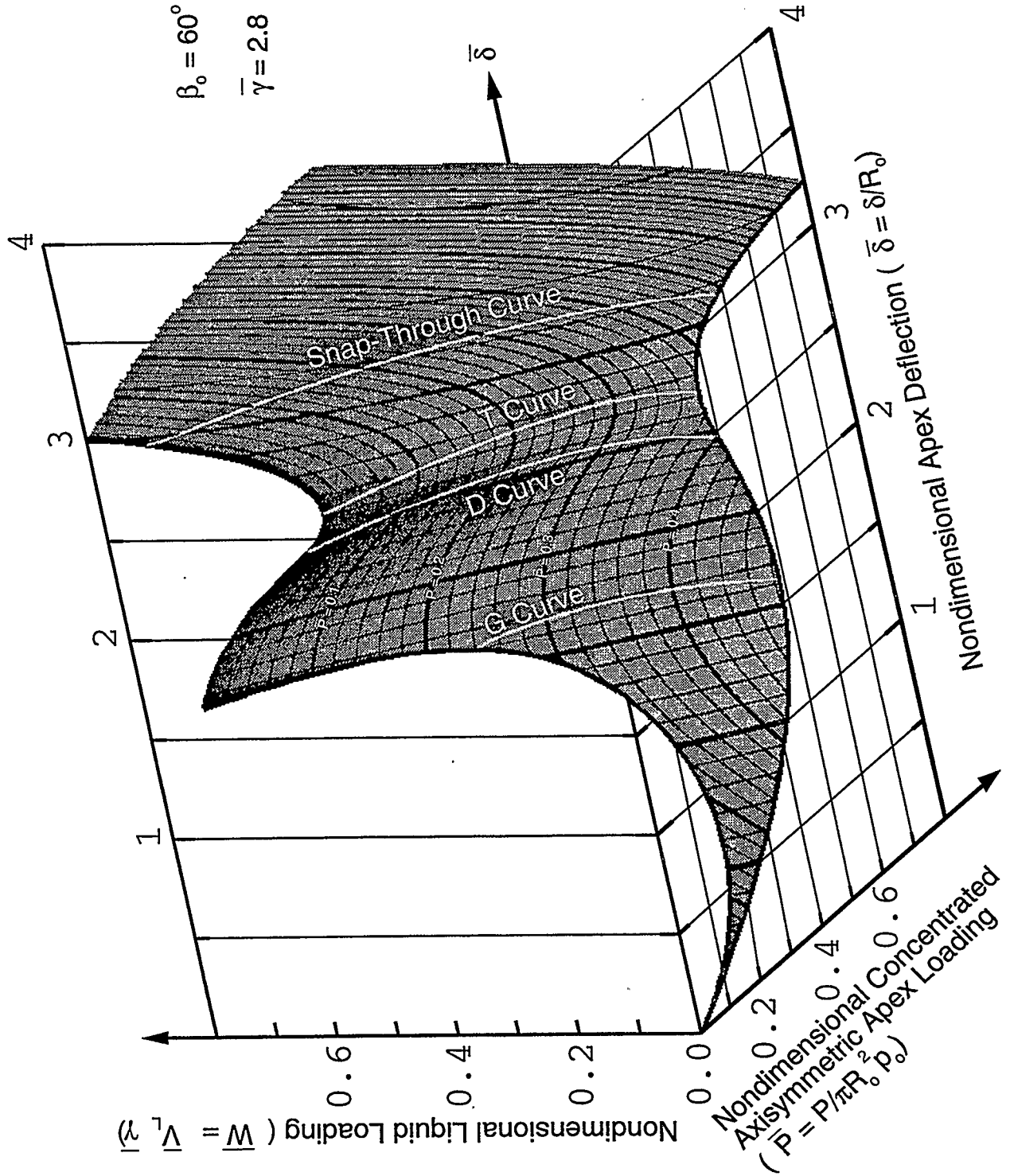


Figure 4.3: Load-Deflection Surface for a Spherical Membrane Subjected to Combined Hydrostatic and Concentrated Axisymmetric Apex Loading ($\bar{\gamma} = 2.8$ and $\beta_0 = 60^\circ$)

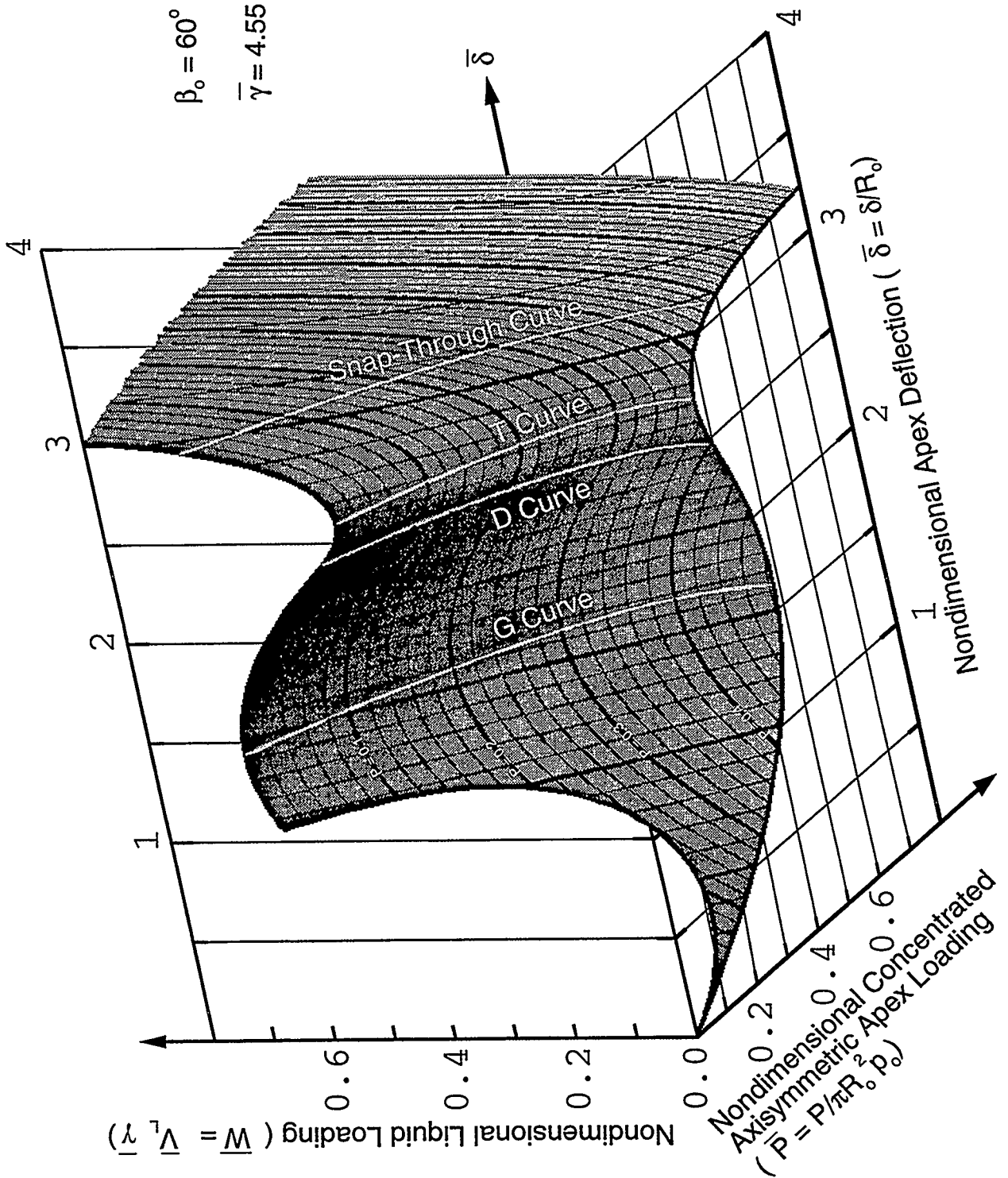


Figure 4.4: Load-Deflection Surface for a Spherical Membrane Subjected to Combined Hydrostatic and Concentrated Axisymmetric Apex Loading ($\bar{\gamma} = 4.55$ and $\beta_0 = 60^\circ$)

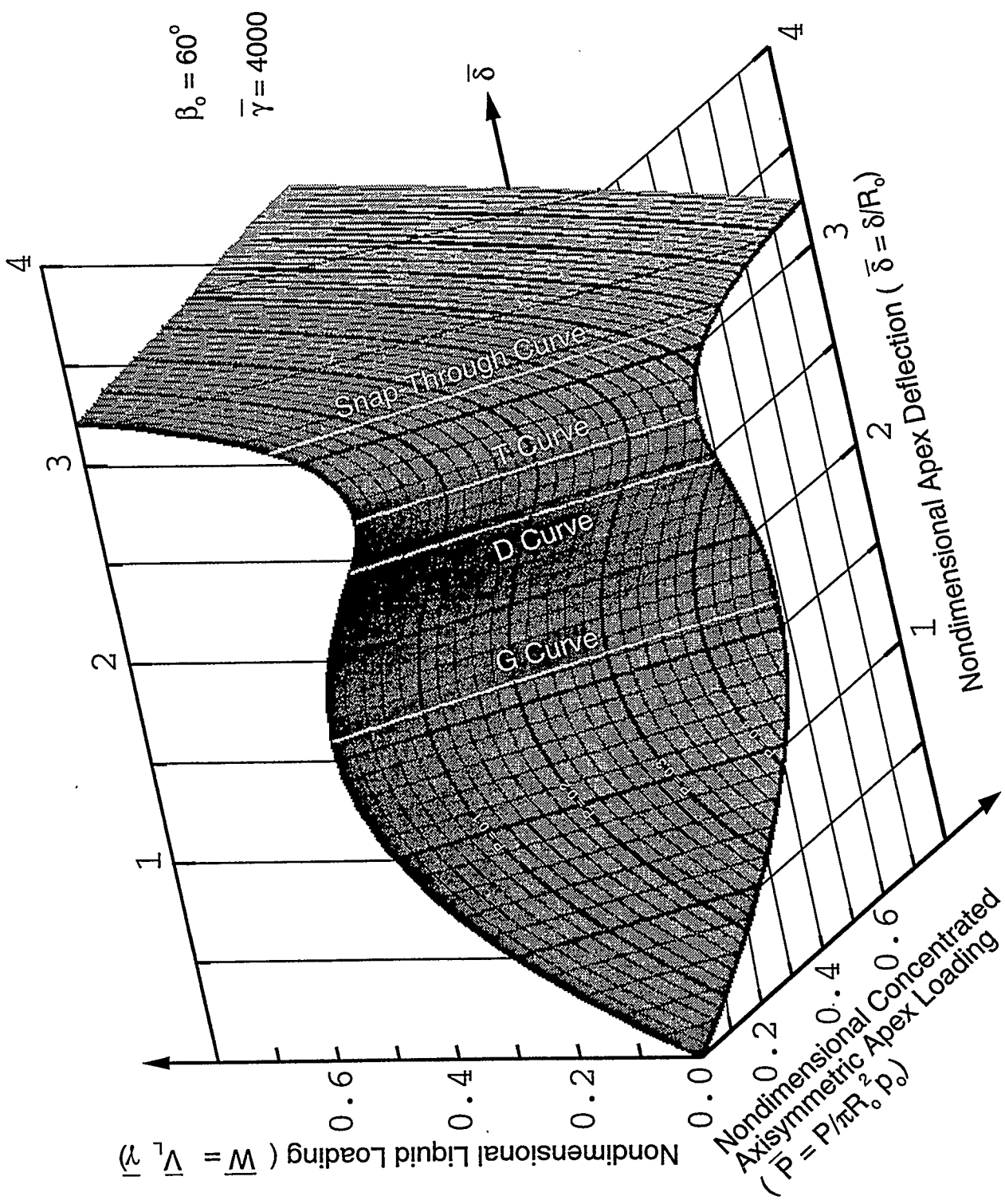


Figure 4.5: Load-Deflection Surface for a Spherical Membrane Subjected to Combined Hydrostatic and Concentrated Axisymmetric Apex Loading ($\bar{\gamma} = 4000$ and $\beta_o = 60^\circ$)

4.5, it can be determined that, as the nondimensional density increases, the curves straighten. It is believed that, in the limit when the nondimensional density approaches infinity, the G, T, D and Snap-Through curve would become straight lines since the hydrostatic and concentrated axisymmetric apex load load-deflection curves would become identical. On the other hand, when the nondimensional density decreases, the C curve will intersect and truncate the G curve as seen on Figure 4.3 for $\bar{\gamma} = 2.8$. This means that all of the points on the C curve in the direction of increasing apex deflection from C curve's intersection point with the G curve are unstable. As this is not the case for the load-deflection surface for $\bar{\gamma} = 4.55$, the change of behavior must occur between the two nondimensional densities. In fact, as was indicated in Chapter 3, when the nondimensional density is $\bar{\gamma} = 3.4$ the G curve, C curve, and hydrostatic loading curve all intersect at one point, C_H . The crucial point, however, is that in Chapter 3 it was stated that for $\bar{\gamma} < 3.4$ there was no stable portion of the main load-deflection curve. This is still correct, but it can be seen from Figure 4.3 that, when combined hydrostatic and concentrated axisymmetric apex loading is applied, there is a stable portion of the load-deflection surface for $\bar{\gamma} < 3.4$. In fact there is a stable portion for every concentrated axisymmetric apex load between $\bar{P} = 0$ to $\bar{P} = 0.484$. It also indicates that, when the membrane is loaded solely by hydrostatic loading, a point of equilibrium exists at the origin which was not indicated in Chapter 3.

The next effect discussed was the effect of the nondimensional density on the value of the hydrostatic load for the ultimate curve. As Figures 4.3 through 4.5 do not include the ultimate curve due to space requirements, reference will first be made to the results in Chapter 3 and then inferences can be made as to the behavior of

load-deflection surfaces. When the nondimensional liquid load is examined for the ultimate point at a given central half angle for Figures 3.11 through 3.24, it is apparent that, as the nondimensional density increases, so too does the final nondimensional liquid load. This is a natural consequence based on the fact that, for a fixed volume of liquid, the total load will increase if a liquid with a higher density is substituted. This is also the case for the ultimate curve on a load-deflection surface. If a higher nondimensional density is used, the ultimate curve will terminate at a higher nondimensional liquid load. In fact, as the nondimensional density approaches infinity, the ultimate curve will not be reached just as in the case for the ultimate point for concentrated axisymmetric apex loading. On the other hand, if the nondimensional density is decreasing in value, the nondimensional liquid load level of the ultimate curve also decreases. In fact, as the nondimensional density approaches $\bar{\gamma} = 0$, the ultimate curve will approach the D curve. An example of this phenomenon is shown on Figure 4.6 which will be presented later in this section.

The most dramatic effect the nondimensional density has on the behavior exhibited on the load-deflection surface concerns the C curve. It is obvious from Figures 4.3 through 4.5 that, as the nondimensional density increases, the amount of surface area excluded from the load-deflection surface decreases, due to the formation of completely filled membrane depressions. Even though it appears that there is no C curve on Figure 4.5, there is one, but the scale is too large for it to be seen. A natural consequence of having a smaller C curve is that point C_M occurs at a smaller value of \bar{P}_M . In the limit, as the nondimensional density approaches infinity, the C curve will vanish at the origin.

On the other hand, it is evident that as the nondimensional density decreases, the

amount of surface area excluded from the load-deflection surface increases. As was previously stated, the G curve for Figure 4.3 has been interrupted by the C curve resulting in a portion of the C curve being in a state of unstable equilibrium. However, it is important to note that the point C_M on the C curve is in stable equilibrium. In practice, the engineer would be restricted to concentrated axisymmetric apex loads between $\bar{P} = 0$ and $\bar{P} = \bar{P}_M$. Thus, for a particular nondimensional density, as long as point C_M is in stable equilibrium, then that nondimensional density can be legitimately used in design. It will be shown later that all nondimensional densities are legitimate but not necessarily practical for design purposes.

It is believed that, as the nondimensional density decreases below $\bar{\gamma} = 2.8$, the C curve will continue to exclude surface area on the load-deflection surface. In fact, it is proposed that, when the nondimensional density reaches $\bar{\gamma} = 0$, the entire load-deflection surface will be excluded except that of the concentrated axisymmetric apex load's load-deflection curve which will also correspond to the C curve. The reasoning is as follows: as the nondimensional density decreases, the liquid adds less and less weight to the total load applied to the structure. The result is that a very low density liquid will cause negligible additional deflection of the membrane allowing the depression to be filled more easily than if a more dense liquid had been used. In the limit, when $\bar{\gamma} = 0$, the depression is completely filled with a hypothetical ponding medium which adds no additional load and causes no additional deflection to the structure. The result is that only the concentrated axisymmetric apex load's load-deflection curve exists. As proof, using Figure 3.5 in Chapter 3, the point C_H for $\bar{\gamma} = 0$ occurs at $\bar{W} = 0.0$ and $\bar{\delta} = \pi + 2$ which corresponds to the end point of the main curve for concentrated axisymmetric apex loading. This means the hydrostatic

load-deflection curve for $\bar{\gamma} = 0$ consists of a single point, and furthermore, that point lies on the concentrated axisymmetric apex load's load-deflection curve.

It is believed that the point C_M on the C curve will always remain in the stable portion of the load-deflection surface as the nondimensional density decreases. It is further proposed that, in the limit when the nondimensional density reaches $\bar{\gamma} = 0$, the point C_M will coincide with the G point for concentrated axisymmetric apex loading. The basis for this statement is that point C_M is defined by the maximum concentrated axisymmetric apex load which will produce a completely filled depression. When the nondimensional density is $\bar{\gamma} = 0$ the C curve is identical to the load-deflection curve for concentrated axisymmetric apex loading. Therefore, the point C_M must lie on the concentrated axisymmetric apex load's load-deflection curve. Further, as the point C_M must correspond to the maximum concentrated axisymmetric apex load which produces a completely filled membrane, the G point for concentrated axisymmetric apex loading must also be point C_M .

In summary, as the nondimensional density approaches infinity, the load-deflection surface becomes symmetrical about a plane oriented at 45° to the concentrated axisymmetric apex loading and apex deflection plane. This is due to the fact that the hydrostatic loading mimics the concentrated axisymmetric apex loading when the nondimensional density reaches infinity. In the other extreme, when the nondimensional density is $\bar{\gamma} = 0$, then the load-deflection surface corresponds to the load-deflection curve for concentrated axisymmetric apex loading.

4.5.2 Central Half Angle

To aid in examining the effects of the central half angle on the load-deflection behavior exhibited by a spherical membrane, Figures 4.6, 4.7, and 4.8 were produced. The central half angle used were $\beta_o = 120^\circ$, $\beta_o = 60^\circ$, and $\beta_o = 30^\circ$ while the nondimensional density was held constant at $\bar{\gamma} = 4.55$.

In actuality, the central half angle has only one effect on load-deflection surfaces, namely, where the load-deflection surface deviates from the main load-deflection surface for a given nondimensional density. Only the portion of the load-deflection surface which has deviated from the main load-deflection surface has unique characteristics based on the central half angle.

By examining Figures 4.7 and 4.8, it is apparent that, as long as the central half angle causes the deviation from the main load-deflection surface to occur at a configuration located in a direction of increasing apex deflection from the G curve, there will be an unstable portion of the main load-deflection surface and snap-through can occur. As the central half angle decreases, the unstable portion of the main load-deflection surface enlarges and the effects of snap-through become more pronounced. It should be noted, that the G curve consists of individual G points each of which has a unique angle ϕ_E . Thus, there is a transition domain in which the deviation from the main load-deflection surface occurs across the G curve. In other words, the D curve will intersect and truncate the G curve such that only concentrated axisymmetric apex loads possessing a G point on the load-deflection surface will exhibit snap-through behavior. This being the case, the smallest value of the central half angle which would guarantee that no snap-through behavior is exhibited, no

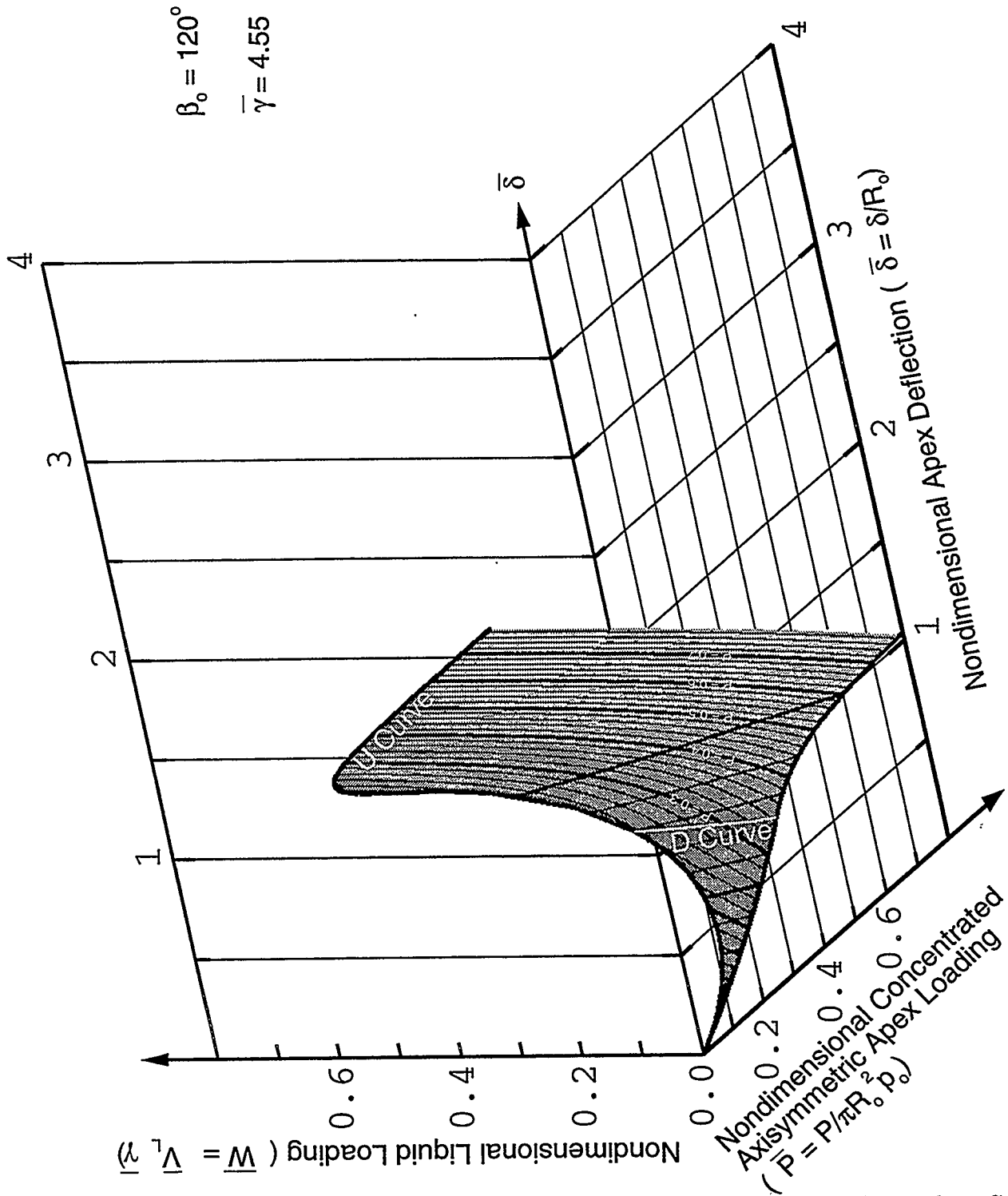


Figure 4.6: Load-Deflection Surface for a Spherical Membrane Subjected to Combined Hydrostatic and Concentrated Axisymmetric Apex Loading ($\bar{\gamma} = 4.55$ and $\beta_0 = 120^\circ$)

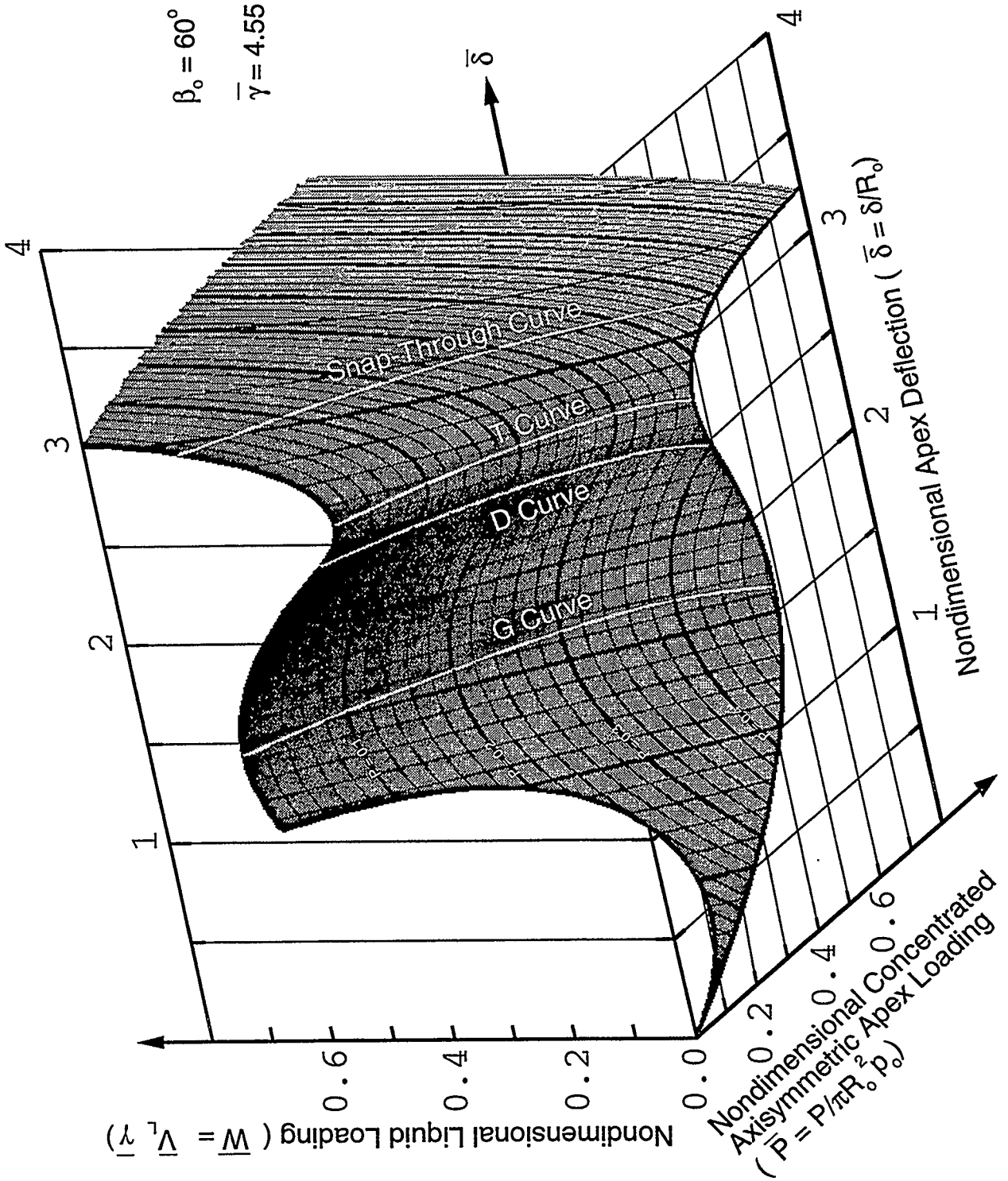


Figure 4.7: Load-Deflection Surface for a Spherical Membrane Subjected to Combined Hydrostatic and Concentrated Axisymmetric Apex Loading ($\bar{\gamma} = 4.55$ and $\beta_0 = 60^\circ$)

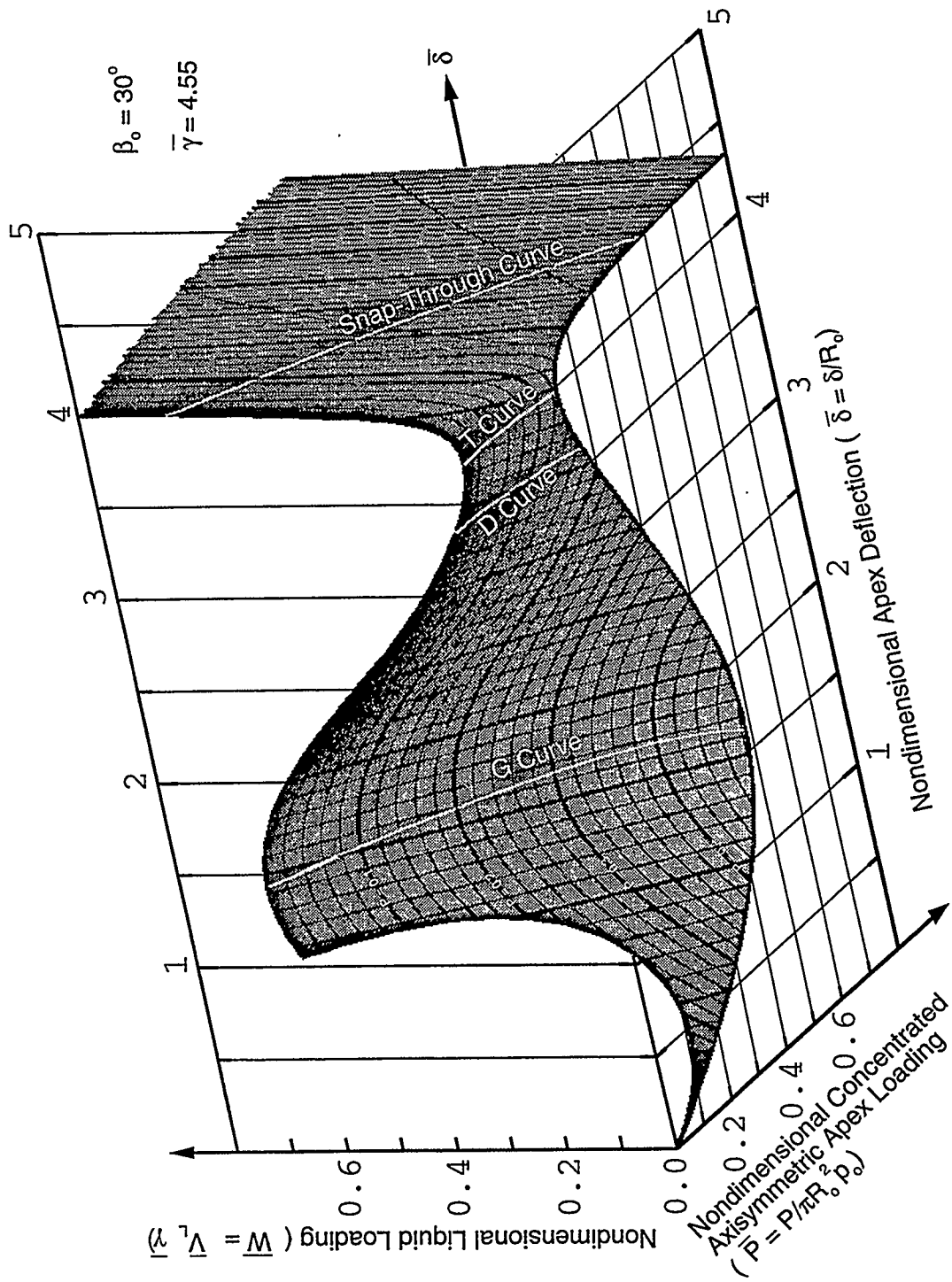


Figure 4.8: Load-Deflection Surface for a Spherical Membrane Subjected to Combined Hydrostatic and Concentrated Axisymmetric Apex Loading Neglecting Support Wrinkling ($\bar{\gamma} = 4.55$ and $\beta_0 = 30^\circ$)

matter what the loading, is $\beta_o = \pi - \phi_{E_{HG}}$ where $\phi_{E_{HG}}$ corresponds to the value of ϕ_E of the G point for hydrostatic loading. This is because angle ϕ_E for hydrostatic loading's G point is the minimum value of all the angles of ϕ_E along the G curve. Whenever the central half angle is greater than $\beta_o = \pi - \phi_{E_{HG}}$, only the D curve exists and the main load-deflection surface only exhibits monotonically stiffening behavior.

However, if the central half angle is increased such that $\beta_o > \pi - \phi_{E_{HC}}$, where $\phi_{E_{HC}}$ corresponds to angle ϕ_E of the C point for hydrostatic loading, then the deviation from the main load-deflection surface will occur on the C curve. In this case, a deviated portion of the C curve exists. This type of behavior can be seen in Figure 4.6. It is interesting to note that, no matter how large the central half angle, there will always be a load-deflection surface in which the concentrated axisymmetric apex load can range from $\bar{P} = 0$ to $\bar{P} = \infty$.

Characteristics of the deviated portion of the load-deflection surface will now be discussed. In general, the deviated portion of the load-deflection surface falls into one of three categories of behavior. The first category exhibits only monotonically stiffening behavior for concentrated axisymmetric apex loads between $\bar{P} = 0$ and $\bar{P} = \infty$ and occurs if the central half angle can be described by $\beta_o > \pi - \phi_{E_{HG}}$. In such cases the G, T and snap-through curves do not exist as the load-deflection surface deviates before their characteristics manifest themselves. This type of behavior is shown in Figure 4.6. The second category has a deviated portion of the load-deflection surface which exhibits unstable behavior for a certain range of concentrated axisymmetric apex loads and then switches to monotonically stiffening behavior for the remainder. For this to occur the central half angle must be de-

scribed as $\pi - \phi_{EHG} > \beta_o > \pi - \phi_{EPG}$ where ϕ_{EPG} is the angle ϕ_E for the G point for concentrated axisymmetric apex loading. The transition between unstable and monotonically stiffening behavior once again occurs where the D curve intersects and truncates the G curve. Let the concentrated axisymmetric apex load which corresponds to the intersection point of the D and G curve be defined as \bar{P}_G . For the second category of behavior, it can now be said that for concentrated axisymmetric apex loads between $\bar{P} = 0$ and $\bar{P} = \bar{P}_G$, the deviated portion of the load-deflection curve has an unstable region whereas for concentrated axisymmetric apex loads between $\bar{P} = \bar{P}_G$ and $\bar{P} = \infty$ only monotonically stiffening behavior is exhibited. Finally, the third category occurs if $\beta_o < \pi - \phi_{EPG}$ where all values of the concentrated axisymmetric apex load that deviate from the main load-deflection surface have an unstable region. In such cases, the entire D curve falls to the right of the G curve. For all concentrated axisymmetric apex loads which have an unstable region on its deviated load-deflection surface, the unstable region ceases at the T curve. Figures 4.7 and 4.8 exhibit category three behavior for their deviated portion of the load-deflection surface.

The last characteristic on the deviated portion of the load-deflection surface to be affected by the central half angle is the ultimate curve. As the central half angle increases, the final volume available to be filled in the ultimate configuration decreases. As the nondimensional density is constant, a smaller volume causes the final nondimensional liquid load, \bar{W} , to be lower at the ultimate configuration. It is evident in Figure 4.6 as the ultimate curve can be seen due to the large value of the central half angle.

The last topic to be discussed with respect to the central half angle is support

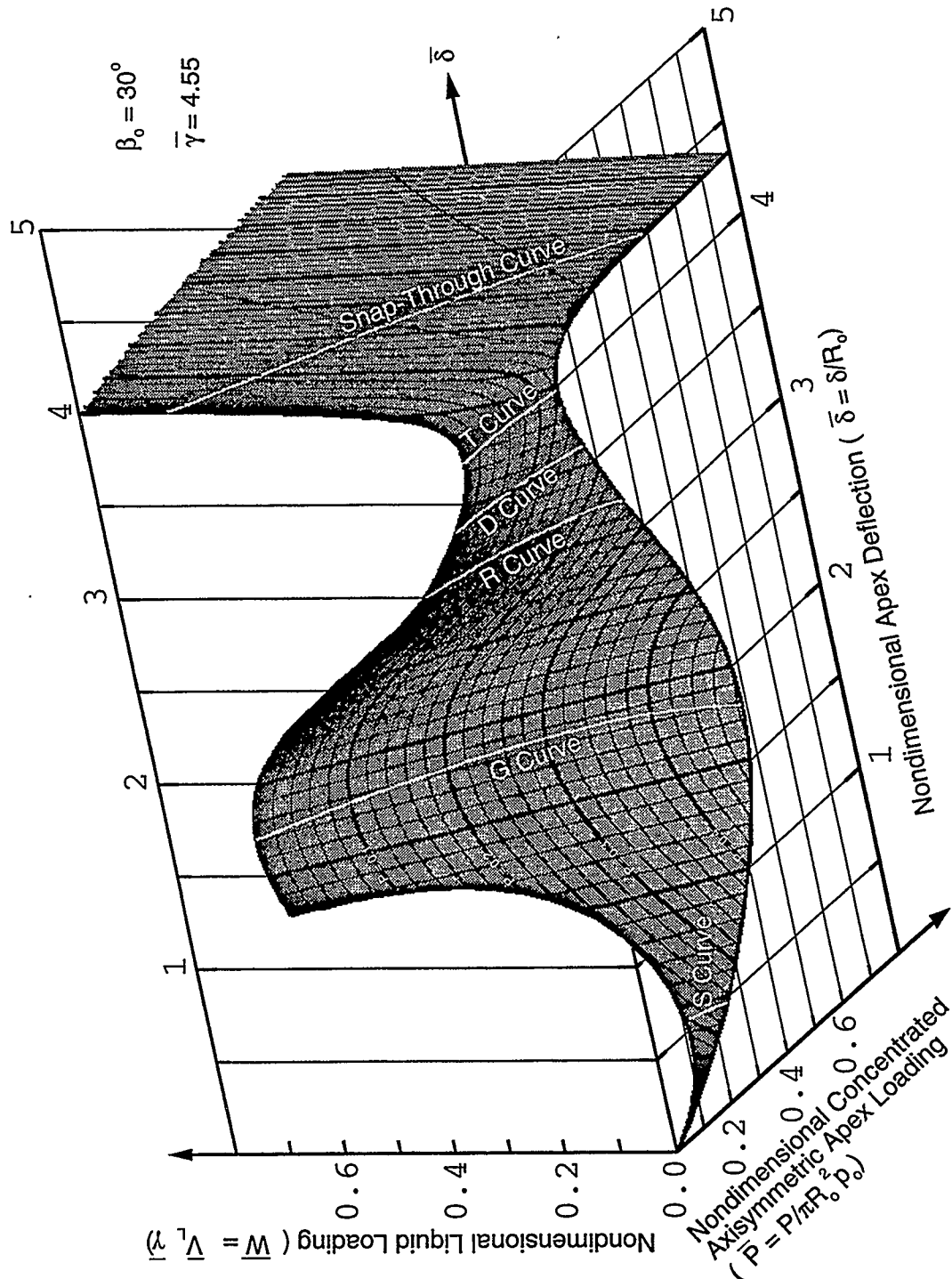


Figure 4.9: Load-Deflection Surface for a Spherical Membrane Subjected to Combined Hydrostatic and Concentrated Axisymmetric Apex Loading with Support Wrinkling ($\bar{\gamma} = 4.55$ and $\beta_0 = 30^\circ$)

wrinkling. The occurrence of support wrinkling is dependent on two variables, the total nondimensional load, \bar{F} , and the central half angle. As the G point for hydrostatic loading has the largest value of total nondimensional load, \bar{F} , on the main load deflection surface, this is where the onset of support wrinkling will occur if the central half angle is lower than the critical value of β_o as determined by Equation 2.38, where $\bar{P}_L = \bar{F}$. This value for the central half angle also corresponds to the minimum value of the central half angle such that no effects of support wrinkling appear on the load-deflection surface.

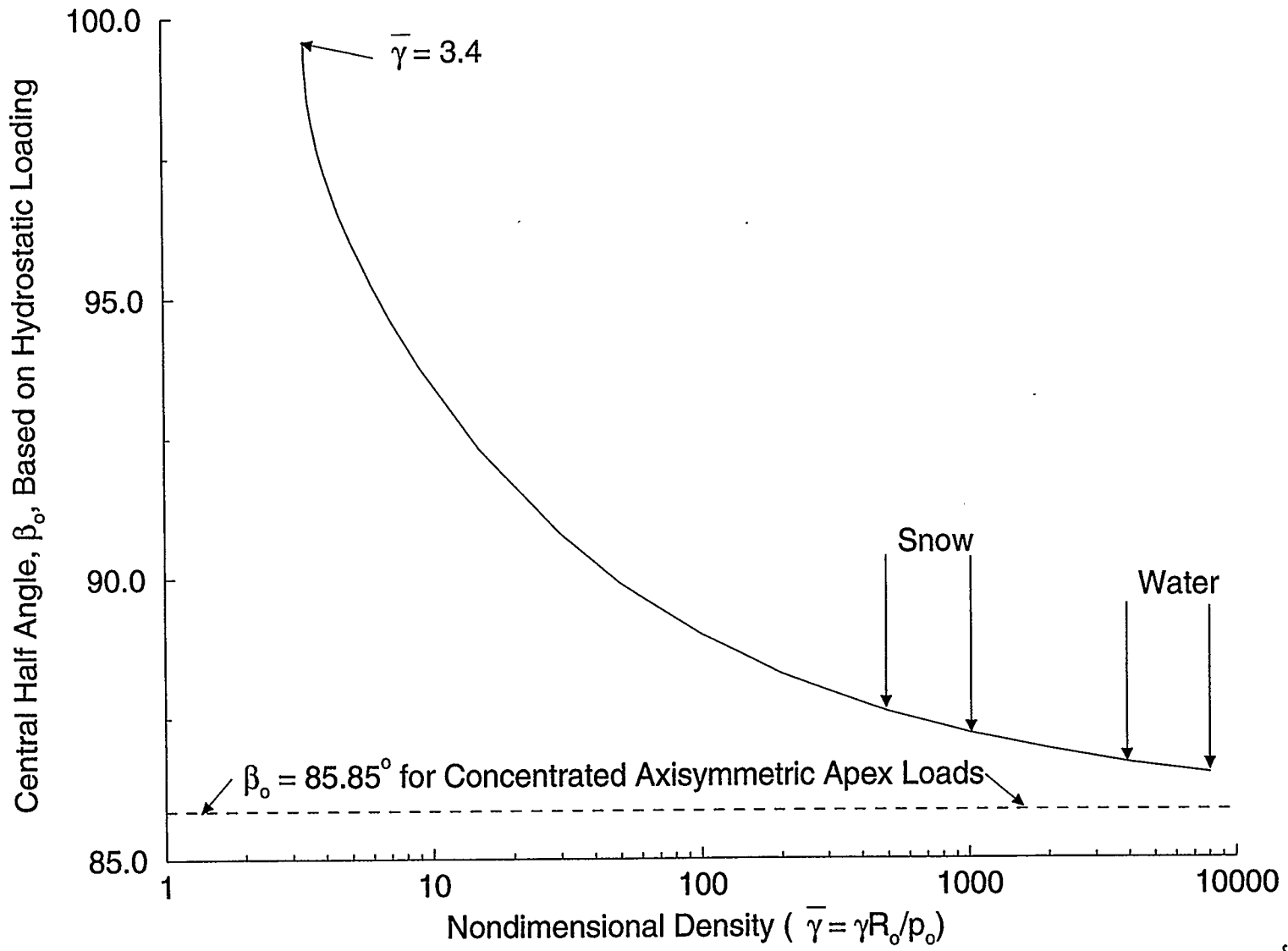
Figure 4.9 shows the load-deflection surface of Figure 4.8 when support wrinkling is included. The only difference between the two Figures is that a larger deflection occurs between the R and S curves on the main load-deflection surface. The S curve indicates the onset of support wrinkling while the R curve marks the end of support wrinkling effects, both of which are shown in Figure 4.9. For central half angles small enough to cause support wrinkling at the G point for hydrostatic loading yet not small enough to cause support wrinkling at the G point for concentrated axisymmetric apex loading, the S and R curves will meet at a point on the G curve. As can be seen from Figure 4.9, support wrinkling has no effect and never will effect the Snap-Through curve, T curve, D curve or any portion of the deviated portion of the load-deflection surface as the membrane is completely wrinkled. Finally, as the central half angle decreases in value, the additional deflection the apex incurs will increase. This is a natural consequence of Equation 2.40.

4.5.3 Design

In practice, the engineer wants to design a structure so that it will not collapse. For the structures discussed in this thesis, failure of the structure can be defined as an unreasonable deflection of the apex or the occurrence of snap-through behavior. The first definition of failure is included as the structure may not incur snap-through yet undergo an apex deflection large enough to render the structure useless. It is not the purpose of this thesis to determine what an unreasonable value of apex deflection is as it is dependent on the use of the structure. Instead, this subsection will focus on the prevention of snap-through behavior. This being the case, the engineer must be cautious in the use of the geometry of the structure, which is controlled by the central half angle, and with the applied loading. However, the engineer can only control the concentrated axisymmetric apex load since the hydrostatic loading is determined by the weather which is unpredictable. Thus, in designing the structure, the engineer can freely choose from the entire range of central half angles or any concentrated axisymmetric apex load but not both.

At this point it is advantageous to provide a range of values for the nondimensional density for substances the engineer is likely to encounter, rain and snow. The equation used to determine the nondimensional density is $\bar{\gamma} = \frac{\gamma R_o}{p_o}$. In all cases, it will be assumed that the internal overpressure, p_o , is a quarter of an inch of water or 62 Pa. The radius of the structure, R_o , on the other hand, is likely to vary depending on the application. For the purposes of this thesis, it is felt that a range between 25 m and 50 m adequately represents the values likely to be used for storage, sports, and green house facilities. Finally, the density of rain water is $9810 N/m^3$ while that

Figure 4.10: Minimum Allowable Central Half Angle for a Given Nondimensional Density



of freshly fallen snow was taken as $1256N/m^3$ from Mark's Standard Handbook for Mechanical Engineers [5]. The result is that for rain water the range of nondimensional densities is between $\bar{\gamma} = 4000$ and $\bar{\gamma} = 8000$ while for snow it varies from $\bar{\gamma} = 500$ to $\bar{\gamma} = 1000$.

If the engineer is restricted to the use of a specific concentrated axisymmetric apex load and if, for the nondimensional density which is applicable, it exceeds the critical value for the concentrated axisymmetric apex load, P_M , the engineer must restrict the geometry of the structure such that snap-through is impossible. In Subsection 4.5.2, it was pointed out that the entire load-deflection surface would be in stable equilibrium if the central half angle was greater than $\pi - \phi_{E_{HG}}$, where $\phi_{E_{HG}}$ is the value of angle ϕ_E for the G point when the membrane is subjected to hydrostatic loading. With this in mind, Figure 4.10 shows a curve which provides the minimum allowable central half angle for a specific nondimensional density. It is recommended that additional safety factors be included. On Figure 4.10, it can be seen that the curve terminates at $\bar{\gamma} = 3.4$. This is due to the fact that, for hydrostatic loading, the G point is nonexistent below $\bar{\gamma} = 3.4$ as the load-deflection curve is already unstable at its C point. As the practical range for nondimensional densities is considerably greater than $\bar{\gamma} = 3.4$ it is not a problem. The practical ranges are also indicated on Figure 4.10. As the corresponding range of central half angles is moderately lofty, the engineer can use shallow geometries with confidence.

On the other hand, if the engineer is required to use a central half angle for which snap-through is a possibility, the design must focus on using a concentrated axisymmetric apex load below the critical concentrated axisymmetric apex load, P_M , for the given nondimensional density. Figure 4.11 provides the nondimensional

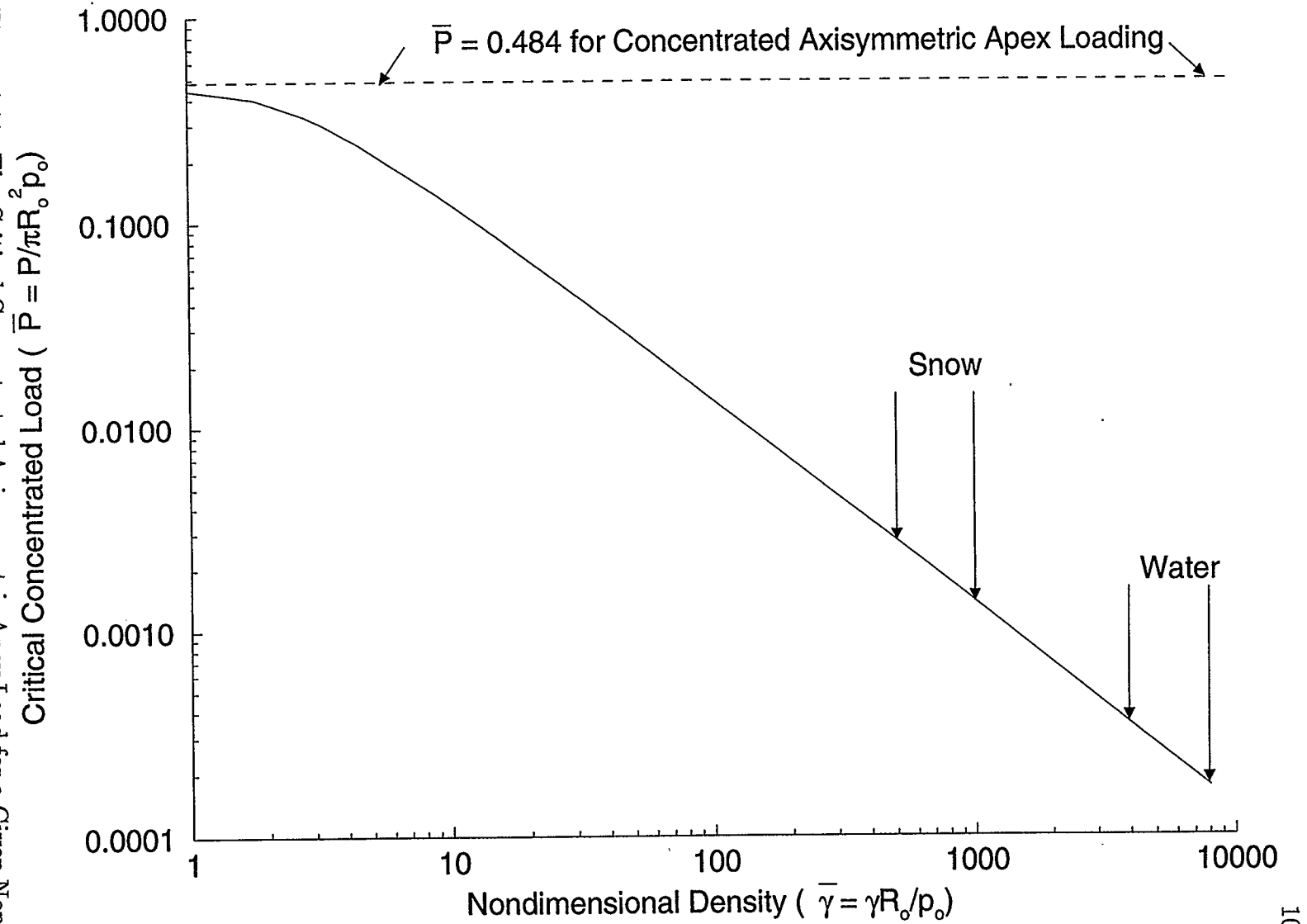
critical concentrated axisymmetric apex load when a specific nondimensional density has been chosen. This curve was first produced by Szyszkowski and Glockner [14] who found that the linear portion of the curve could be approximated by

$$\bar{P} = \frac{1.109}{\bar{\gamma}^{0.9636}} \quad (4.33)$$

As a side note, Figure 4.11 confirms the statement made in subsection 4.5.1 to the effect that, as the nondimensional density approaches $\bar{\gamma} = 0.0$, the value of the critical concentrated axisymmetric apex load approaches $\bar{P} = 0.484$.

Of particular interest is the value of the critical concentrated axisymmetric apex load and the depth of the critical depression for the upper range of the nondimensional density, $\bar{\gamma} = 8000$, for water. The equation used in determining the concentrated axisymmetric apex load is $P = \bar{P}\pi R_o^2 p_o$. Using $\bar{P} = 0.000172$, from Figure 4.11, a radius of 50 m and an internal overpressure of 62 Pa, the critical concentrated axisymmetric apex load is 84 N. This is an extremely small load for the size of the structure. The depth of the critical depression, which would allow the structure to collapse due to hydrostatic loading alone, is determined by the height of the liquid at the apex which is $H_o = \bar{H}_o R_o$. Using the value $\bar{H}_o = 0.000309$, the corresponding depth of the depression is 1.545 cm. This is alarmingly small as a defect in the arc length for a structure with a 50 m radius may easily exceed this value. This situation can be alleviated by increasing the internal overpressure for large radius structures. It also points out that large radii, flat, structures are more likely to be susceptible to ponding failure. However, it is recommended that the design also incorporate a shallow central half angle to eliminate the possibility of snap-through behavior.

Figure 4.11: The Critical Concentrated Axisymmetric Apex Load for a Given Nondimensional Density



4.6 Summary

This concludes the presentation on results for various loading conditions of a spherical inflatable membrane. Chapter 5 will summarize the findings, as well as make recommendations for future research.

Chapter 5

DISCUSSION AND CONCLUSIONS

5.1 Limitations

This section will discuss the limitations of the computer model, the reason for each limitation, and how, if possible, to adapt to the limitation such that its effect will be minimized.

The first limitation to be discussed is that equilibrium configurations for the membrane would not converge for central half angles below $\beta_o = 5^\circ$. This results in the main load curve for concentrated axisymmetric apex loading and the “takeoff” curve for hydrostatic loading to terminate prematurely. The data for these curves was extrapolated below $\beta_o = 5^\circ$ based on the points for central half angles greater than $\beta_o = 5^\circ$. The end point of the curves can be deduced from the geometry of the structure. The reason for the limitation is that, at very lofty geometries, the problem becomes highly unstable and the variables used by the computer do not have enough precision. At this point the computer program variables are quadruple precision and no further improvement can be achieved. This limitation exists for all three loading conditions described in this thesis.

The second limitation, however, only affects combined hydrostatic and concentrated axisymmetric apex loading cases. The difficulty lies in the fact that the concentrated axisymmetric apex load cannot be set to zero. When this is attempted it results in a singularity in the differential equations defining the behavior of the

membrane at the apex. This results from the fact that the assumption was made that the wrinkled region begins at the apex. In Chapter 3 the reason for using an inverted sphere from the apex to point A was to eliminate the singularity at point A that would have resulted if wrinkling began at the apex. For combined loading, however, the load-deflection behavior can be determined for $\bar{P} = 0$ by choosing a concentrated axisymmetric apex load close to $\bar{P} = 0$, determining its load-deflection value, and then reducing the concentrated axisymmetric apex load. This process is repeated until the change in load-deflection values becomes negligible. The only problem with this procedure is that the resulting values of $\bar{\delta}$ and \bar{W} for combined loading, although close, did not match those predicted in Chapter 3 for Hydrostatic loading. The reason lies in the fact that the behavior at the apex is assumed to be different in the two chapters. In Chapter 3 there is an inverted sphere at the apex while in Chapter 4 the wrinkling begins immediately at the apex. The two cases will never reconcile.

The next limitation in the computer model is that, whenever hydrostatic loading occurs, the nondimensional density's upper limit is restricted as it attempts to approach infinity. In the case of this thesis the nondimensional density produced acceptable results for $\bar{\gamma} = 8000$ but failed when $\bar{\gamma} = 16000$ was attempted. The reason this occurred was that, as the nondimensional density increases, the points A, B, and C on the membrane move closer together. Finally, the B and C points are so close that they are both within a single increment of the arc length. The program attempts to execute both the test for the B and C point at the same time and the program fails. The solution to this limitation is that, for larger nondimensional densities, the step size used for the nondimensional arc length must be decreased.

The final limitation in the computer model to be discussed is the fact that, when C points are generated, the depression is never completely filled. The test used to determine if the depression was full is to check if $\phi_C = 0$. When the program was executed, however, the closest angle ϕ_C came to passing the test was typically $\phi_C = -0.001$. At first it was felt that this resulted since the nondimensional liquid height, \bar{H}_o , was within one increment of the nondimensional arc length from being completely filled. When the increment used for the nondimensional arc length was reduced, however, no noticeable improvement for the value of ϕ_C was obtained. It then became apparent that the method used to predict angle ϕ_D at point C fails when $\phi_C = 0$ as Equation 4.29 becomes identical to Equation 4.28. Fortunately, the values for $\bar{\delta}$ and \bar{F} do not change significantly once the value of angle ϕ_C is less than -0.01 radian.

5.2 Conclusions

A summary of the major points presented in this thesis are as follows:

- The load-deflection characteristics have been clearly developed for a spherical membrane subjected to concentrated axisymmetric apex loads, hydrostatic loads, or a combination of hydrostatic and concentrated axisymmetric apex loading.
- Snap-through behavior is exhibited by spherical inflatable structures, given a sufficiently small central half angle, when subjected to concentrated axisymmetric apex loads, hydrostatic loads, or a combination of hydrostatic and concentrated axisymmetric apex loading.

- When the spherical membrane is subjected solely to concentrated axisymmetric apex loading, the engineer can avoid snap-through behavior by ensuring the nondimensional concentrated axisymmetric apex load is less than $\bar{P} = 0.484$ regardless of the geometry of the structure.
- When the spherical membrane is subjected solely to concentrated axisymmetric apex loading, the engineer can avoid snap-through behavior by ensuring the central half angle for the structure is greater than $\beta_o = 85.5^\circ$ regardless of the concentrated axisymmetric apex load applied.
- When the spherical membrane is subjected to hydrostatic loading, load-deflection curves exist for nondimensional densities ranging from $\bar{\gamma} = 0$ to $\bar{\gamma} = \infty$.
- When the nondimensional density for hydrostatic loading approaches infinity, the load-deflection behavior of the spherical membrane approaches the behavioral characteristics of a membrane subjected to concentrated axisymmetric apex loading.
- When the nondimensional density for hydrostatic loading ranges between $\bar{\gamma} = 3.4$ and $\bar{\gamma} = \infty$, The load-deflection curves deviate from the “Takeoff” curve in a state of stable equilibrium.
- When the nondimensional density for hydrostatic loading ranges between $\bar{\gamma} = 3.4$ and $\bar{\gamma} = 0$, the load-deflection curves deviate from the “Takeoff” curve in a state of unstable equilibrium.
- The “Takeoff” curve terminates at $\bar{W} = 0$ and $\bar{\delta} = 2 + \pi$ when the nondimensional density is $\bar{\gamma} = 0$. This corresponds to the end of the main curve for

concentrated axisymmetric apex loading.

- As hydrostatic loads result from precipitation, the loading and unloading of hydrostatic loads is unpredictable. Also, when subjected to hydrostatic loading all load-deflection curves, with a sufficiently small central half angle, exhibit snap-through behavior. As this is the case, the only equilibrium configuration which can be relied upon not to collapse is the one involving a completely filled depression since any additional loading is rejected. These configurations make up the “Takeoff” curve for various nondimensional densities.
- In practice, the engineer will likely encounter structures which are initially loaded by a concentrated axisymmetric apex loads. The resulting depression is available to initiate hydrostatic loading of the structure.
- Load-deflection surfaces rather than curves are better equipped to describe the load-deflection characteristics of a spherical membrane subjected to a combination of hydrostatic and concentrated axisymmetric apex loads.
- As the nondimensional density approaches infinity, the load-deflection surface becomes symmetrical about a plane oriented at 45° to the plane defined by the nondimensional concentrated axisymmetric apex load axis and the nondimensional apex deflection axis.
- As the nondimensional density approaches $\bar{\gamma} = 0$, the load-deflection surface decreases in area until it is reduced to the concentrated axisymmetric apex load’s load-deflection curve.

- Once again, equilibrium configurations with completely filled depressions afford the only guarantee against snap-through behavior when small central half angles are employed. These configurations comprise the C curve on load-deflection surfaces. The maximum concentrated axisymmetric apex load which produces a completely filled membrane is designated as \bar{P}_M .
- As the value of \bar{P}_M is insignificant for the practical range of nondimensional densities corresponding to rain water, it is recommended the engineer employ a shallow geometry to prevent snap-through behavior.
- Support wrinkling of the structure occurs for all loading conditions discussed in this thesis if the central half angle is sufficiently small. The load wrinkling and the support wrinkling domains never interact. The result of support wrinkling on the structure's load-deflection characteristics is an additional settlement of the apex.

5.3 Future Research

To conclude this thesis, a few potential new areas for research are suggested:

- The effect of stove pipe supports and support interference on the load-deflection behavior of spherical membranes subjected to hydrostatic loads or combined hydrostatic and concentrated axisymmetric apex loads.
- The effect of nonaxisymmetric concentrated loads on a spherical membrane's load-deflection characteristics.

- The load-deflection characteristics of a spherical membrane subjected to symmetric ring and hydrostatic loads.
- The effect on the load-deflection characteristics of a spherical membrane if the assumption of a constant internal overpressure is relaxed.

Bibliography

- [1] Ahmadi, G. and Glockner, P. G. (1983). *Ponding Instability of Inflated Imperfect Membranes*. Proc. ASCE, 109, No. 2, J. Struct. Division, 297 - 313.
- [2] Ahmadi, G. and Glockner, P. G. (1983). *Collapse by Ponding of Pneumatic Elastic Spherical Caps under Distributed Loads*. Can. J. Civ. Eng. 10, 740 - 747.
- [3] Ahmadi, G. and Glockner, P. G. (1983). *Ponding Instability of Air-Supported Elastic Spherical Membranes*. Engineering Transactions, Polish Academy of Sciences, 31, No. 3, 361 - 378.
- [4] Ahmadi, G. and Glockner, P. G. (1984). *Effect of Imperfection on Ponding Instability*. Proc. ASCE, 110, No. 8, J. E. M. Division, 1167 - 1173.
- [5] Avallone, E. A. & Baumeister III, T. *9th Mark's Standard Handbook for Mechanical Engineers* McGraw Hill. New York. 1987.
- [6] Dacko, A. K. & Glockner, P. G. (1988). *Spherical Inflatables Under Axisymmetric Loads: Another Look*. Int. J. Non-Linear Mechanics. 23: 393 - 407.
- [7] Dacko, A. K. & Glockner, P. G. (1989a). *On the Large-Deflection and Stability Behaviour of Spherical Inflatables Under Symmetric Plate and Cylinder Loads*. Eng. Struct. 11: No. 2, 97 - 111.
- [8] Dacko, A. K. & Glockner, P. G. (1989b). *The Effect of Support Interference on the Behaviour of High-Rise Spherical Inflatables*. Thin-Walled Structures. 8: 41 - 53.

- [9] Dacko, A. K. & Glockner, P. G. (1989c). *Behaviour of Spherical Pneumatics Subjected to Axisymmetric Ring Loads*. Int. J. Non-Linear Mechanics. **24**: No. 4, 41 - 53.
- [10] Dym, C. L. *Introduction to the Theory of Shells*. Pergamon Press. New York. 1974.
- [11] Eisenhart, L.P. *Differential Geometry of Curves and Surfaces*. Dover. New York. 1960.
- [12] Eisenhart, L.P. *Riemannian Geometry*. Princeton University Press. 1926.
- [13] Green, A.E. and Zerna, W. *Theoretical Elasticity*. Oxford University Press. 1954.
- [14] Glockner, P. G. & Szyszkowski, W. (1983). *Some Stability Considerations of Inflatable Structures*. Shell and Spatial Struct. in Eng. IASS Symp. Rio de Janeiro. 116 - 134.
- [15] Griffiths, D. V. & Smith, I. M. *Numerical Methods for Engineers*. Blackwell Scientific Publications. Oxford. 1991.
- [16] Kraus, H. *Thin Elastic Shells*. John Wiley & Sons. New York. 1967.
- [17] Lukasiewicz, S.A. and Glockner, P.G. (1983). *Collapse by Ponding of Shells*. Int. J. Solids and Structures, 19, No. 3, 251 - 261.
- [18] Lukasiewicz, S.A. and Glockner, P.G. (1983). *Ponding Instability of Air-Supported Spherical Membranes with Initial Imperfections*. Int. J. Non-Linear Mechanics, 18, No. 1, 1 - 9.

- [19] Lukasiewicz, S.A. and Glockner, P.G. (1983). *Lateral Stability of Lofty Air-Supported Spherical Membranes*. Int. J. Non-Linear Mechanics, 18, No. 6, 491 - 499.
- [20] Malcolm, D. J. & Glockner, P. G. (1981). *Collapse By Ponding of Air-Supported Spherical Caps*. Proc. Am. Soc. Civ. Engrs ST9. 1731 - 1742.
- [21] Sokolnikoff, I.S. *Tensor Analysis*. John Wiley and Sons. New York. 1951.
- [22] Sokolnikoff, I.S. *Mathematical Theory of Elasticity*. McGraw-Hill Book Co. 1956.
- [23] Stanuszek, M. & Glockner, P. G. (1992). *The Ponding Problem of Very Lofty Spherical Inflatables: Another Look*. Proc. IASS-CSCE, Int. Congress on "Innovative Large Span Structures". Toronto. 1: 790 - 799.
- [24] Stanuszek, M. & Glockner, P. G. (1995). *Further Results on the Response of Spherical Inflatables Under Axisymmetric Hydrostatic Loads*. Computers and Structures. 57: No. 1, 35 - 45.
- [25] Szyszkowski, W. & Glockner, P. G. (1984a). *Finite Deformation and Stability Behaviour of Spherical Inflatables Under Axisymmetric Concentrated Loads*. Int. J. Non-Linear Mechanics. 19: No. 5, 489 - 496.
- [26] Szyszkowski, W. & Glockner, P. G. (1984b). *Finite Deformation and Stability Behaviour of Spherical Inflatables Subjected to Axisymmetric Hydrostatic Loading*. Int. J. Solids & Structures. 21: No. 11/12, 1021 - 1036.
- [27] Szyszkowski, W. & Glockner, P. G. (1987). *Spherical Membranes Subjected to Concentrated Loads*. Eng. Struct. 9: 45 - 52.

- [28] Timoshenko, S.P. *Theory of Shells and Plates*. McGraw-Hill. New York. 1940.
- [29] Timoshenko, S.P. and Goodier, J.N. *Theory of Elasticity*. McGraw-Hill: New York. 1951.
- [30] Weatherburn, C.E. *Differential Geometry of three dimensions*. Cambridge University Press. Cambridge.